

THE PENNSYLVANIA STATE UNIVERSITY  
SCHREYER HONORS COLLEGE

DEPARTMENT OF BIOENGINEERING

A CORRELATIVE STUDY OF FLUID MECHANICS AND EVIDENCE OF  
THROMBUS FORMATION WITHIN THE PENN STATE 50 CC V-2 LEFT  
VENTRICULAR ASSIST DEVICE

STEPHEN ROBERT TOPPER  
Spring 2012

A thesis  
submitted in partial fulfillment  
of the requirements  
for a baccalaureate degree  
in Bioengineering  
with honors in Bioengineering

Reviewed and approved\* by the following:

Dr. Keefe B. Manning  
Associate Professor of Bioengineering and Surgery  
Thesis Supervisor

Dr. Peter J. Buter  
Associate Professor of Bioengineering  
Honors Adviser

Dr. Steven Deutsch  
Senior Scientist Emeritus  
Thesis Reader

\* Signatures are on file in the Schreyer Honors College.

## ABSTRACT

Ventricular assist devices (VADs) are important alternatives for patients with insufficient cardiac function due to congestive heart failure. With limited donors, heart transplants are often not available. As an alternative to heart replacement, VADs are bridge-to-recovery or life prolonging devices. Clinically, thrombus formation may occur both within the pump and at the cannula junctions and may embolize leading to strokes. Here, we correlate the velocity and shear fluid dynamics obtained from particle image velocimetry (PIV) in a pulsatile VAD against regions on the sac surface within an explanted VAD from a bovine study with particular attention to low shear areas and platelet and fibrin deposition. The bovine study was conducted at the Penn State Hershey Medical Center where a model of the 50 cc Penn State V-2 VAD was implanted and maintained at a constant beat rate of 75 beats per minute (bpm). At the conclusion of the study, the device was explanted and the sac surface was analyzed using scanning electron microscopy (SEM) and, after immunofluorescent labeling for platelets and fibrin, confocal microscopy. Areas were examined based on PIV measurements, with special attention to low shear regions where platelet and fibrin deposition are most likely to occur. To mimic physiological conditions *in vitro*, a mock circulatory loop was used with a blood analog that matched blood's viscoelastic behavior. Under normal physiologic pressures and for a heart rate of 75 bpm as in the *in vivo* study, PIV data was acquired and shear maps were produced. Data collected within the outlet port in a direction normal to the front wall of the VAD shows that areas experience shear rates less than  $500 \text{ s}^{-1}$ . Shear rates below this value indicate insufficient washing along the device walls and

increase the likelihood of platelet and fibrin deposition. This is quantified by the thrombus susceptibility potential, a calculation to correlate low shear with deposition. Computational fluid dynamics confirms the microscopy and PIV data and together, these studies provide information about VADs that will improve their design and increase their clinical effectiveness.

## TABLE OF CONTENTS

LIST OF FIGURES .....	iv
ACKNOWLEDGEMENTS .....	vii
Chapter 1 Introduction .....	1
Chapter 2 Methods .....	10
2.1 Blood Sac Surface Evaluation .....	10
2.2 <i>In Vitro</i> Experiments .....	15
2.3 Computational Fluid Dynamics .....	20
Chapter 3 Results .....	21
3.1 Blood Sac Surface Evaluation .....	21
3.2 Particle Image Velocimetry .....	31
3.3 Computational Fluid Dynamics .....	40
Chapter 4 Discussion .....	43
4.1 Correlations between PIV, microscopic analysis, and CFD .....	43
4.2 Normal and parallel plane correlations between microscopic analysis and TSP .....	44
4.3 Limitations .....	48
Chapter 5 Conclusion .....	49
5.1 Summary of findings .....	49
5.2 Future Work .....	50
References .....	52
Appendix A Complete set of fluorescent images acquired with confocal microscopy .....	55
Appendix B Complete set of images acquired with scanning electron microscopy ...	78

## LIST OF FIGURES

<b>Figure 1-1:</b> The coagulation cascade according to the NIH. ....	4
<b>Figure 1-2:</b> Design iterations of the Penn State 50 cc LVAD. ....	7
<b>Figure 1-3:</b> Inlet and outlet valve orientations within a VAD. ....	8
<b>Figure 2-1:</b> Data points were collected in 1 mm increments along the red curve for each normal plane in Figure 2-2. The arc length of the red curve is 35 mm. ....	11
<b>Figure 2-2:</b> Locations of normal planes from which PIV data was acquired. ....	12
<b>Figure 2-3:</b> Subsectioning of removed blood sac samples. $S_1$ and $S_2$ are sections removed for SEM preparation, $F_1$ and $F_2$ are sections labeled with fluorescent antibodies to be viewed by confocal microscopy. ....	13
<b>Figure 2-4:</b> Locations of the 6 images acquired on each subsection using both SEM and confocal microscopy. ....	14
<b>Figure 2-5:</b> Rear (A) and inlet-side (B) views of the Penn State 50 cc V-2 LVAD. ...	16
<b>Figure 2-6:</b> The Penn State mock circulatory loop. ....	17
<b>Figure 2-7:</b> Inlet-side view of the V-2 LVAD. ....	19
<b>Figure 3-1:</b> Images acquired from the rear wall, 17 mm along the curvature from the origin (Figure 2-1) on the (A) 19.5 mm, (B) 26.9 mm, (C) 34.24 mm, (D) 42.5 mm and (E) 50.8 mm normal planes. (scale bar = 20 microns).....	23
<b>Figure 3-2:</b> Images acquired from the front region of the bottom curve, 1 to 2 mm along the curvature from the origin (Figure 2-1) on the normal planes (A) 19.5 mm, (B) 26.9 mm, (C) 34.24 mm, (D) 42.5 mm and (E) 50.8 mm. (white bar = 20 microns).....	25
<b>Figure 3-3:</b> Images acquired from the center region of the bottom curve, 3 to 6 mm along the curvature from the origin (Figure 2-1) on the normal planes (A) 19.5 mm, (B) 26.9 mm, (C) 34.24 mm, (D) 42.5 mm and (E) 50.8 mm. (white bar = 20 microns).....	27
<b>Figure 3-4:</b> Images acquired from the bottom curve, 7 to 10 mm along the curvature from the origin (Figure 2-1) on the normal planes (A) 19.5 mm, (B)	

26.9 mm, (C) 34.24 mm, (D) 42.5 mm and (E) 50.8 mm. (white bar = 20 microns) .....	29
<b>Figure 3-5:</b> Confirmation of confocal surface analysis by SEM. A and C show regions of the sac with little, or no, platelet and fibrin deposition. B and D show images of platelet and fibrin deposition on the sac surface. (Top, fluorescent microscopy, white bar = 20 microns; Bottom, SEM, scale bar = 50 microns) .....	30
<b>Figure 3-6:</b> Velocity contour maps of flow in the plane 1 mm parallel to the rear wall during diastole within the Penn State V-2 LVAD at a beat rate of 75 bpm. Percentages are during diastole. ....	32
<b>Figure 3-7:</b> Velocity contour maps of flow in the plane 1 mm parallel to the rear wall during systole within the Penn State V-2 LVAD at a beat rate of 75 bpm. Percentages are of the systolic duration.....	33
<b>Figure 3-8:</b> Diagram showing wall location measurements on the normal planes.....	34
<b>Figure 3-9:</b> Wall shear plots of flow during diastole, normalized by $500 \text{ s}^{-1}$ at locations from 0 to 30 mm along the wall curvature (Figure 3-8) on the 19.5, 26.9, 34.24, 42.5 and 50.8 mm normal planes.....	35
<b>Figure 3-10:</b> A TSP plot of wall locations on the 19.5 mm normal plane. A TSP value of 1 indicates a high potential of thrombus formation, 0 indicates a low potential. ....	36
<b>Figure 3-11:</b> A TSP plot of wall locations on the 26.9 mm normal plane. A TSP value of 1 indicates a high potential of thrombus formation, 0 indicates a low potential. ....	37
<b>Figure 3-12:</b> A TSP plot of wall locations on the 34.24 mm normal plane. A TSP value of 1 indicates a high potential of thrombus formation, 0 indicates a low potential. ....	37
<b>Figure 3-13:</b> A TSP plot of wall locations on the 42.5 mm normal plane. A TSP value of 1 indicates a high potential of thrombus formation, 0 indicates a low potential. ....	38
<b>Figure 3-14:</b> A TSP plot of wall locations on the 50.8 mm normal plane. A TSP value of 1 indicates a high potential of thrombus formation, 0 indicates a low potential. ....	38
<b>Figure 3-15:</b> Circumferential measurements of the LVAD wall on the 1 mm parallel plane.....	39

- Figure 3-16:** A TSP plot of wall locations on the 1 mm parallel plane. A TSP value of 1 indicates a high potential of thrombus formation, 0 indicates a low potential. .... 40
- Figure 3-17:** Computational fluid dynamics modeling of wall shear in the Penn State V-2 LVAD for flow in the 1 mm parallel plane during diastole at a beat rate of 75 bpm. Percentages are of the diastolic duration. .... 41
- Figure 3-18:** Computational fluid dynamics modeling of wall shear in the Penn State V-2 LVAD for flow in the 1 mm parallel plane during systole at a beat rate of 75 bpm. Percentages are of the systolic duration. .... 42
- Figure 4-1:** Comparisons between microscopy of specific regions of the explanted sac along the 1 mm parallel plane with the TSP for the same regions. .... 45
- Figure 4-2:** Comparisons of confocal microscopy and SEM of specific regions of the explanted sac along the 1 mm parallel plane with the TSP for the same regions. .... 47

## ACKNOWLEDGEMENTS

I would first like to thank my advisor, mentor and friend, Dr. Keefe Manning. His constant input, support and guidance made this thesis possible and the past three years of work in the Artificial Heart Lab a lasting experience. I would also like to sincerely thank the other members of the Artificial Heart Lab, especially Dr. Steven Deutsch, Dr. Margaret Slattery, and Dr. Peter Butler, my first graduate mentor, Jason Nanna, and Mike Navitsky, for their help, guidance and contributions to this work. At the Huck Institute, John Cantolina and Missy Hazen offered great instruction and support for the microscopy included in this project. This opportunity to supplement my undergraduate education was largely made possible by the Schreyer Honors College, The Pennsylvania State University Summer Discovery Grant and the National Institutes of Health through grant NHLBI HL60276. Finally, I would like to thank my family and friends for their love, support and understanding through my years at Penn State. I could not have done it without you.

## **Chapter 1**

### **Introduction**

Cardiovascular disease (CVD) is a leading medical malady within the United States. It is estimated that 82.6 million American adults live with one or more forms of CVD and in past years, CVD has caused over 55% of all deaths in the United States, which is more than any other type of disease.<sup>1</sup> While the best treatment for patients with end stage heart failure is a transplant, this is not often viable due to the limited number of available donors. In the United States, the ratio of heart transplant recipients to patients on a waiting list approaches 1:10.<sup>2</sup> Ventricular assist devices (VADs) are an alternative to heart transplants for people suffering from congestive heart failure. In most cases, a patient eligible for a VAD would receive a left ventricular assist device (LVAD), since the left ventricle supplies most of the blood to the body and is more prone to failure. LVADs supplement the native heart's ability to supply blood to the body, making them useful as bridge-to-transplant, bridge-to-recovery or destination therapy devices.

The success of patients who have received VADs has improved with new designs of these devices. In 2001, the Randomized Evaluation of Mechanical Assistance in the Treatment of Congestive Heart Failure (REMATCH) reported a 52% survival rate for patients who received a VAD after one year and just 23% after two years.<sup>3</sup> According to the Interagency Registry For Mechanical Circulatory Support (INTERMACS) second annual report of 2010, the survival rates from the beginning of the decade increased to

74% after one year and 55% after two years.<sup>4</sup> Though promising improvements, there are still significant challenges to the success of VADs, specifically in their tendency to cause life-threatening thrombosis.

To address this problem, a thorough understanding of hemocompatibility is necessary. Platelets are disc-shaped cellular fragments – implying they contain no nucleus – typically 2 – 4 microns in diameter, within blood that can be activated to form aggregates. Fibrin is another structure that forms during platelet activation and together they entrap other cellular components such as red blood cells. This process is part of a more complex coagulation cascade, shown in Figure 1-1.<sup>5</sup> This pathway is often triggered by a physiologic event, sometimes associated with injury, trauma or, in the case of VADs, the introduction of a foreign material into the body. Penn State VADs are lined with a sac made of polyurethane, a material that is one of the more biocompatible materials available. However, polyurethane, like every biomaterial, exhibits a level of protein absorption upon exposure to a physiological system.

The physiological response stems from several factors. On a microscopic scale the surface topography of the polyurethane material is not perfectly smooth, providing crevices that catch passing blood components like platelets. These crevices result from the manufacturing process, a limitation of the available technology. Fluid flow also causes a physiological response in the activation of certain blood components such as platelets and fibrin. For example, areas of high shear, as often observed with stenoses, activate platelets and regions of low shear cause fibrin deposition.<sup>6</sup> Both of these

contribute to thrombus formation. Within a vessel, a protruding thrombus disturbs the local blood flow causing turbulence and subsequent tissue damage. Detachment is another possibility if the thrombus is subjected to sufficient shear. This, termed thromboembolism, could likely cause tissue damage or more serious physiological problems such as necrosis, heart attacks or strokes.

Anticoagulants are prescribed to patients who receive VADs to help prevent thrombus formation by inhibiting specific factors along the coagulation pathway.<sup>7</sup> Heparin is a commonly used short-term anticoagulant because of its abilities to inactivate thrombin (Figure 1-1) and other coagulation factors. However, long-term use of heparin causes thrombocytopenia, low platelet counts in the patient.<sup>8</sup> For long-term anticoagulant use, warfarin sodium (Coumadin®) is used because it inhibits vitamin K, which in turn inhibits several coagulation factors such as prothrombin, Factor VII, Factor IX and Factor X (Figure 1-1).<sup>7</sup>

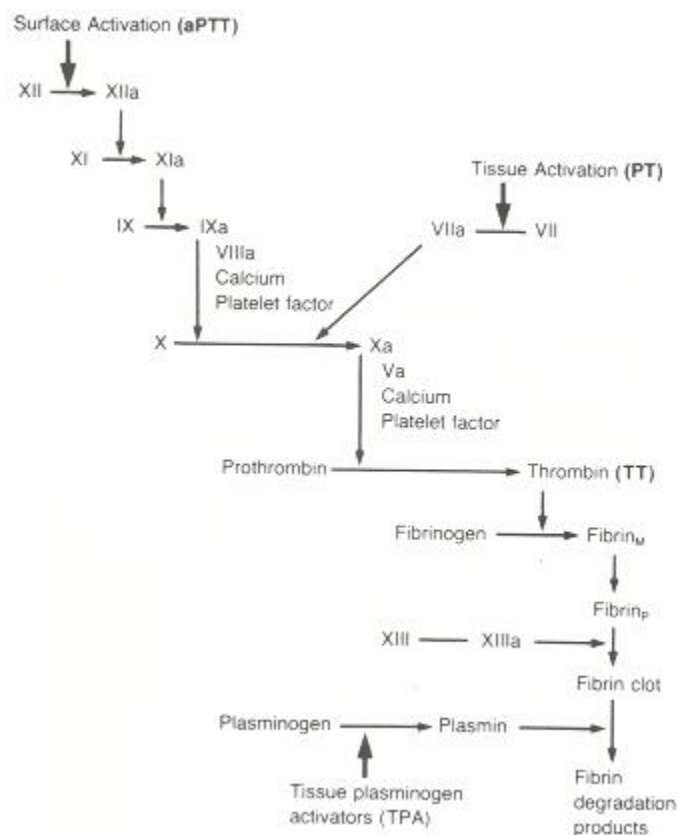


**Figure 1-1:** The coagulation cascade according to the NIH.<sup>5</sup>

Considering the challenges of hemocompatibility, The Pennsylvania State University has studied and developed LVADs in the Division of Artificial Organs since the 1970s. VADs, with sizes ranging from 10 cc to 100 cc were developed and in 2001, the first, fully implantable LVAD, the 70 cc LionHeart™, reached clinical trials and showed remarkably little evidence of thrombus formation.<sup>9</sup> Clinicians found, however, that the 70 cc device was too large for most patients. Considerable efforts have been ongoing to develop a 50 cc device to accommodate the size-limitations of patients. Because size scaling affects the flow through the device, thrombus formation studies of the 50 cc device are necessary to improve its design.

Yamanaka *et al.* concluded after a 3-day *in vivo* bovine study that platelet and fibrin aggregation, and consequently clot formation, are region dependent within an LVAD, making fluid mechanics studies necessary.<sup>7</sup> Such studies are conducted *in vitro* and help to identify areas of low shear rates within VADs throughout the cardiac cycle. At The Pennsylvania State University, an experimental fluid dynamics approach has been ongoing for several decades and current techniques include fluid dynamics studies using particle image velocimetry (PIV), shear studies using a rotating disc system (RDS), computational fluid dynamics modeling and microscopic surface evaluation of biomaterials from explanted LVADs. Using these different fluid mechanics techniques, areas within LVADs susceptible to platelet and fibrin deposition can be identified and the theory behind these phenomena explained.

To confirm the suspected thrombus-prone regions within LVADs, bovine studies are conducted. Devices are implanted in bovine and after a period ranging from 3 to 30 days, the devices are explanted and the sacs lining the LVADs undergo surface evaluation. Immunochemistry is a technique that utilizes antibodies to fluorescently label features found on samples. This technique proves useful in the surface evaluation of the polyurethane sacs within VADs. Platelets and fibrin present proteins such as the  $\alpha\text{IIb}\beta$  integrin (CD41) and fibrinogen, respectively, that can be labeled and viewed via immunofluorescence (IF) microscopy and identified with certainty. A scanning electron microscope (SEM) provides further surface evaluation.

Understanding the interactions between blood components and the polyurethane biomaterial requires microscale evaluation. One commonly used method for quantifying platelet adhesion is the rotating disc system (RDS). Yamanaka performed preliminary RDS experiments by placing circular samples of biomaterials in platelet rich plasma (PRP) and spinning them at several different, fixed rates.<sup>10</sup> Chorprenning expanded on this work by performing both steady and pulsatile experiments, determining that there is in fact a relationship between the shear rates experienced by the platelets on the material and their adhesion coefficients when examining areas of the disc at specified distances from the center.<sup>11</sup> Milner *et al.* observed similar results in that low platelet adhesion coefficients were observed at shear rates above 500 s<sup>-1</sup>.<sup>12</sup> In Equation 1, the adhesion coefficient (AC) is the ratio of the number of platelets adhered to a unit area of polyurethane surface to the number of platelets that are transported to the polyurethane surface throughout the experiment,

$$AC(\%) = 100 \frac{N}{jt} \quad (1)$$

where  $N$  is the number of platelets per mm<sup>2</sup>,  $j$  is the platelet flux (platelets/sec/mm<sup>2</sup>) and  $t$  is the experiment duration (sec). The ability to correlate shear rates to platelet adhesion for a particular material with certainty allows wall shear estimations using other fluid mechanics techniques to be appropriate spatial predictors for thrombus formation within VADs.

Hochareon *et al.* conducted PIV studies on the Penn State 50 cc V-0 LVAD (Figure 1-2), calculated shear rates within an acrylic VAD model and identified regions within the VAD that have shear rates below  $500 \text{ s}^{-1}$ .<sup>13</sup> The value of  $500 \text{ s}^{-1}$  was determined to be a threshold of platelet adhesion by Hubbell and McIntire, below which the likelihood of thrombus formation increases on polyurethane, a material similar to the blood sac used in Penn State VADs.<sup>14</sup> Subsequent PIV studies have been conducted to determine whether that threshold is attained in many specific, thrombus-prone regions within different VAD models, at various beat rates and with various blood analogs.<sup>15</sup> From the studies conducted on VADs, design changes and valve orientations<sup>16</sup> were suggested to increase the likelihood that a greater number of regions within the device would experience shear rates above  $500 \text{ s}^{-1}$ , thereby preventing platelet adhesion and aggregation.

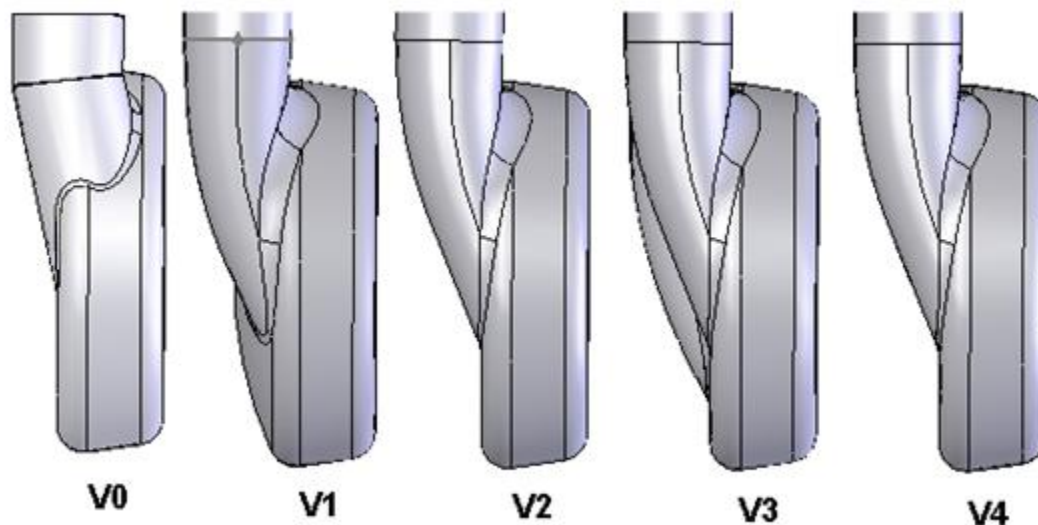


**Figure 1-2:** Design iterations of the Penn State 50 cc LVAD.<sup>17</sup>

One aspect of VAD design that affects shear rates within the device is valve orientation. Krieder *et al.* examined the effects of rotating the inlet valve.<sup>16</sup> They observed that by rotating the major orifice of the inlet valve through different orientations the resulting jet during diastole provides greater washing to more thrombus-prone areas and for longer durations within the LVAD. Of the four valve housing orientations examined, two were found to provide the best results. By rotating the major orifice away from the pusher plate and toward the front wall by 30° and 45° (Figure 1-3)<sup>15</sup>, significantly more of the bottom area within the VAD was subjected to higher shears.<sup>16</sup>

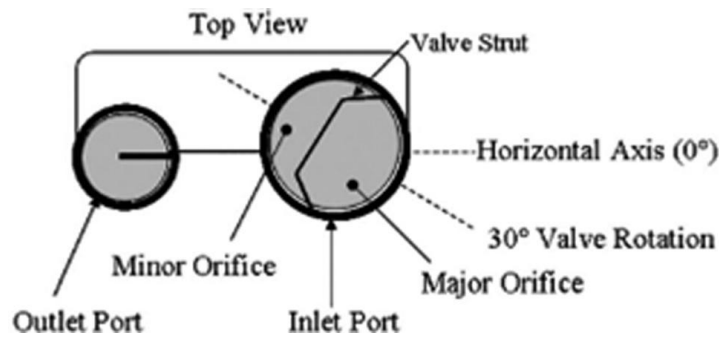


**Figure 1-3:** Inlet and outlet valve orientations within a VAD.<sup>15</sup>

In conjunction with valve orientation, several different models of the 50 cc VAD were designed to determine the shape of the front wall and the orientation of the inlet and outlet ports that best facilitates washing within the pump (Figure 1-2). The V-1 model consisted of a rounded back wall and inlet and outlet ports oriented to direct flow along the device walls. Later iterations, the V-2, V-3 and V-4 models, had similar pump geometries with different outlet port orientations.<sup>17</sup> The V-2 model is characterized by a straight rear wall and ports equidistant from the midline of the pump parallel to one

another. This pump was determined to be the best design based on shear measurements in thrombus-prone regions.<sup>18</sup>

Computational simulations add another dimension to fluid mechanics studies and offers support to observations made clinically and *in vitro*. The models of LVADs previously discussed have been recreated computationally by Medvitz *et al.*<sup>19</sup>

Results from previous studies show surface analysis of explanted sacs from animal studies, flow characterization from PIV and computational modeling of the Penn State V-2 LVAD, however the results have been viewed independently. The objective of this study is to use this multi-dimensional approach to correlate surface deposition observed *in vivo* with fluid velocities and wall shear rates calculated from *in vitro* studies and CFD modeling. To limit variability, the same beat rate is used for the animal study at The Hershey Medical Center, PIV imaging and computational modeling, and the areas under examination remain constant across the study. These correlations provide a better understanding of how local fluid behavior affects platelet and fibrin deposition within areas of the LVAD predicted to be susceptible to thrombus formation.

## Chapter 2

### Methods

#### 2.1 Blood Sac Surface Evaluation

After the completion of a 30-day, one bovine study at the Hershey Medical Center during which a 50 cc V-2 LVAD was implanted, maintained at 75 bpm for the entirety of the study and then removed, the polyurethane blood contacting sac was processed for analysis. Immediately after explantation, the sac was first flushed with saline then with a 1% paraformaldehyde fixative to preserve formations on the surface. The sac was then stored in a 0.9% saline solution until it was sectioned for evaluation. Eight sections corresponding to the areas designated by Yamanaka *et al.*<sup>10</sup> were immediately removed prior to the evaluation done here.

Of the remaining regions, specific areas were removed that correspond to areas already studied with PIV. Along the red line in Figure 2-1, 4 mm by 8 mm samples were removed beginning at the origin of the red line through the curve connecting the bottom and back walls and centered on the 35 mm location for each of the normal planes in Figure 2-2. This allows a portion of the back wall and the entire 10.16 mm of the bottom wall to be imaged along the specified normal planes, enabling comparisons to be made to the PIV data collected in the same locations. After removal, each section was further divided into four 2 mm by 4 mm sub-sections, two designated for fluorescence labeling followed by imaging with a confocal microscope and two for dehydration series

preparation followed by SEM imaging (Figure 2-3). When looking at the inside, blood-contacting surface of the sac samples, the upper, right-hand corner was removed to distinguish the outside surface from the inside surface during sample preparation and imaging.

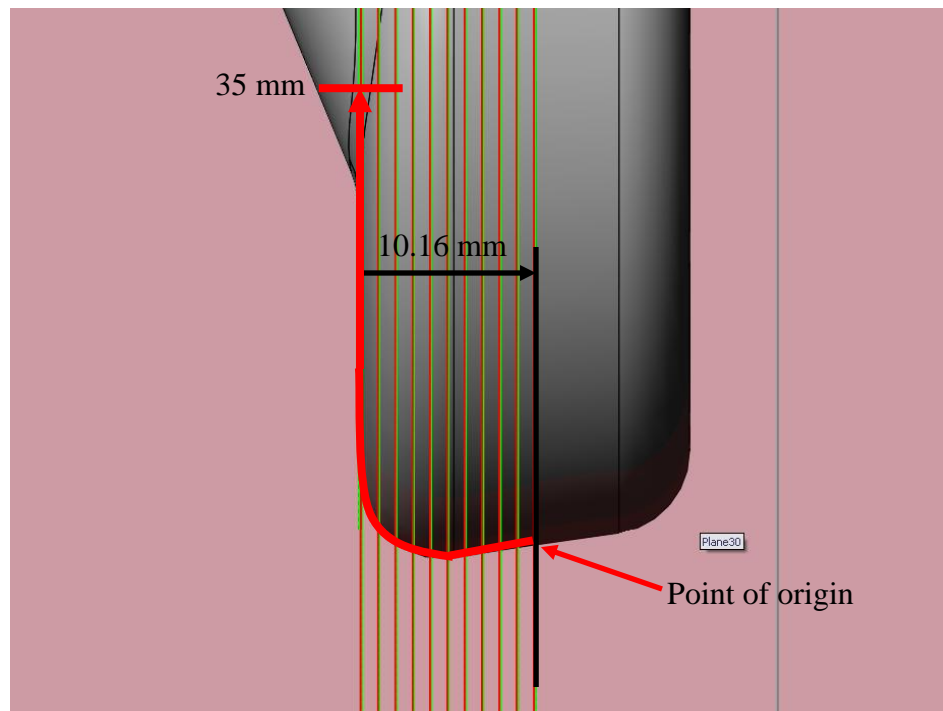


**Figure 2-1:** Data points were collected in 1 mm increments along the red curve for each normal plane in Figure 2-2. The arc length of the red curve is 35 mm.

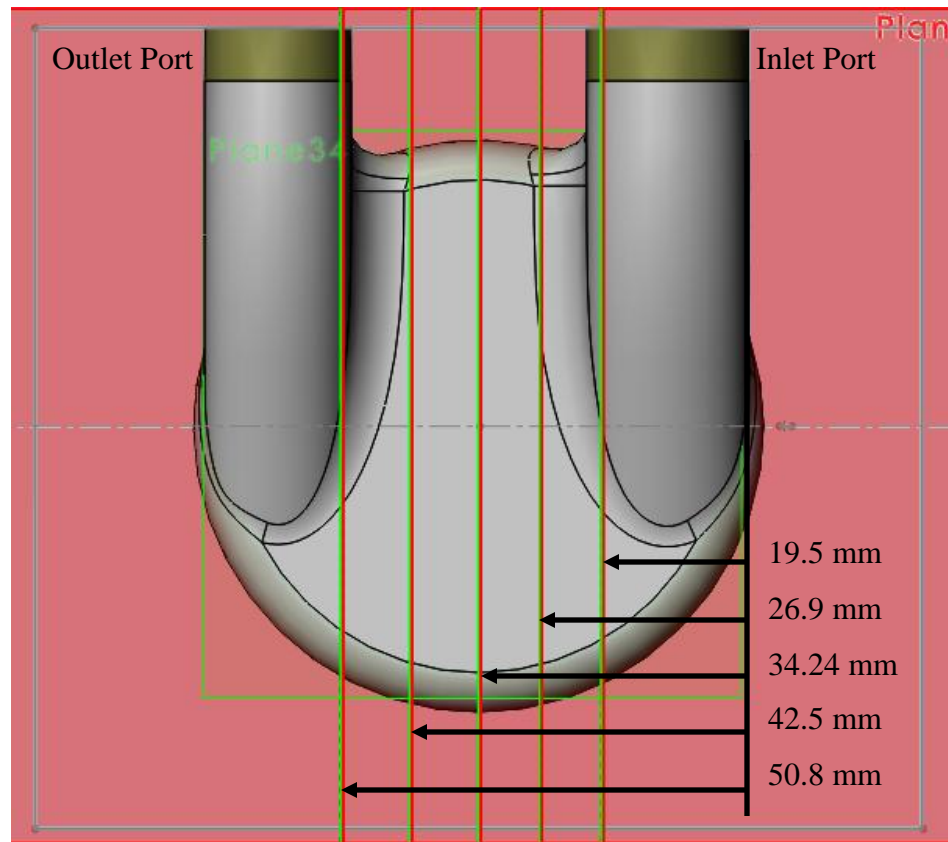


**Figure 2-2:** Locations of normal planes from which PIV data was acquired.

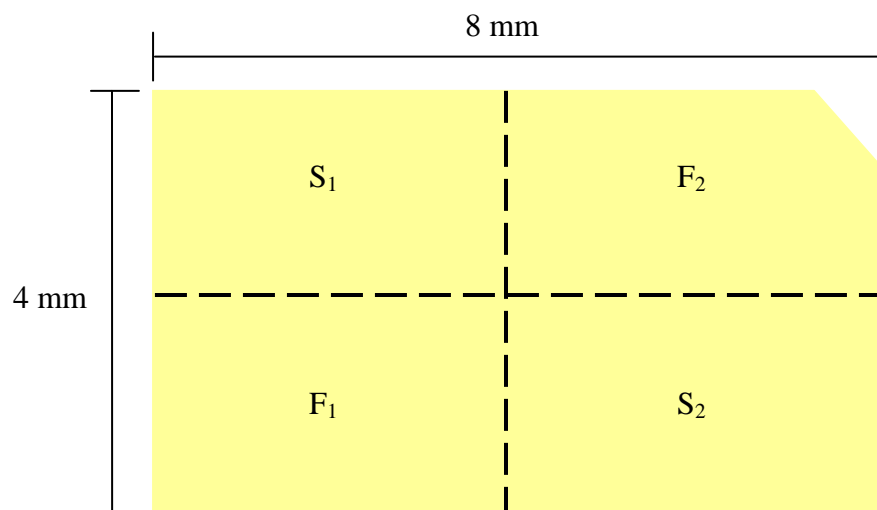


**Figure 2-3:** Subsectioning of removed blood sac samples. S<sub>1</sub> and S<sub>2</sub> are sections removed for SEM preparation, F<sub>1</sub> and F<sub>2</sub> are sections labeled with fluorescent antibodies to be viewed by confocal microscopy.

The samples to be examined under SEM were prepared according to the procedure recommended by the Huck Institute at Penn State and described here. The samples were first fixed in a 2.5% gluteraldehyde solution (0.1M Sodium ACOH buffer, pH 7.4) overnight at 4°C. The samples were then dehydrated using an alcohol dehydration series with ethanol concentrations of 25, 50, 70, 85, 95 and 100%. In each concentration, the samples incubated for 5 minutes at room temperature. The 100% ethanol step was performed 3 times. Samples were immediately transferred in pure ethanol to a critical point dryer where the ethanol solvent was replaced with bone dry CO<sub>2</sub>. Once completely dry, the samples were mounted on SEM stubs with carbon tape, sputter coated and then imaged at 500x under the SEM. Six images were captured for each sample from the following orders (1 – first, 2 – second, etc.) and approximate locations (Figure 2-4).

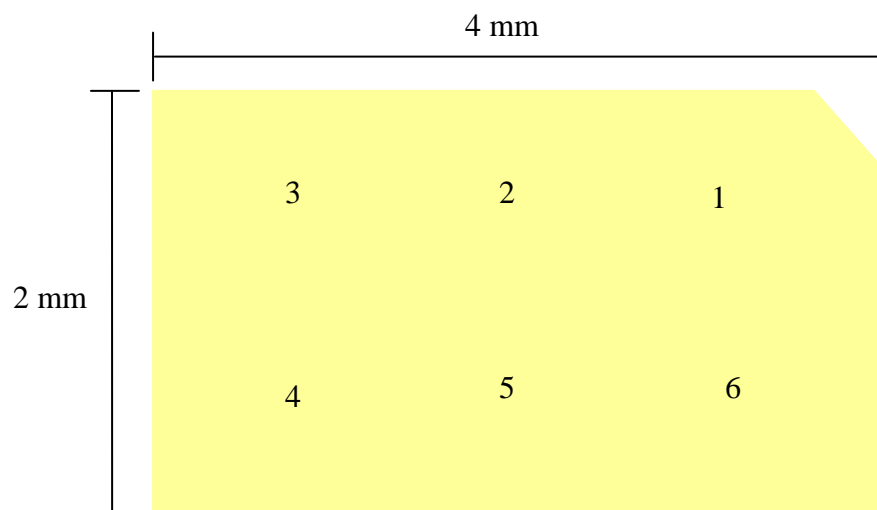


**Figure 2-4:** Locations of the 6 images acquired on each subsection using both SEM and confocal microscopy.

The remaining samples were labeled using fluorescent antibodies and then examined using a confocal microscope. The samples were placed in a 1% chicken and 1% rabbit blocking agent and allowed to incubate at room temperature for 1 hour prior to labeling with primary antibodies. Concentrations of 1.5 microliters ( $\mu\text{L}$ ) of CAPP2A and 1.0  $\mu\text{L}$  of goat anti-bovine fibrinogen per milliliter (mL) of blocking agent were added to the samples, labeling platelets and fibrin, respectively. Samples incubated overnight at 4  $^{\circ}\text{C}$  and were then washed with PBS. The PBS was again replaced with the blocking agent. At this point, fluorescent secondary antibodies were added. Two  $\mu\text{l}$  of Alexa Fluor 488 chicken anti-mouse per mL of PBS labeled platelets and 2  $\mu\text{l}$  of Alexa Fluor 555 rabbit anti-goat per mL of PBS were added to label fibrin. After incubating in the dark for 1 hour at 37  $^{\circ}\text{C}$ , these samples were washed with PBS to remove non-specifically bound antibodies. Each sample was mounted to a slide and viewed under a confocal microscope.

Six images were acquired of each sample as described for SEM (Figure 2-4). Images were analyzed qualitatively for platelet and fibrin deposition.

## **2.2 *In Vitro* Experiments**

The V-2 model (Figure 2-5) has been determined to be the most successful design in terms of thrombus prevention and therefore, a model of that device was used for this study. The back half of the device *in vitro* consists of a polyurethane diaphragm allowing a Superpump, positive displacement piston system including a head, amplifier and ViViGen Waveform Generator (StarFish Medical, Victoria, B.C.) to drive fluid through the system. A programmable waveform generator controlled the pump to mimic both the cardiac rhythm and the motion of clinical LVADs in terms of systolic duration and stroke length, which are fixed at 38% and 15 mm, respectively. The beat rate for this study was 75 bpm to correspond with the studies conducted *in vivo*. Bjork-Shiley Monostrut 23 mm inlet (mitral) and 21 mm outlet (aortic) tilting disc valves were used. The inlet valve was oriented so that the major orifice axis was rotated 30° toward the back wall of the LVAD model (Figure 1-3).

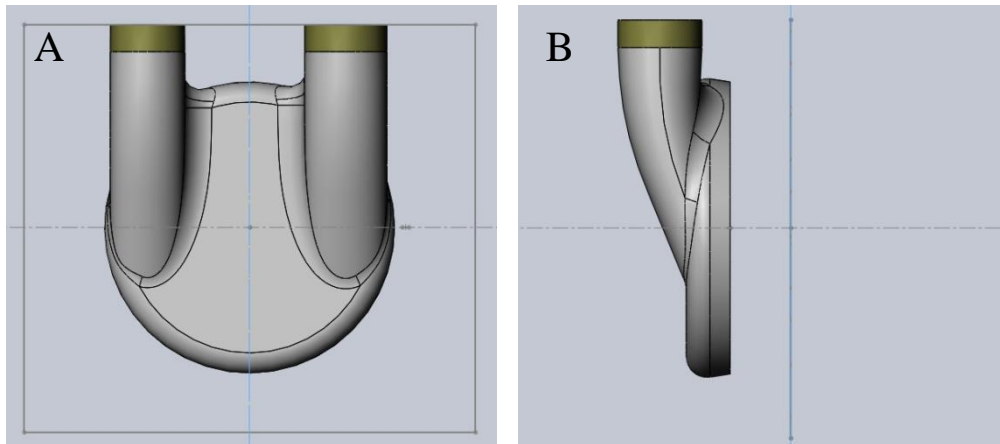


**Figure 2-5:** Rear (A) and inlet-side (B) views of the Penn State 50 cc V-2 LVAD.

The LVAD model was the central component of a mock circulatory loop designed by Rosenberg (Figure 2-6).<sup>20</sup> This loop mimics physiologic conditions. In addition to the LVAD model and the hydraulic pump, the loop includes a venous reservoir, aortic and arterial compliance chambers and a resistance plate that are connected using Tygon tubing. Pressure transducers (Argon Medical Devices, Athens, TX) measure the arterial pressures throughout the course of the cycle. Arterial pressures were maintained at 120 / 80 mmHg while venous pressures were maintained at 30 / 5 mmHg. Ultrasonic flow probes (Transonic Systems, Inc., Ithaca, NY) attached to the loop's tubing monitored the volume of fluid being pumped throughout each cycle at the inlet and outlet of the device.

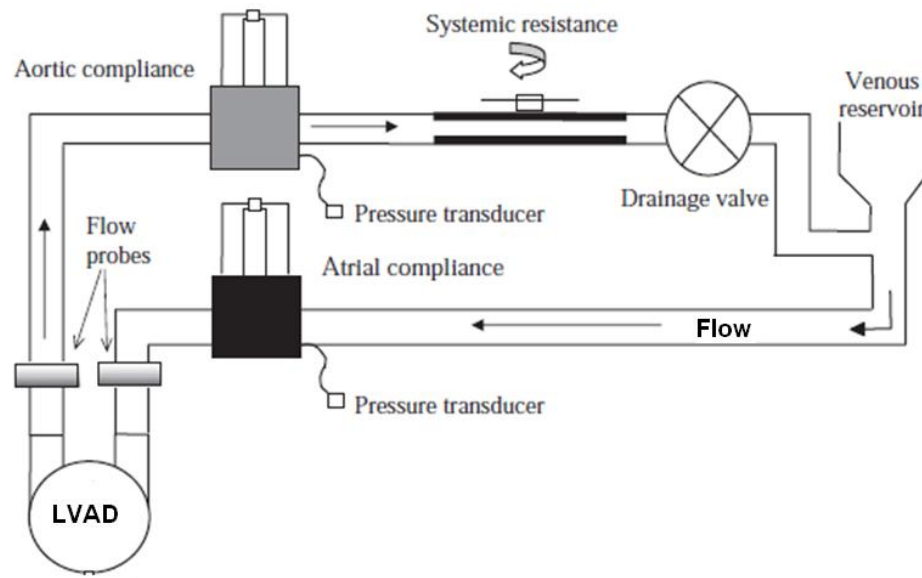


**Figure 2-6:** The Penn State mock circulatory loop.

A blood analog was used to match the properties of 40% hematocrit blood. Weight volumes of 0.03% xanthan gum, 16% glycerin, 33.97% water and 50% NaI were mixed to a clear solution. Xanthan gum and glycerin-water serve to reproduce the elasticity and viscosity of blood, respectively. NaI is added to help match the index of refraction of the acrylic model (1.49) for imaging purposes. The viscoelasticity of the fluid was measured and verified using a viscoelastic analyzer (Vilastic-3, Vilastic Scientific, Inc., Austin, TX). The fluid was then seeded with 10-micron glass beads (Potters Industries, Inc., Valley Forge, PA) for imaging purposes.

To image flow, a Nd:YAG laser, part of a Gemini PIV 15 system (New Wave Research, Inc., Fremont, CA), is pulsed twice at a specified time depending on the particular operating conditions. The laser is focused with a cylindrical and a spherical

lens producing a light sheet 300  $\mu\text{m}$  thick. This light sheet illuminates the glass beads at particular locations within the LVAD acrylic model. For each laser pulse, a synchronized, two megapixel CCD camera (TSI, Inc., Shoreview, MN) with a Nikon 50 mm F1.8 lens (Nikon Corporation, Tokyo, Japan) captures an image of flow within the acrylic model. Two hundred image pairs are collected at each measurement plane for every 7% of the cardiac cycle. Using Insight<sup>TM</sup> 3G software (TSI, Inc., Shoreview, MN), the light reflected from the glass particles is captured by the camera for each laser pulse and particles are statistically correlated from one image to the next. Insight<sup>TM</sup> 3G software calculates flow velocities by dividing particle displacements by the pulse separation.

Further post-processing, using an in-house MATLAB (The MathWorks, Inc., Natick, MA) algorithm developed by Horchareon,<sup>21</sup> calculates wall shear rate values from these velocities. These shear rates are calculated using Equation 2,

$$\frac{du}{dy} = \frac{u_t - u_w}{y_t - y_w} \quad (2)$$

At the LVAD wall, the no-slip boundary condition applies, making  $u_w$  zero. The origin of each measurement is  $y_w$ , giving that a value of zero as well. Therefore, the shear rate here is two dimensional, dependent only on  $u_t$ , the tangential fluid velocity approaching and immediately next to the wall, and  $y_t$ , the distance from the wall.

The areas of interest for this study included regions from both the bottom of the model and the back wall of the model (Figure 2-7). Data was collected from planes both

normal and parallel to the back wall of the model. The normal planes are located 19.5, 26.9, 34.24, 42.5 and 50.6 millimeters (mm) from the outermost edge of the inlet port (Figure 2-2). More specifically, on these normal planes, data was collected at locations along the curved bottom of the device. With the origin on the bottom of the device measured 10.16 mm from the plane of the back wall (the depth of the acrylic model used in the mock circulatory loop), data was collected in 1 mm increments along the bottom and up the back of the device for 35 mm (Figure 2-1). Attention was focused on the outlet side of the pump where previous PIV and computational data have shown areas of low shear.

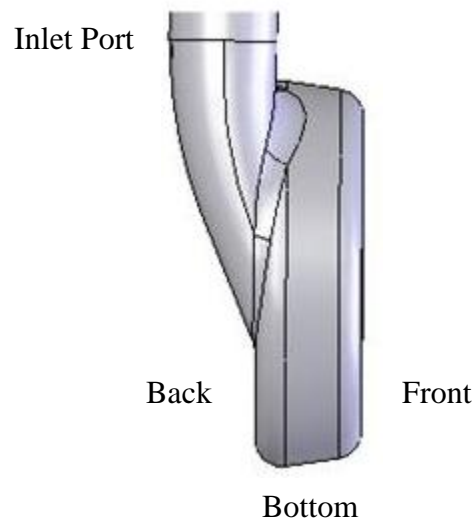


**Figure 2-7:** Inlet-side view of the V-2 LVAD.

### 2.3 Computational Fluid Dynamics

Medvitz *et al.* designed a computational fluid dynamics model to simulate pulsatile flow through the V-2 50 cc LVAD.<sup>22</sup> Flow conditions of 75 bpm were set to validate both PIV and *in vivo* studies. Mitral and aortic valve orientations were modeled numerically to match *in vitro* studies. Computational fluid dynamics studies allow for qualitative flow pattern comparisons with *in vitro* PIV results and velocity field and shear map generation for areas within the positive displacement pump. Two dimensional velocity and wall shear data were extracted from grid intersections nearest the locations specified in Figures 2-1 and 2-2. Velocity plots, wall shear plots and qualitative flow analysis were compared to both PIV results and microscopic analysis of explanted blood sacs.

## Chapter 3

### Results

#### 3.1 Blood Sac Surface Evaluation

The analysis performed on both confocal images and images from the SEM were primarily qualitative. Because of the low contrast between structures observed on the sac material and the material itself, image processing is difficult. A complication of imaging polyurethane is the material's ability to autofluoresce when excited by lasers used for microscopy. Confocal microscopes reduce this effect by creating a 2-D image composed of maximum pixel intensities for each location from a z-series of images and stacks images obtained by differing only the z-position. As a result, structures, such as platelets and fibrin, can be observed despite autofluorescence because the fluorescent signal transmitted at the pixels where these structures exist is stronger for multiple slices within a stack. This offers a distinct advantage over traditional bright-field microscopy with a wavelength-specific filter as autofluorescence of the polyurethane masks bound structures. SEM was used to confirm the surface topography and structures found on fluorescently labeled samples. However, because of sample preparation requirements, the same samples were not able to be examined with both SEM and fluorescence, limiting the usefulness of the comparison.

An inherent difficulty with microscopy is focusing the microscope in the correct region and on the correct plane. With these particular experiments, the goal is to

determine whether platelets and fibrin exist on sac samples from specific regions within the pump. In regions where thrombus and platelet deposition is expected to be low, no evidence of these structures implies that there is either no deposition present or the microscope is out of focus. To ensure the former, the intensity of the laser is increased to bring any structure present into focus. However, this results in structures that are neither platelets nor fibrin becoming visible, possibly through autofluorescence. This is less an issue on the outlet side when the presence of fibrin and platelet clots provides definite contrast between these structures of interest and superfluous debris. This problem is avoided in post-processing by manually raising the threshold of these images so that the background intensity is approximately the same as in images where clear and definite fibrin or platelets are the only structures present.

From the rear wall of the pump, representative images of those collected from samples removed 17 mm from the origin on each of the normal planes are shown in Figure 3-1. Figures 3-1 A,B and C show little, if any, fluorescent activity, indicating there are no platelets or fibrin, while the images acquired from samples removed from the outlet side of the pump, Figures 3-1 D and E, show higher fluorescent activity. In these images, there appears to be significant coverage by both platelets and fibrin. The green (platelets) are on the order of 2-4 microns ( $\mu\text{m}$ ), a size typical of platelets. The red (fibrin) appears as both microclots, on the same size-order as platelets, and as splayed, web-like structures on the sac surface. The intensity of the fluorescence of both the fibrin and platelets in contrast to the background in these images provide strong assurance of their identity.

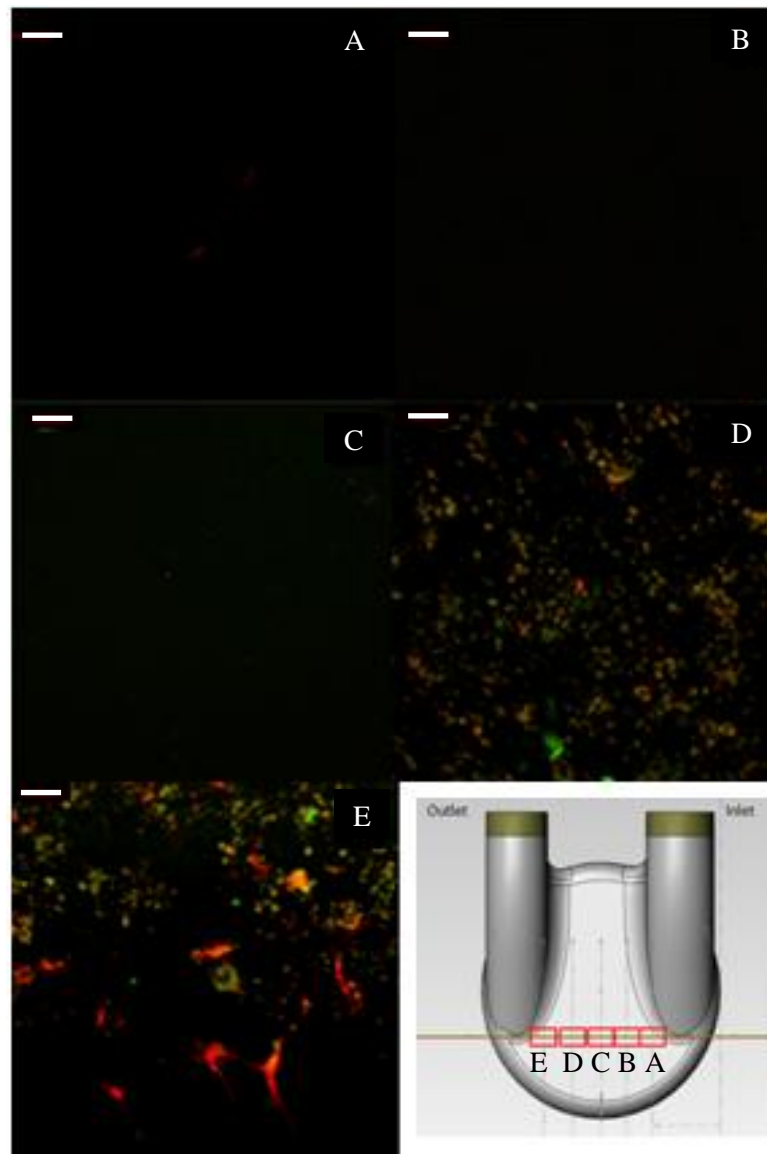


**Figure 3-1:** Images acquired from the rear wall, 17 mm along the curvature from the origin (Figure 2-1) on the (A) 19.5 mm, (B) 26.9 mm, (C) 34.24 mm, (D) 42.5 mm and (E) 50.8 mm normal planes. (scale bar = 20 microns)

The bottom section of the blood sac was divided into three general regions to simplify its analysis. From the point of origin in Figure 2-1, the front section of the bottom wall refers to locations 1 mm and 2 mm from the origin in the direction of the back wall. The center region refers to locations along the wall 3 mm to 6 mm from the

origin. Finally, the curve, the region of the pump where the back wall transitions to the bottom wall, is located 7 mm to 10 mm from the point of origin. Subdividing the bottom region into these three sections allows a more general spatial analysis of the bottom of the pump in relation to the normal planes.

Figure 3-2 shows representative images acquired from the front section of the bottom wall of the pump. Images acquired from the normal planes on the inlet side and at the center of the pump, 19.5 mm (Figure 3-2A), 26.9 mm (Figure 3-2B) and 34.24 mm (Figure 3-2C), show very little if any fluorescent activity. Figures 3-2 D and E, however, show strong red fluorescence. This indicates the presence of larger, fibrin clots on the sac surface. The clot from the 42.5 mm plane measures approximately 20  $\mu\text{m}$  in length, while the clots from the 50.8 mm plane measure from 20 to 40  $\mu\text{m}$ . The fluorescence of these fibrin structures is bright enough to overcome background fluorescence, though individual, green platelet structures are visible on the 42.5 mm plane. Platelets in proximity to the clots on the 50.8 mm plane may either be nonexistent or hidden by the fluorescence of fibrin formations.

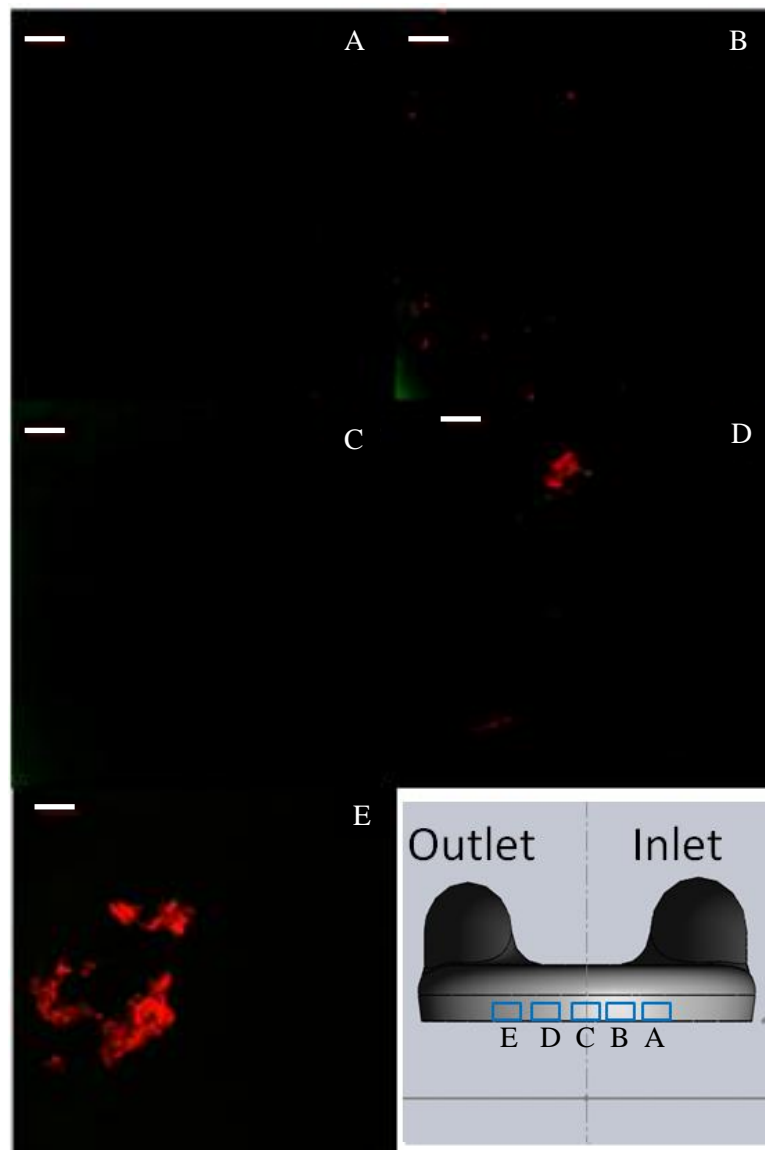


**Figure 3-2:** Images acquired from the front region of the bottom curve, 1 to 2 mm along the curvature from the origin (Figure 2-1) on the normal planes (A) 19.5 mm, (B) 26.9 mm, (C) 34.24 mm, (D) 42.5 mm and (E) 50.8 mm. (white bar = 20 microns)

The center region of the bottom curve (Figure 3-3) shows similar trends with more deposition on the sac samples from the outlet side normal planes than the inlet side normal planes. Again, the 19.5 mm normal plane and the 26.9 mm normal plane show little or no sign of platelet and fibrin deposition. From the center region, however, the

34.24 mm plane does have evidence of fibrin deposition with both long, narrow fibrin clots approximately 40  $\mu\text{m}$  by 5  $\mu\text{m}$  and small, round fibrin clots approximately 5 to 10  $\mu\text{m}$  in diameter. The normal planes nearest the outlet port, 42.5 mm 50.8 mm, show larger, 30 – 40  $\mu\text{m}$  clots in this region. Few platelets are observed.

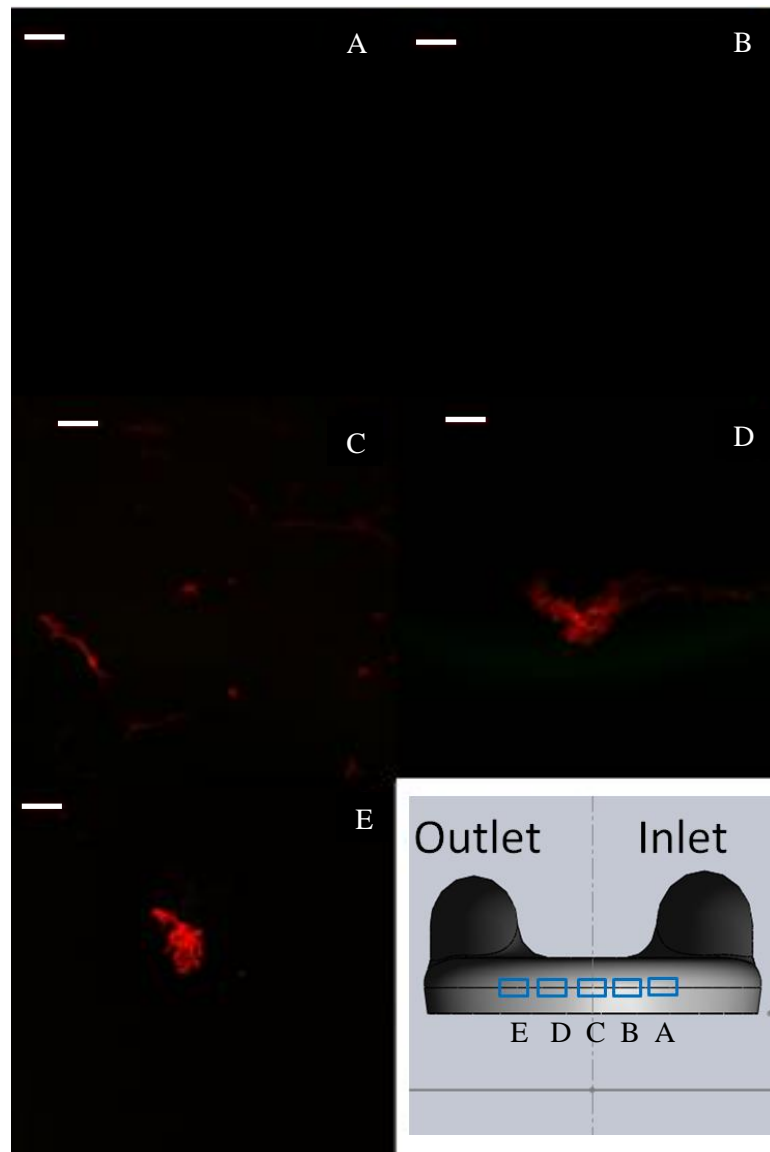


**Figure 3-3:** Images acquired from the center region of the bottom curve, 3 to 6 mm along the curvature from the origin (Figure 2-1) on the normal planes (A) 19.5 mm, (B) 26.9 mm, (C) 34.24 mm, (D) 42.5 mm and (E) 50.8 mm. (white bar = 20 microns)

Figure 3-4 shows images acquired from sac samples along the curve joining the bottom wall and the back wall. This region displays fewer large clots than the two regions shown in Figures 3-2 and 3-3. Images from the inlet-side planes (Figures 3-4 A and B) show little to no fluorescent activity, while images from the center and outlet-side planes

show deposition. The 34.24 mm and 42.5 mm normal planes have evidence of small, fibrin clots in this region instead of the large, isolated clots seen previously. The fluorescent spots measure between 3 and 10  $\mu\text{m}$ , though distinguishing all of the fluorescent activity as fibrin versus background noise and debris proves difficult. Samples from the 50.8 mm normal plane appear to show isolated clots approximately 20  $\mu\text{m}$  in diameter, as seen on this plane along the front and center regions.

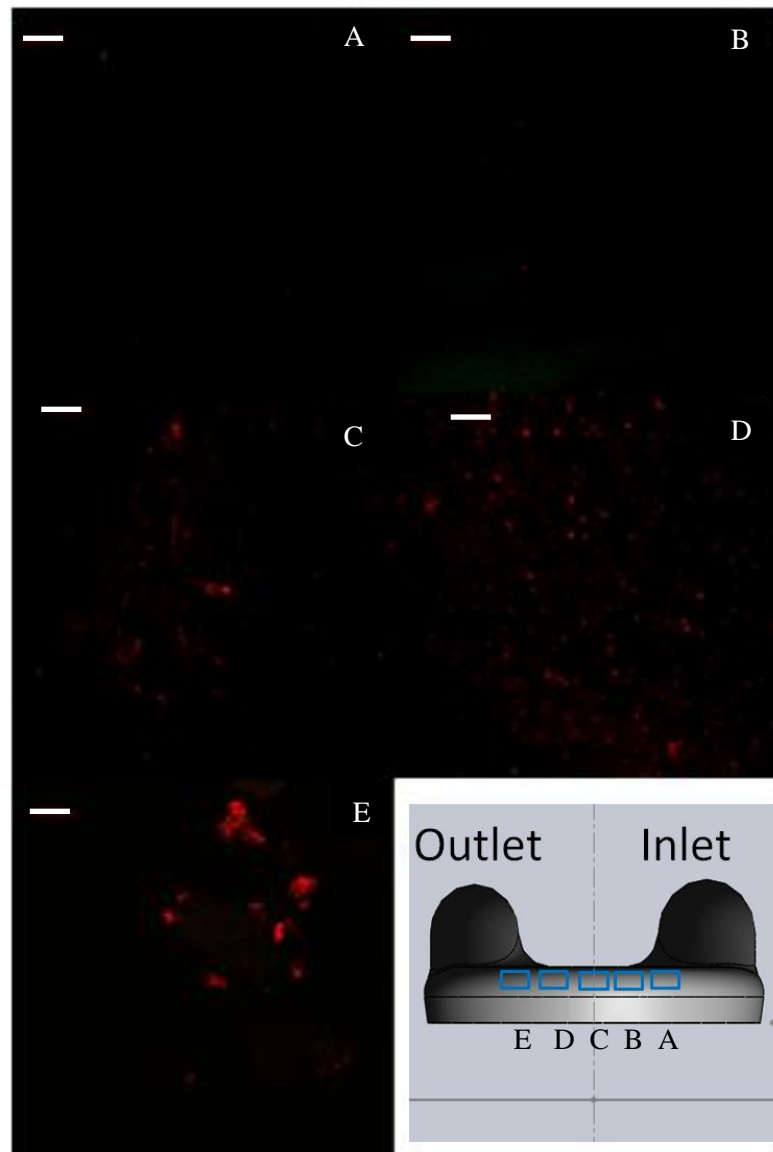


**Figure 3-4:** Images acquired from the bottom curve, 7 to 10 mm along the curvature from the origin (Figure 2-1) on the normal planes (A) 19.5 mm, (B) 26.9 mm, (C) 34.24 mm, (D) 42.5 mm and (E) 50.8 mm. (white bar = 20 microns)

To confirm the fluorescent labeling, surface evaluation of samples next to those observed with confocal imaging (Figure 2-3) was also performed using SEM. Figure 3-5 compares fluorescent and SEM images acquired from corresponding normal planes. Figures 3-5 A and C show areas of the sac where few structures are deposited. Figures 3-

5 B and D show areas of the explanted sac where fibrin and platelet deposition are evident. Because SEM does not use structural labeling, the features in the image are not confirmed to be platelets or fibrin as they are in the confocal images. Similar SEM images were acquired for each of the corresponding confocal images. The complete set of SEM images is found in Appendix B.

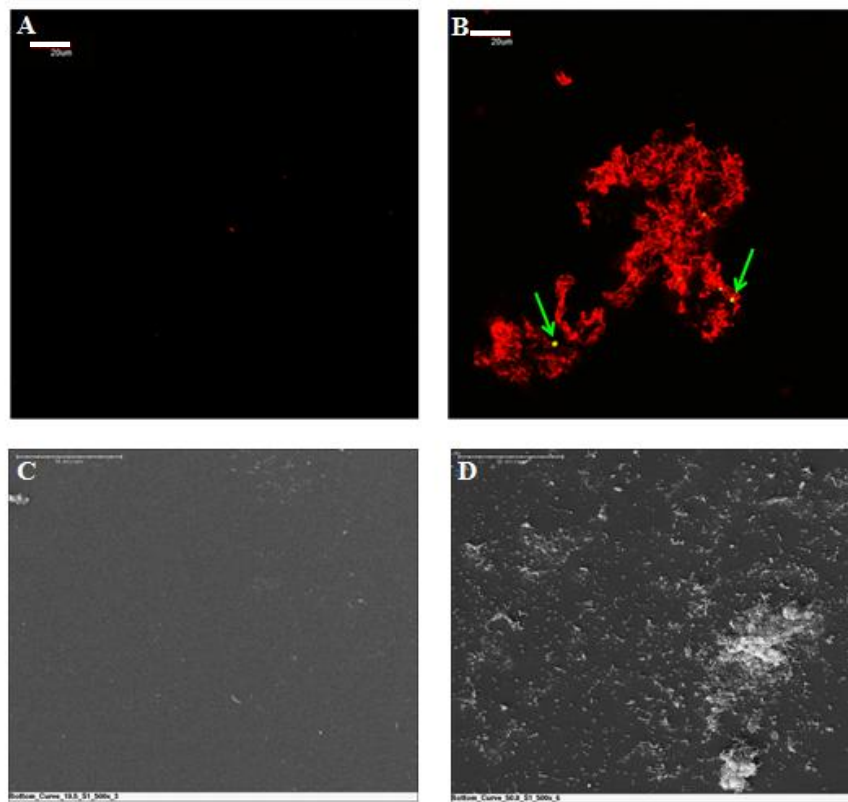


**Figure 3-5:** Confirmation of confocal surface analysis by SEM. A and C show regions of the sac with little, or no, platelet and fibrin deposition. B and D show images of platelet and fibrin deposition on the sac surface. (Top, fluorescent microscopy, white bar = 20 microns; Bottom, SEM, scale bar = 50 microns)

### 3.2 Particle Image Velocimetry

PIV is a technique used to image flow within the LVAD. From these images, velocity maps and shear plots were generated to characterize flow both in the normal and parallel directions.<sup>23</sup> Figure 3-6 shows velocity flow maps within the LVAD at 7, 35, 64 and 92% of diastole. As the pusher plate of the mock circulatory loop retracts, the pressure within the model drops, causing the onset of diastole. An inlet jet enters the mitral valve with a peak velocity magnitude of approximately 1.4 meters per second (m/s). As the model continues to fill, the jet washes the inlet wall and the bottom curve, approaching the mid-line of the pump. The jet then detaches from the wall and recirculates in the center of the pump until the onset of systole. Velocity magnitudes along the outlet side of the pump never exceed 0.8 m/s.

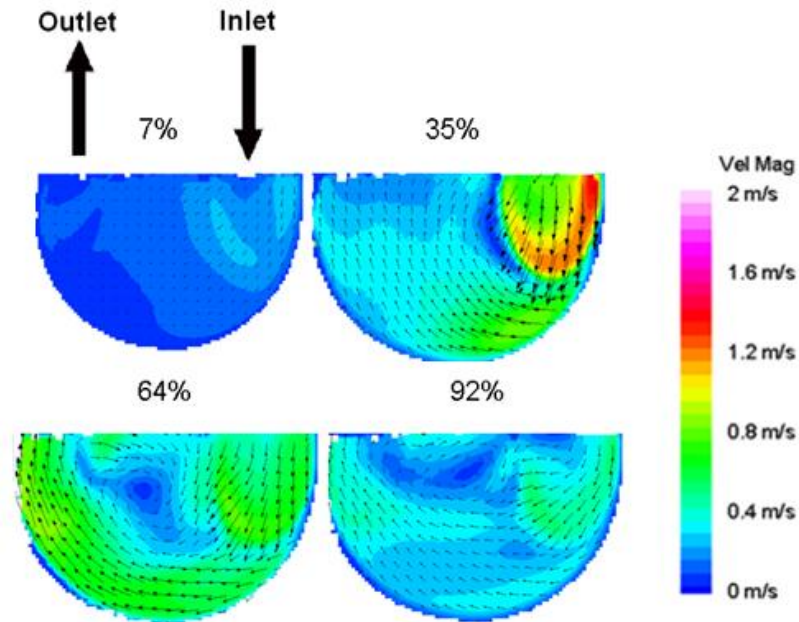


**Figure 3-6:** Velocity contour maps of flow in the plane 1 mm parallel to the rear wall during diastole within the Penn State V-2 LVAD at a beat rate of 75 bpm. Percentages are during diastole.

Velocity maps during systole show magnitudes that are lower than those seen in diastole. As the pusher plate moves toward the rear wall and the pressure within the model increases, flow is ejected out the aortic valve. The PIV data of each percentage of systole in Figure 3-7 shows velocity magnitudes below 0.8 m/s, with the magnitudes in many areas falling to near 0 m/s.

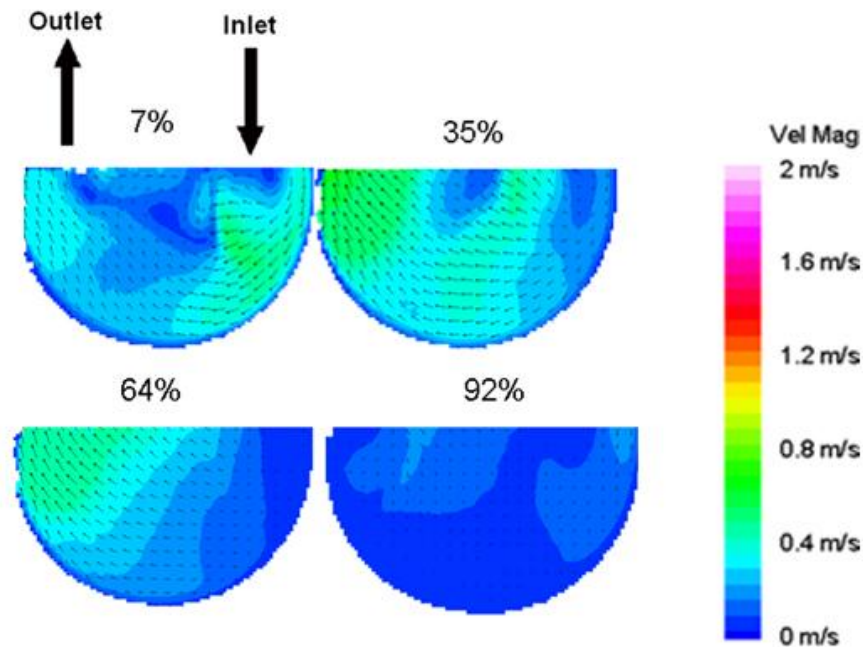


**Figure 3-7:** Velocity contour maps of flow in the plane 1 mm parallel to the rear wall during systole within the Penn State V-2 LVAD at a beat rate of 75 bpm. Percentages are of the systolic duration.

The flow velocity magnitudes where the inlet jet leaves the wall during diastole are typically smaller, causing less washing in that region. Because platelet and fibrin deposition is a significant function of wall shear rates, small velocities observed during diastole are the focus of study in predicting regions susceptible to cellular deposition. Figure 3-8 shows the wall locations corresponding to the shear plots in Figure 3-9. In Figure 3-9, shear rates are calculated based on the velocities measured during diastole of the cardiac cycle with 0% corresponding to the onset of diastole and 100% the conclusion of diastole. Wall shear rates are normalized to  $500 \text{ s}^{-1}$ ; a value of -1 equals a wall shear value of  $-500 \text{ s}^{-1}$ . Negative values (blue) correspond to flow moving toward the bottom of the pump and positive values (red) correspond to flow moving toward the top of the

pump. The highest wall shear rates are found on the 19.5 mm normal plane in the 20 to 30 mm section of the back wall. This region of the pump has the largest shear rates within each of the normal planes. The lowest wall shear rates for all of the planes occur in the 0 to 10 mm region, indicating that the bottom of the pump, especially those areas closest to the 0 mm location, has the highest susceptibility for thrombus formation.

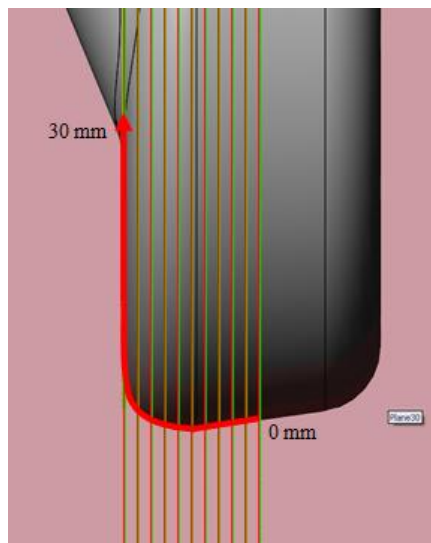


**Figure 3-8:** Diagram showing wall location measurements on the normal planes.

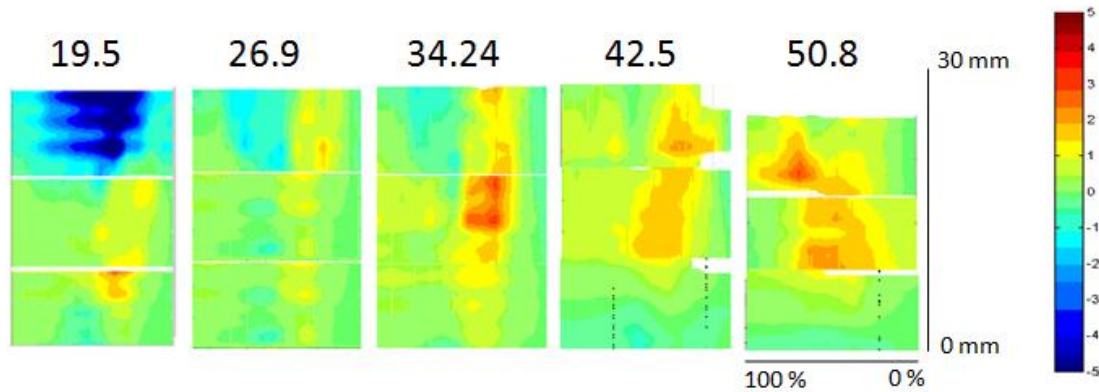


**Figure 3-9:** Wall shear plots of flow during diastole, normalized by  $500 \text{ s}^{-1}$  at locations from 0 to 30 mm along the wall curvature (Figure 3-8) on the 19.5, 26.9, 34.24, 42.5 and 50.8 mm normal planes.

A quantitative method for determining the likelihood of thrombus formation in areas within a LVAD was developed by Medvitz using computational fluid dynamics studies on the LVAD.<sup>19</sup> The thrombus susceptibility potential (TSP), which has been adapted and now applied to the PIV measurements, is based in part on wall shear rates and flow exposure time. Equation 3,

$$TSP = 1 - \sum_0^N \frac{\Delta t \gamma_w}{\gamma_{cutoff} t_{crit}} \times \frac{e^{\left(\frac{\gamma_w - \gamma_{peak}}{\gamma_{cutoff} - \gamma_{peak}}\right)} - 1}{e^1 - 1} \quad (3)$$

produces a value between 0 and 1, with 1 indicating a high risk of thrombus formation and 0 a low risk of thrombus formation. In the TSP equation, N is the number of time steps taken through the cardiac cycle,  $\Delta t$  is the amount of time between image acquisitions for PIV,  $\gamma_w$  is the wall shear rate,  $\gamma_{peak}$  is set to  $500 \text{ s}^{-1}$ ,  $\gamma_{cutoff}$  is set to  $1000 \text{ s}^{-1}$  and  $t_{crit}$  is set to twice the value of  $\Delta t$ . TSP calculations for this study were conducted

over the entire cardiac cycle. Figures 3-10 through 3-14 show TSP plots for the 19.5, 26.9, 34.24, 42.5 and 50.8 mm normal planes. The distance on the x-axis corresponds to the wall locations along the curve as shown in Figure 3-8. For each of these planes, the bottom curve of the pump, locations from 0 to approximately 10 mm, show TSP values near 1, indicating strong potential for thrombus formation.

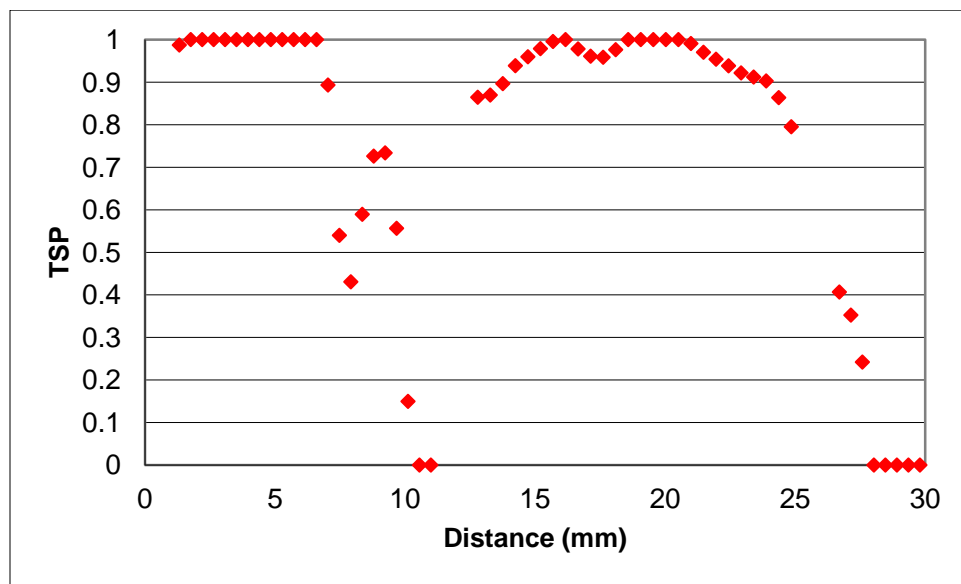


**Figure 3-10:** A TSP plot of wall locations on the 19.5 mm normal plane. A TSP value of 1 indicates a high potential of thrombus formation, 0 indicates a low potential.

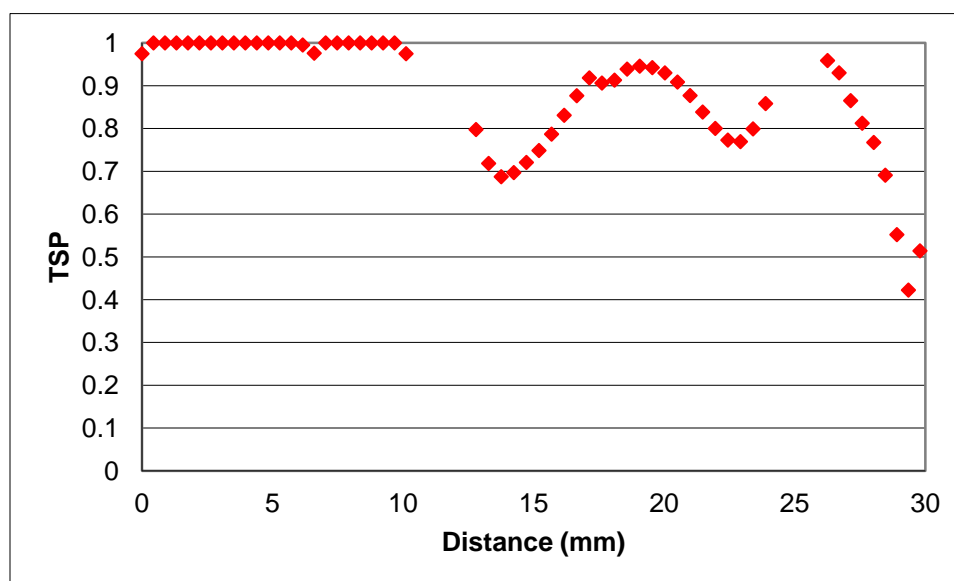


**Figure 3-11:** A TSP plot of wall locations on the 26.9 mm normal plane. A TSP value of 1 indicates a high potential of thrombus formation, 0 indicates a low potential.

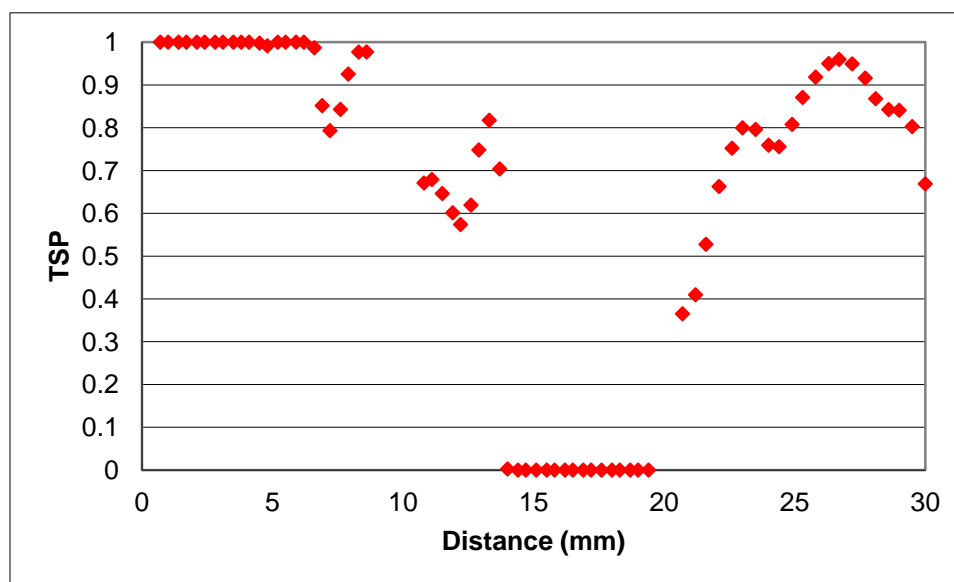


**Figure 3-12:** A TSP plot of wall locations on the 34.24 mm normal plane. A TSP value of 1 indicates a high potential of thrombus formation, 0 indicates a low potential.

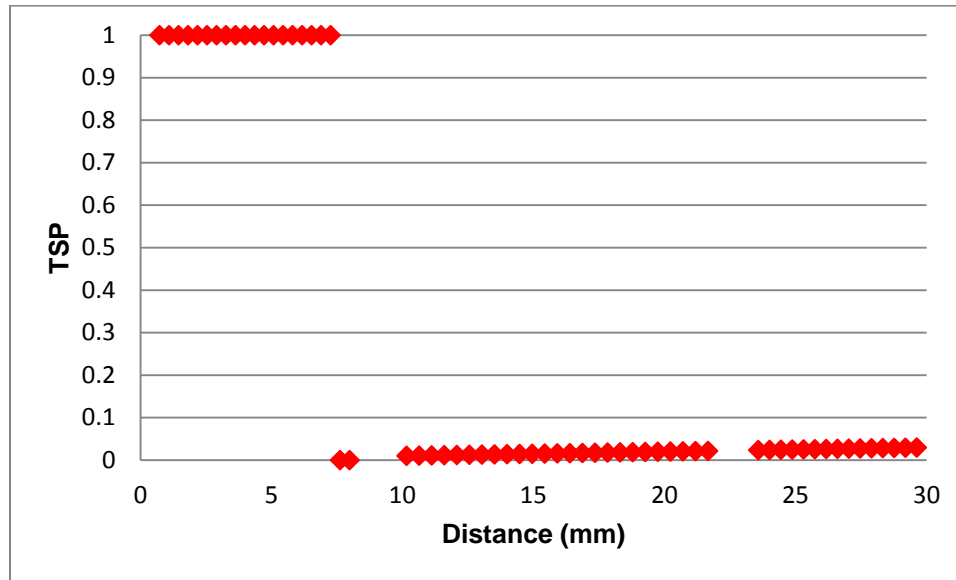


**Figure 3-13:** A TSP plot of wall locations on the 42.5 mm normal plane. A TSP value of 1 indicates a high potential of thrombus formation, 0 indicates a low potential.

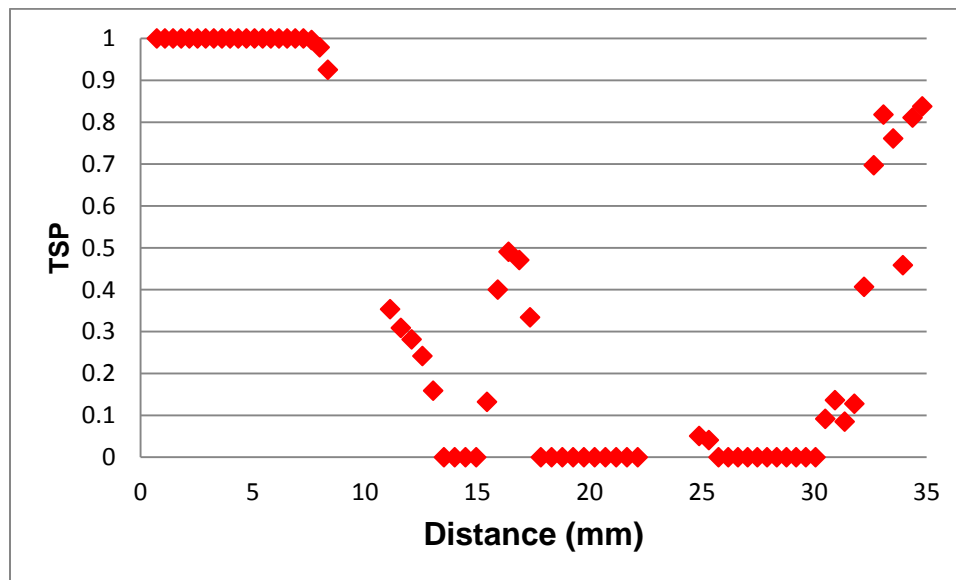


**Figure 3-14:** A TSP plot of wall locations on the 50.8 mm normal plane. A TSP value of 1 indicates a high potential of thrombus formation, 0 indicates a low potential.

In addition to the normal planes, TSP values for the parallel plane, 1 mm from the back wall, were also calculated. Flow in this plane moves parallel to the device face, as opposed to flow visualized in the normal planes, which moves normal to the device face. The wall location measurements for the parallel plane are measured circumferentially along the bottom from 0 mm on the inlet side to 110 mm on the outlet side (Figure 3-15). The majority of TSP calculations for parallel flow show low potential for thrombus formation (Figure 3-16). There are several locations, however, where precursors to thrombi are likely to deposit on the surface of the LVAD. Circumferential distances of approximately 15 to 20 mm and 80 to 95 mm show TSP values near 0.7 and 1, respectively. These are the areas most susceptible to deposition along this plane.

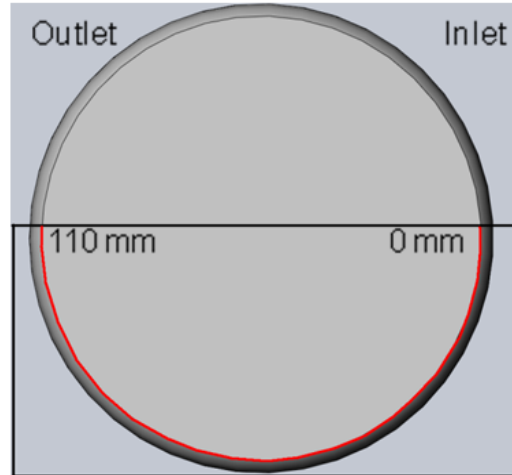


**Figure 3-15:** Circumferential measurements of the LVAD wall on the 1 mm parallel plane.

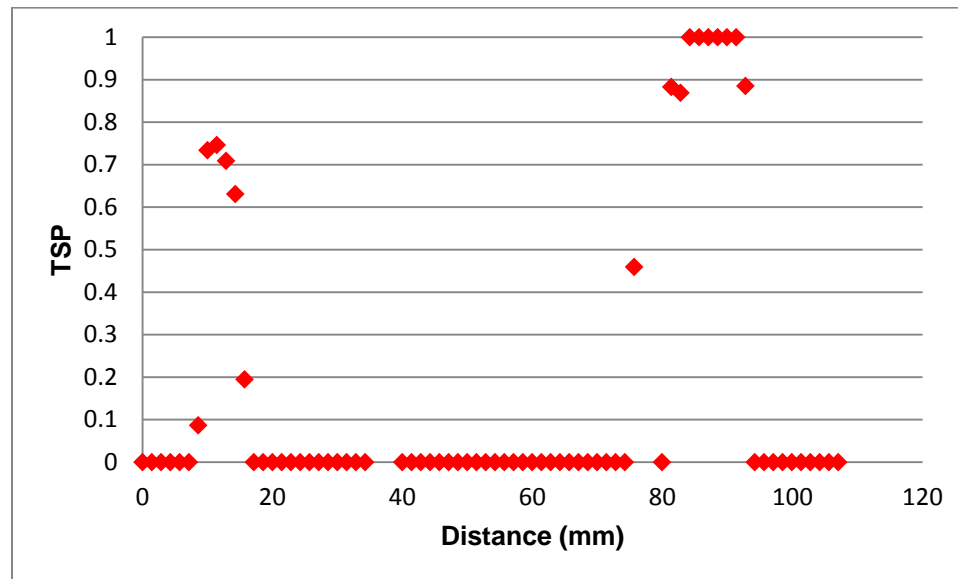


**Figure 3-16:** A TSP plot of wall locations on the 1 mm parallel plane. A TSP value of 1 indicates a high potential of thrombus formation, 0 indicates a low potential.

### 3.3 Computational Fluid Dynamics

Computational fluid dynamics provide another method of flow analysis through the Penn State V-2 LVAD and were completed by Richard Medvitz at the Applied Research Laboratory at The Pennsylvania State University. Figures 3-17 and 3-18 show contour maps of wall shear rates within the LVAD at 7, 35, 64 and 92% of both diastole and systole, respectively. Similar to the velocity plots in Section 3.2, the inlet jet is visualized using CFD. Forming at the onset of diastole, the jet enters the mitral valve and washes along the bottom wall on the inlet side of the model. Toward the end of diastole, the jet detaches from the wall and recirculates in the center of the pump. The jet then reforms as it travels through the aortic valve during systole. This CFD modeling also shows that areas of the highest shear within the jet do not wash along the bottom, outlet

side wall as shown in PIV (Figure 3-6). This insufficient washing leaves that region of the pump susceptible to thrombus formation.

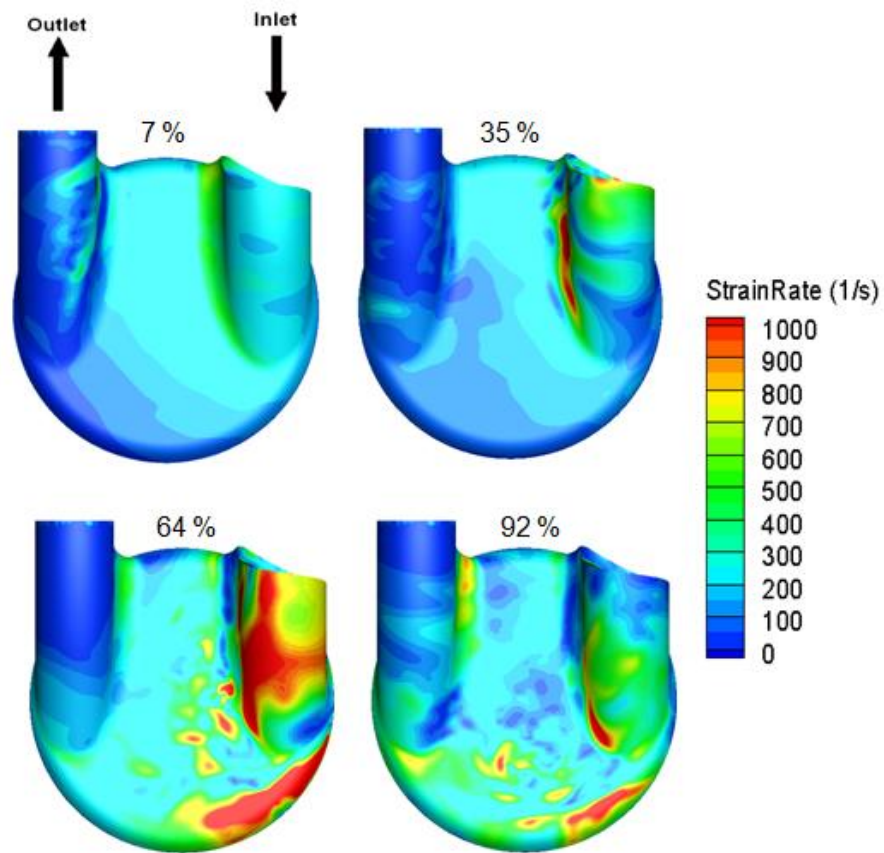


**Figure 3-17:** Computational fluid dynamics modeling of wall shear in the Penn State V-2 LVAD for flow in the 1 mm parallel plane during diastole at a beat rate of 75 bpm. Percentages are of the diastolic duration.

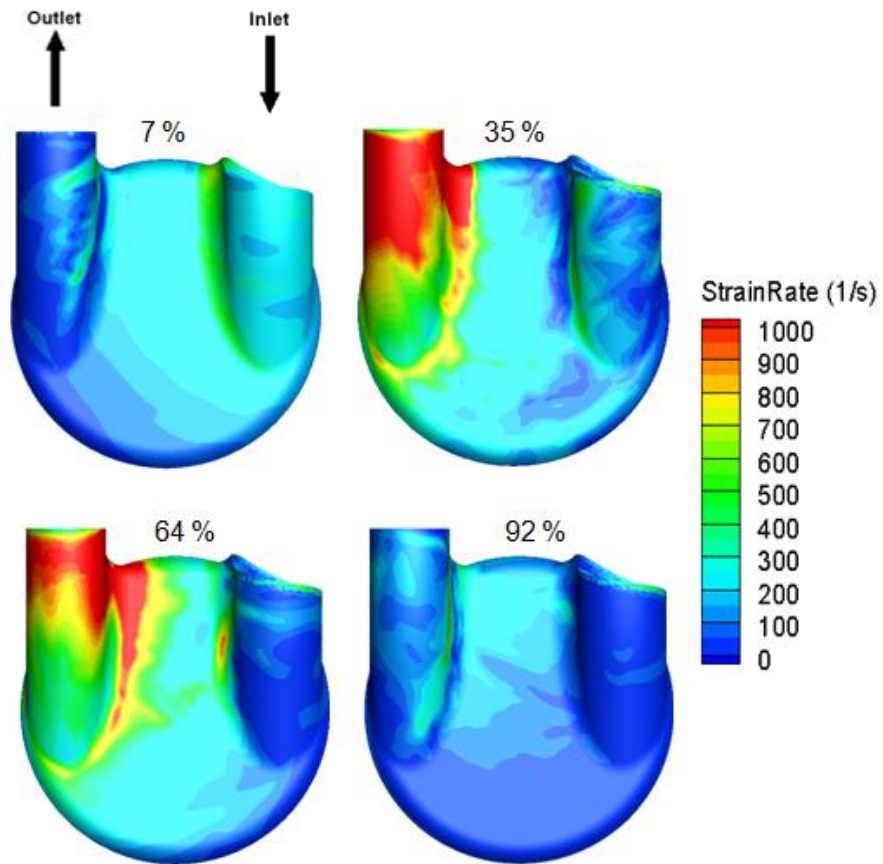


**Figure 3-18:** Computational fluid dynamics modeling of wall shear in the Penn State V-2 LVAD for flow in the 1 mm parallel plane during systole at a beat rate of 75 bpm. Percentages are of the systolic duration.

## Chapter 4

### Discussion

Particle image velocimetry and computational fluid dynamics help to predict platelets and fibrin deposition within a LVAD. For this study, PIV and CFD help to identify areas on the sac surface where deposition is likely and provide a fluid dynamics rationale for the presence based on local fluid velocities and wall shear rates. From these measurements, the potential for thrombus formation is quantified through the thrombus susceptibility potential and microscopic evaluation of explanted sac samples tests the usefulness of *in vitro* experimentation and computational modeling.

#### 4.1 Correlations between PIV, microscopic analysis, and CFD

The overall flow patterns observed with PIV and CFD are similar within the LVAD. However, the values of velocity and shear vary between the two modeling techniques. The major difference between the flow maps of PIV and CFD are the times at which the main inlet jet travels through the pump. The inlet jet as visualized with PIV has left the inlet port and moved toward the bottom of the pump 35% through diastole (Figure 3-6). This main jet reaches approximately the same location on the pump around 60% through diastole using the CFD model (Figure 3-17). Wall shear calculations between PIV and CFD vary considerably, making quantitative comparison limited; however, general flow patterns from each model suggest similarities.

## **4.2 Normal and parallel plane correlations between microscopic analysis and TSP**

Washing in both normal and parallel directions helps to prevent platelet and fibrin deposition. PIV and CFD both show that areas of high wall shear exist on the inlet side of the pump, where the inlet jet washes most thoroughly and for the longest duration. Consequently, these are the areas where platelet deposition is found by microscopic analysis to be minimal. The sections explanted and evaluated with microscopy from the 19.5 and 26.9 mm normal planes show little to no fluorescent activity both on the rear wall and the bottom curve. Additionally, there is little deposition on the 34.24 mm plane until near the curve where the rear and bottom surfaces meet (Figures 3-1 through 3-4). This correlates fairly well with the TSP plots. In the normal directions, there is a TSP value of 1 corresponding to these regions (Figures 3-10 through 3-14) but the parallel TSP plot shows a value of 0 for these regions (Figure 3-16). At 10 to 15 mm from the origin of the parallel flow, the TSP increases, indicating a higher risk of deposition. Because the parallel flow provides sufficient washing to prevent deposition, the fact that normal TSP is 1 is less relevant. Consequently, to utilize TSP as a prediction tool, calculations in both the normal and parallel directions must be considered and correlated.

Figure 4-1 compares the TSP resulting from parallel flow with the microscopy samples from corresponding sections. For locations of 39.69, 47.59, 55 and 63.33 mm along the 1 mm parallel plane, there is little to no fluorescent activity. On the graph of TSP values, each of these locations corresponds to a value of 0. Thrombus formation was seen at the 72.35 and 90 mm locations. The TSP value near 72 mm just precedes a

location where TSP rises from 0, indicating correlations are not present for this region. The 90 mm location has a TSP value of 1, indicating that the evidence of fibrin is expected.

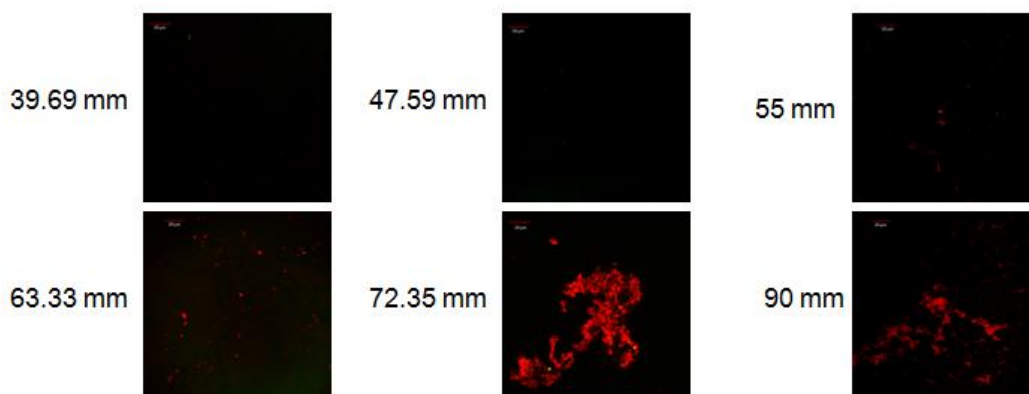
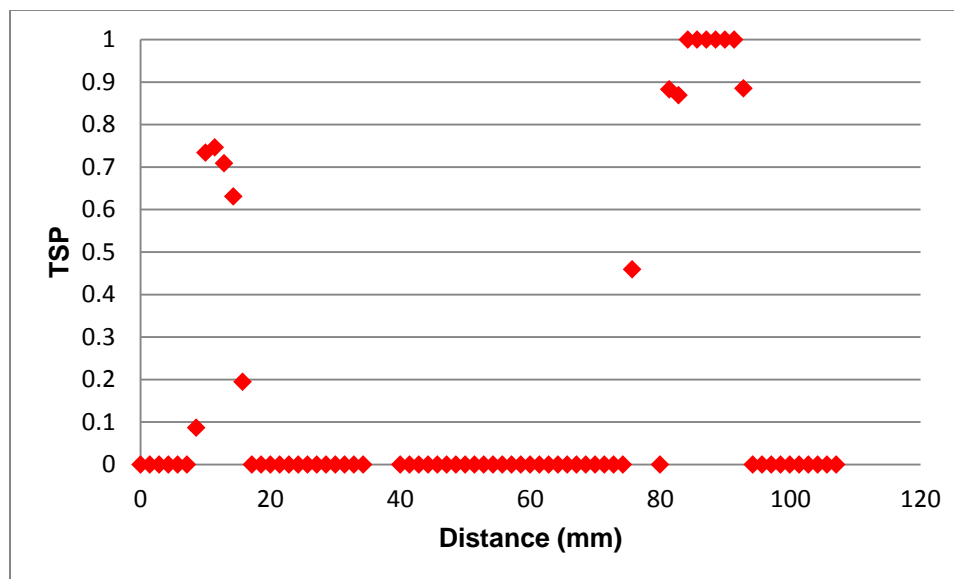


**Figure 4-1:** Comparisons between microscopy of specific regions of the explanted sac along the 1 mm parallel plane with the TSP for the same regions.

The 50.8 mm normal plane is another region where platelet and fibrin deposition correspond well to the TSP calculations. Figure 4-2 shows a spatial comparison of

microscopy from the sac explanted from locations both on the rear wall and the bottom wall with TSP values along the 50.8 mm normal plane. Sac samples from the 0 mm location show high levels of fluorescence, indicating significant fibrin and platelet deposition. This region corresponds to a TSP value of 1. At a location of 17 mm, the TSP graph increases as the potential for thrombus formation increases. Evaluation of the explanted sac from this location shows considerable microclots formed, also corresponding to the TSP value. The next section compared is from the 25 mm location. There is very little fluorescent activity and the structures observed on the SEM do not appear to be platelets or fibrin, rather debris. This corresponds well with the TSP as the value for this location is near 0. Finally, the 35 mm location shows a TSP increase again and the microscopy confirms platelet and fibrin deposition. The correlations between these images and the *in vitro* prediction give confidence to the experimental results obtained.

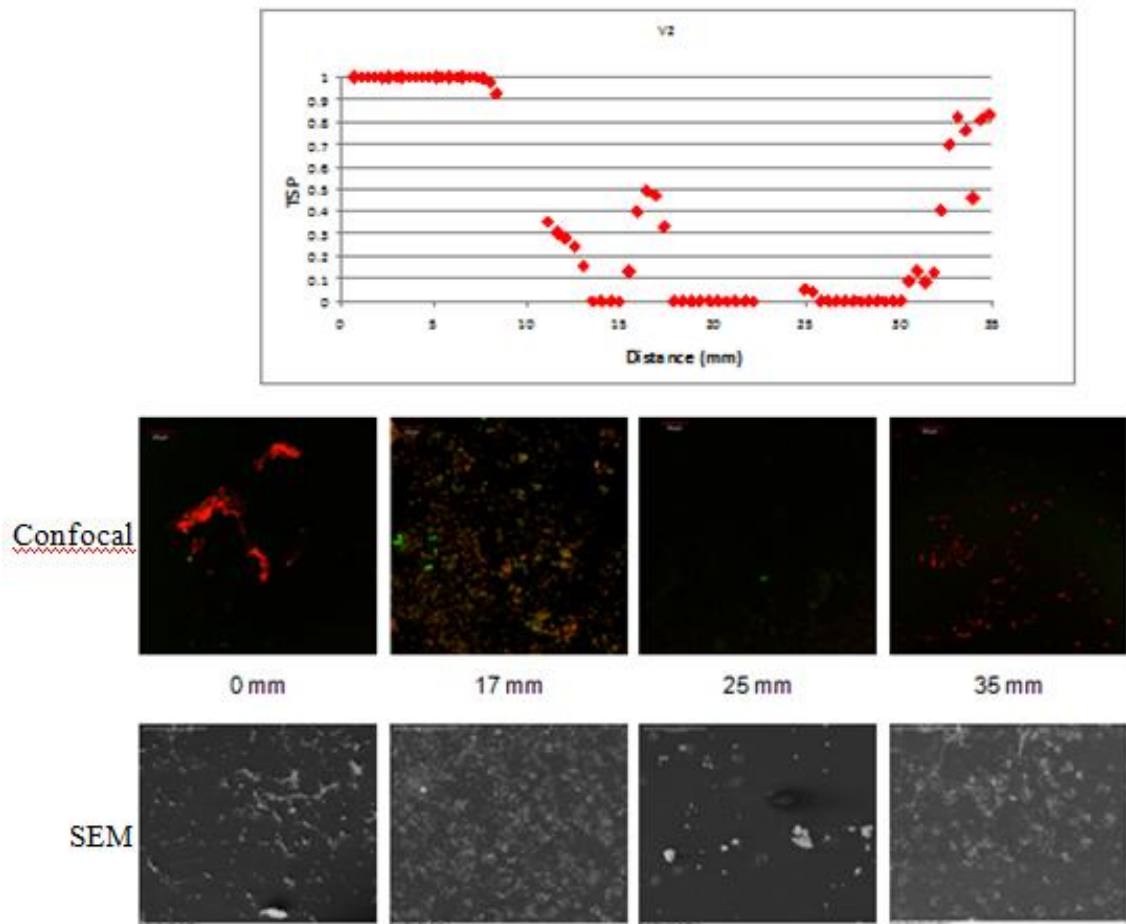


**Figure 4-2:** Comparisons of confocal microscopy and SEM of specific regions of the explanted sac along the 1 mm parallel plane with the TSP for the same regions.

Though the 1 mm parallel plane and the 50.8 mm normal plane show strong correlations with the TSP values for their corresponding locations, the correlations are not as good. TSP is a method for predicting evidence of thrombus deposition but there is an associated error based on the error in calculating normal wall shear rates ( $\pm 90 \text{ s}^{-1}$ ) and parallel wall shear rates ( $\pm 138 \text{ s}^{-1}$ ) from PIV. In addition to errors in calculation, this model is only partially valid for predictions *in vivo* because the shear rates used as limits for deposition and the value for  $\Delta t$ . Shear rates of 500 and  $1,000 \text{ s}^{-1}$  are estimates for a

material similar to the polyurethane used the Penn State LVAD. The value for  $\Delta t$  is acquired from PIV studies, however, the time that regions within the LVAD are exposed to wall shear varies over a 30 day study. Because of these constraints, this model is more useful in comparing LVAD designs than providing a definitive design. Likewise, when explanting the sac samples, the measurements on the sac surface were estimates, despite using dimensioned computer models. These inherent errors provide explanation, for example, as to why there is evidence of fibrin deposition on the 1 mm parallel plane at a location of 78 mm when the TSP value does not increase until closer to 75 mm for the same plane. Though in general, strong correlations have been made between the data constructed from PIV experiments and microscopic evaluation of the explanted LVAD sac.

### **4.3 Limitations**

Animal studies are necessary to test LVADs *in vivo* prior to clinical trials. However, because of the necessary regulations and costs associated with these studies, implanting LVADs in bovine is an expensive and time intensive process. Previous trials have been conducted with LVAD software programmed to vary with the calf's physiologic heart rate, ranging from 90 to 180 bpm. For this study, the LVAD is maintained at a constant beat rate of 75 bpm for the entire 30-day trial, allowing for comparisons with *in vitro* studies. Unfortunately, this is the only trial conducted during which the LVAD remains at a constant rate, limiting the number of available blood sacs for examination.

## Chapter 5

### Conclusion

#### 5.1 Summary of findings

In this study, correlations were made between deposition observed on the polyurethane blood sac of an explanted Penn State 50 cc LVAD and fluid mechanics experiments conducted *in vitro*. Flow in directions both normal and parallel to the rear face of the device contribute to fibrin and platelet deposition on the walls. Normal planes 19.5, 26.9, 34.24, 42.5 and 50.8 mm from the outer edge of the inlet port and a parallel plane 1 mm from the rear face were examined for deposition using microscopy and to calculate flow velocities and wall shear values. Platelet and fibrin structures suspected to exist on explanted sac samples at locations along these planes were labeled with fluorescent antibodies and imaged using a confocal microscope. These images were confirmed with surface analysis using SEM. The flow local to these regions was imaged using PIV, then velocities and wall shear rates were calculated. CFD quantitatively confirmed these flow patterns within the LVAD model.

Microscopic surface evaluation of the explanted sac on both normal and parallel planes showed significantly more fluorescence activity, indicating platelet and fibrin deposition, on the outlet side of the pump. Fibrin clots ranging from 10 to 40  $\mu\text{m}$  in diameter were imaged on the 42.5 and 50.8 mm normal planes along the bottom wall of the pump. On the bottom wall, the clots with the largest diameters were observed near the

origin of these normal planes, approximately 10 mm from the rear wall. Smaller clots that were not as isolated were observed near the bottom curve and on the rear wall.

These findings correspond well to the TSP calculated from PIV wall shear measurements. For the 0 mm region of each normal plane on the outlet side, the TSP value is 1, predicting evidence of thrombus formation where the clots were actually observed. The TSP values for the bottom wall on the inlet-side normal planes is also 1. However, the TSP in the parallel direction for these locations is low, indicating a decreased risk of deposition. Because of the parallel flow through the inlet-side locations, platelet and fibrin deposition were not observed *in vivo*. These findings show that PIV is a strong tool in the prediction of platelet and fibrin deposition within a LVAD.

## 5.2 Future Work

The correlations made in this study provide insight to the relationship between fluid dynamics and the effects it has on platelet and fibrin deposition within an LVAD, specifically along the bottom of the device. This study includes the examination of one blood sac from an *in vivo* LVAD that was maintained at 75 bpm. Studies of additional beat rates are necessary to gain a more complete understanding of the effect flow has on thrombus formation.

Computational modeling is a powerful tool to study many different LVAD parameters without the expense and time necessary for *in vivo* and *in vitro* studies.

Further refinement of the current computational LVAD modeling is necessary to move beyond general flow characteristics correlations and obtain shear and velocity measurements that closely match PIV studies, leading to predictive measures.

## References

1. Roger, V.L. *et al.*, 2011, "Heart Disease and Stroke Statistics—2011 Update, A Report From the American Heart Association," *Circulation*, 123, pp. 18–209.
2. Shreenivas, S., Rame, J., and Jessup, M., 2010, "Mechanical Circulatory Support as a Bridge to Transplant or for Destination Therapy," *Curr. Heart Fail. Rep.*, 7, pp. 159–166.
3. Hernandez, A.F. *et al.*, 2008, "Long-term Outcomes and Costs of Ventricular Assist Devices Among Medicare Beneficiaries," *The Journal of the American Medical Association*, 300(20), pp.2398-2406.
4. Kirklin, J.K. *et al.*, 2010, "Second INTERMACS annual report: More than 1,000 primary left ventricular assist device implants," *The Journal of Heart and Lung Transplantation*, 29(1), pp. 1–10.
5. Raber M.N., "Coagulation Tests," *Clinical Methods: The History, Physical, and Laboratory Examinations*, 3rd edition, Walker H.K., Hall W.D., Hurst J.W., Editors. 1990, Butterworths: Boston, pp. 739–742.
6. Gorbet, M.B., Sefton, M.V., 2004, "Biomaterial-associated thrombosis: roles of coagulation factors, complement, platelets and leukocytes," *Biomaterials*, 25, pp. 5681-5703.
7. Yamanaka, H. *et al.*, 2006, "Short-term In Vivo Studies of Surface Thrombosis in a Left Ventricular Assist System," *ASAIO J.*, 52(3), pp. 257–265.
8. George, J.N, "Heparin-induced thrombocytopenia, in Hemostasis and thrombosis: basic principles and clinical practice," Colman, R.W., Hirsh J., Marder, V.J., Clowes, A.W., George, J.N., Editors. 2001, Lippincott Williams & Wilkins: Philadelphia, pp. 454-455.
9. Mehta S., Pae W., Rosenberg G., Snyder A.J., Weiss W.J., Lewis J.P., Frank D.J., Thompson J.J., Pierce W.S., 2001, "The LionHeart LVD-2000: a completely implanted left ventricular assist device for chronic circulatory support," *Ann. Thorac. Surg.*, 71, pp.156-161.
10. Yamanaka, H., "Investigation of thrombosis at the biomaterial surface in left ventricular assist systems," PhD thesis, The Pennsylvania State University, 2006.

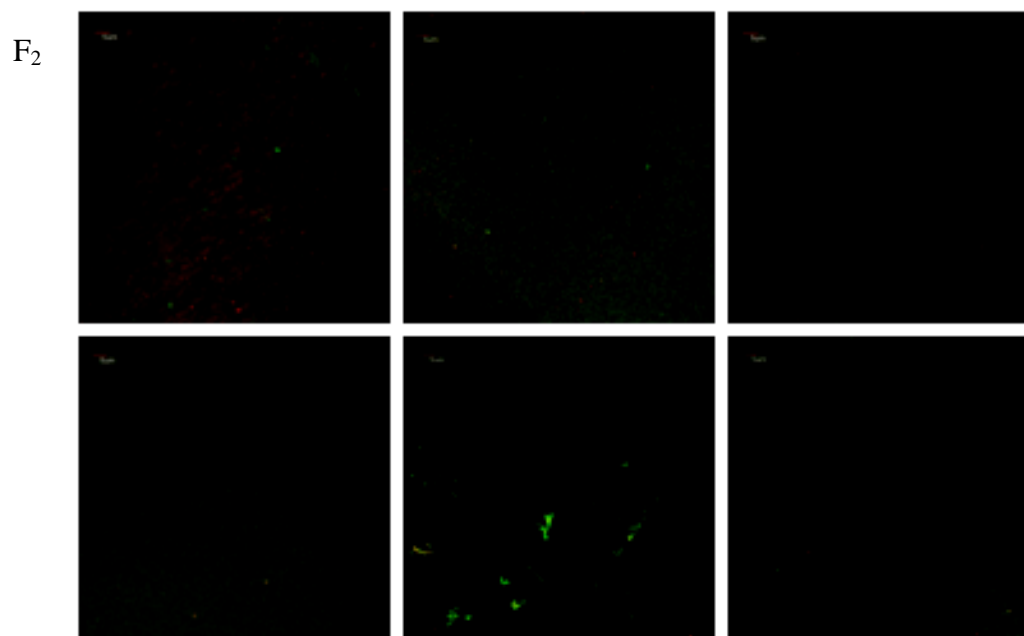
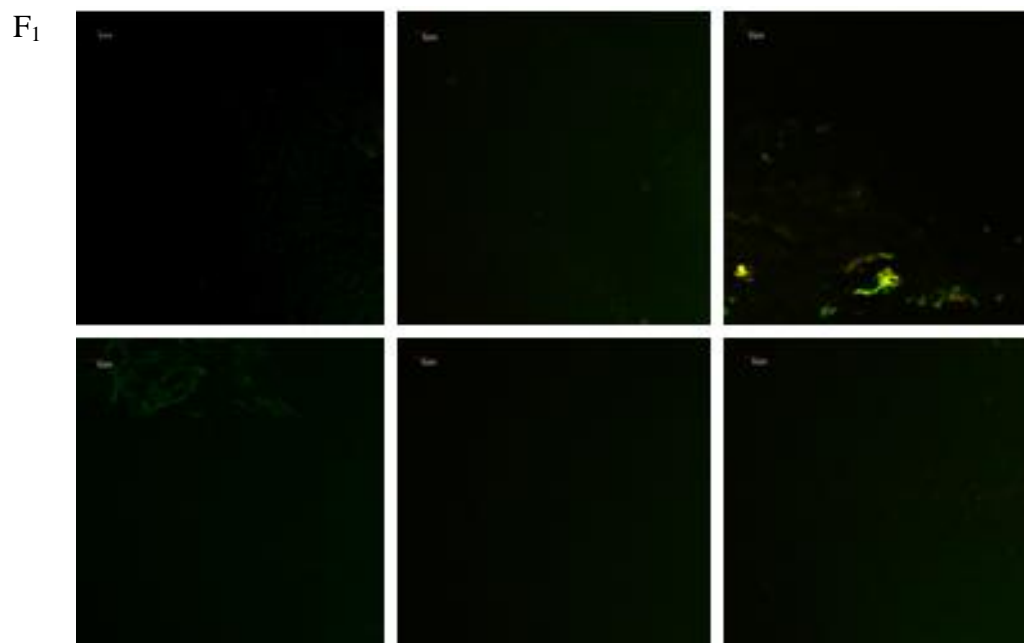
11. Chorpenning, K.A., "Platelet adhesion to polyurethane urea under cardiac pulse," Masters thesis, The Pennsylvania State University, 2010.
12. Milner, K.R., Snyder, A.J., Siedlecki, C.A., 2005, "Sub-micron texturing for reducing platelet adhesion to polyurethane biomaterials," J. Biomed. Mater. Res. 76(A), pp. 561–570.
13. Hochareon P., Manning K., Fontaine A., Tarbell J., Deutsch S., 2004, "Wall shear-rate estimation within the 50cc Penn State artificial heart using particle image velocimetry," J. Biomech. Eng., 126, 430–437.
14. Hubbell J.A., McIntire L.V., 1986, "Visualization and analysis of mural thrombogenesis on collagen, polyurethane and nylon," Biomaterials, 7, pp. 354–63.
15. Kreider, J., Manning, K. B., Oley, L. A., Fontaine, A. A., and Deutsch, S., 2006, "The 50cc Penn State LVAD: a Parametric Study of Valve Orientation Flow Dynamics," ASAIO J., 52, pp. 123–131.
16. Nanna, J.C., Navitsky, M.A., Topper, S.R., Deutsch, S., Manning, K.B., 2011, "A Fluid Dynamics Study in a 50 cc Pulsatile Ventricular Assist Device: Influence of Heart Rate Variability," J. Biomech. Eng., 133(10), pp. 101002.
17. Nanna, J. C., Wivholm, J.A., Deutsch, S., and Manning, K. B, 2011, "Flow Field Study Comparing Design Iterations of a 50 cc Left Ventricular Assist Device," ASAIO J., 57(5), pp. 349-357.
18. Wivholm J., "Flow field study comparing design iterations of a 50cc left ventricular assist device," Masters thesis, The Pennsylvania State University, 2008.
19. Medvitz, R.B., "Development and validation of a computational fluid dynamic methodology for pulsatile blood pump design and prediction of thrombus potential," PhD thesis, The Pennsylvania State University, 2008.
20. Rosenberg G., "A mock circulatory system for *in vitro* studies of artificial hearts," Masters thesis, The Pennsylvania State University, 1972.
21. Hochareon, P., "Development of Particle Image Velocimetry (PIV) for wall shear stress estimation within a 50cc Penn State artificial heart ventricular chamber," Ph.D thesis, The Pennsylvania State University, 2003.
22. Medvitz *et al.*, 2007, "Development and Validation of a Computational Fluid Dynamics Methodology for Simulation of Pulsatile Left Ventricular Assist Devices," ASAIO J. 53(2), pp. 122-131.

23. Navitsky, M.A., Deutsch, S., Manning, K.B., “A thrombus susceptibility comparison of two pulsatile Penn State 50cc left ventricular assist device designs,” In Review, The Pennsylvania State University, 2012.

**Appendix A****Complete set of fluorescent images acquired with confocal microscopy**

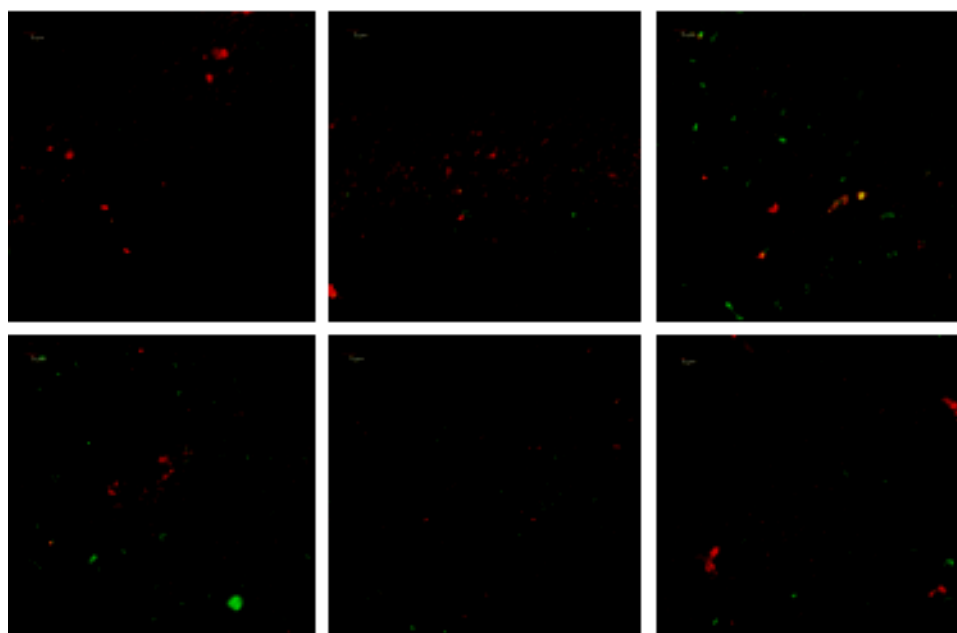
Locations of F<sub>1</sub> and F<sub>2</sub> are shown in Figure 2-1.

19.5 mm normal plane – front region of bottom wall

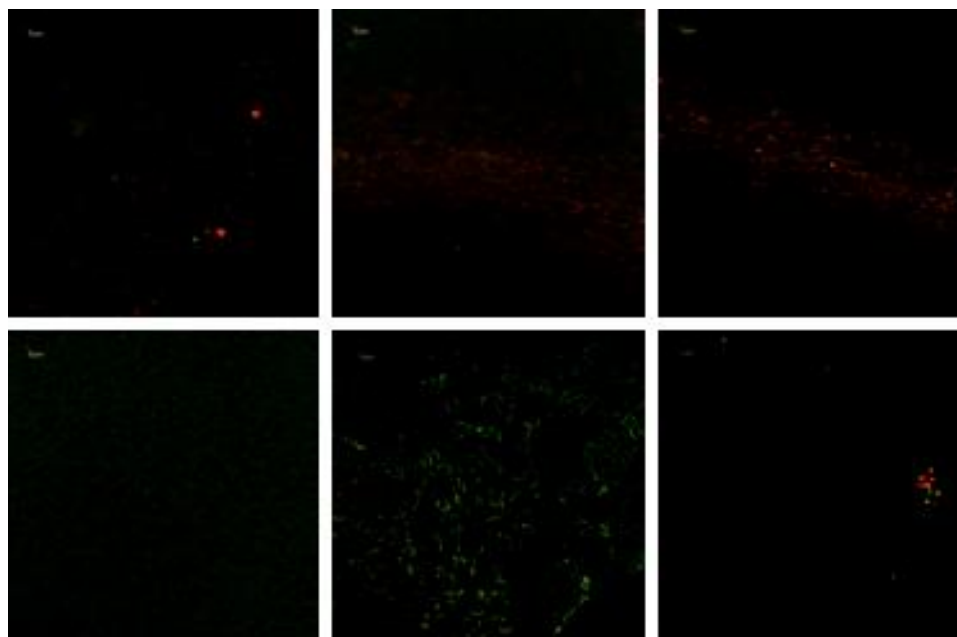


19.5 mm normal plane – center region of bottom wall

F<sub>1</sub>

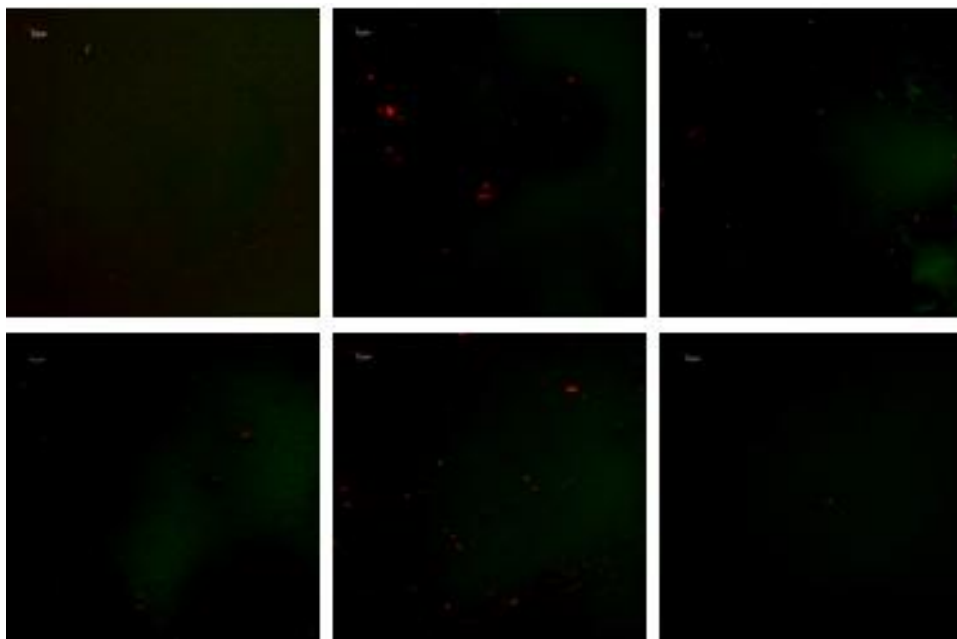


F<sub>2</sub>

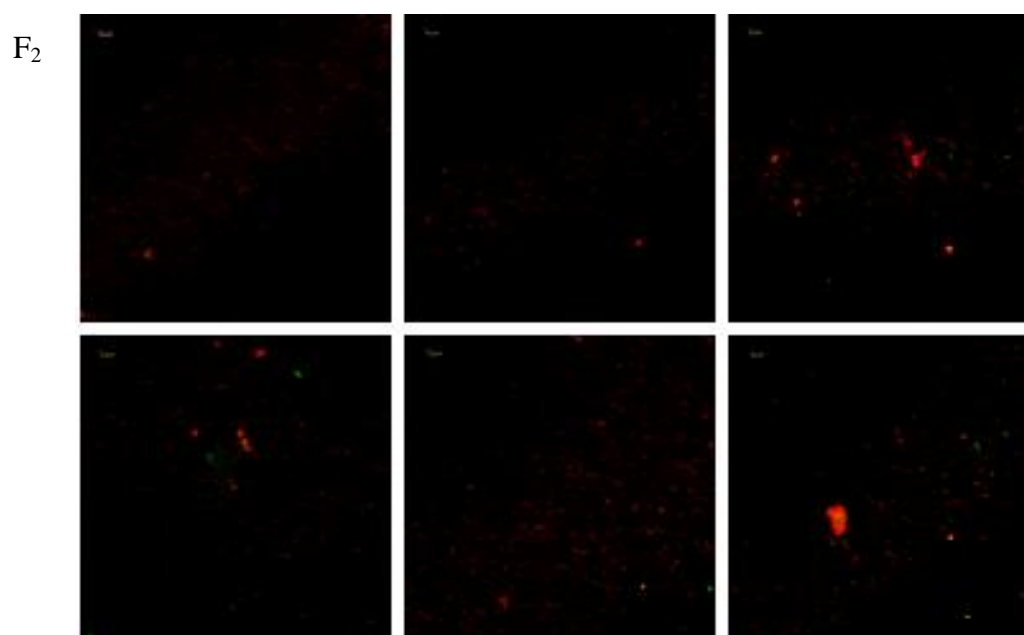
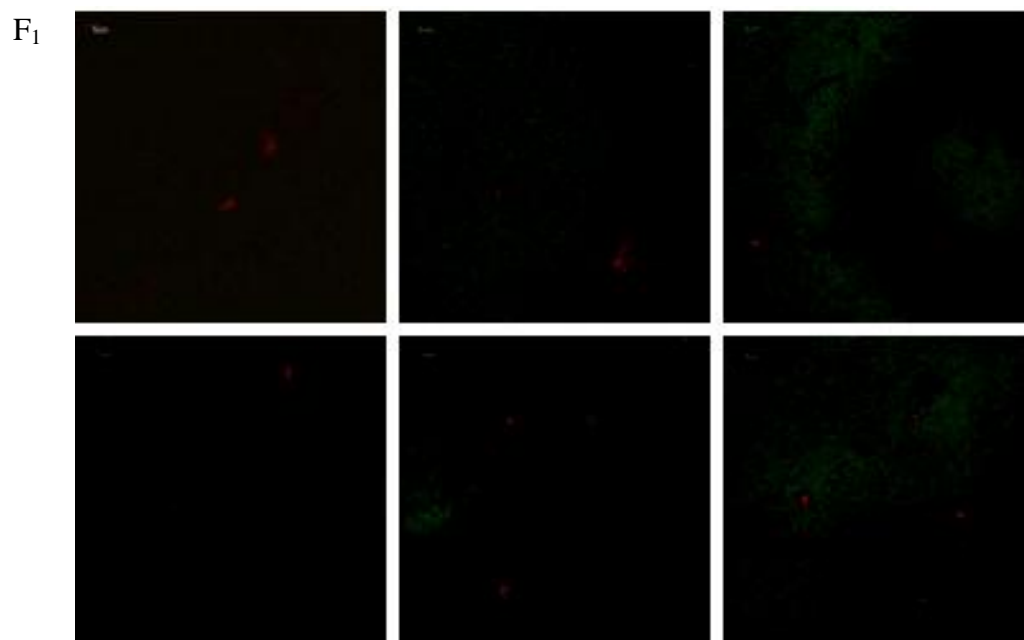


19.5 mm normal plane – rear region of bottom wall

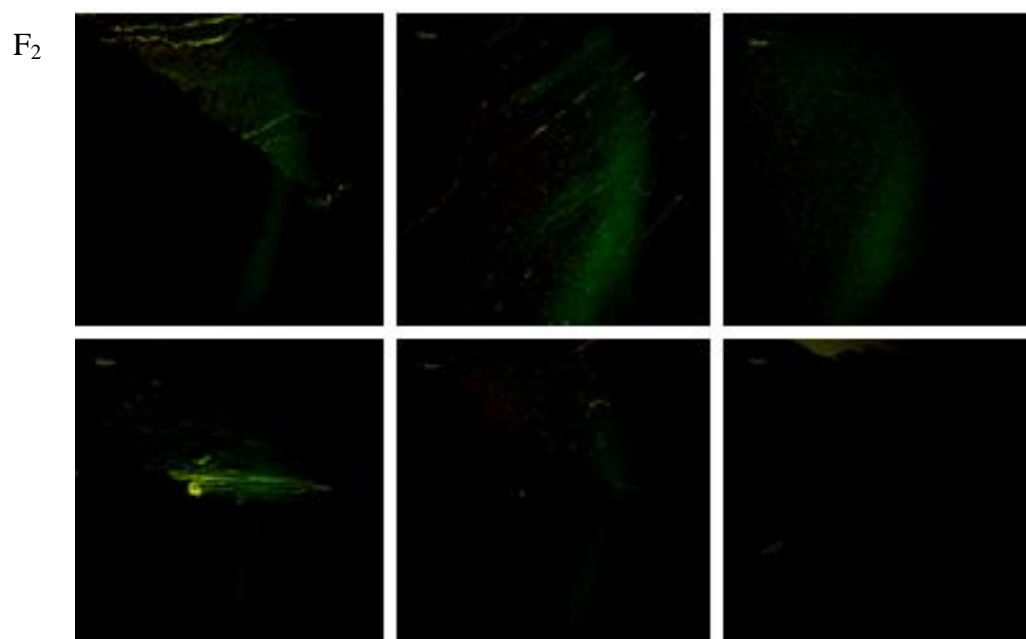
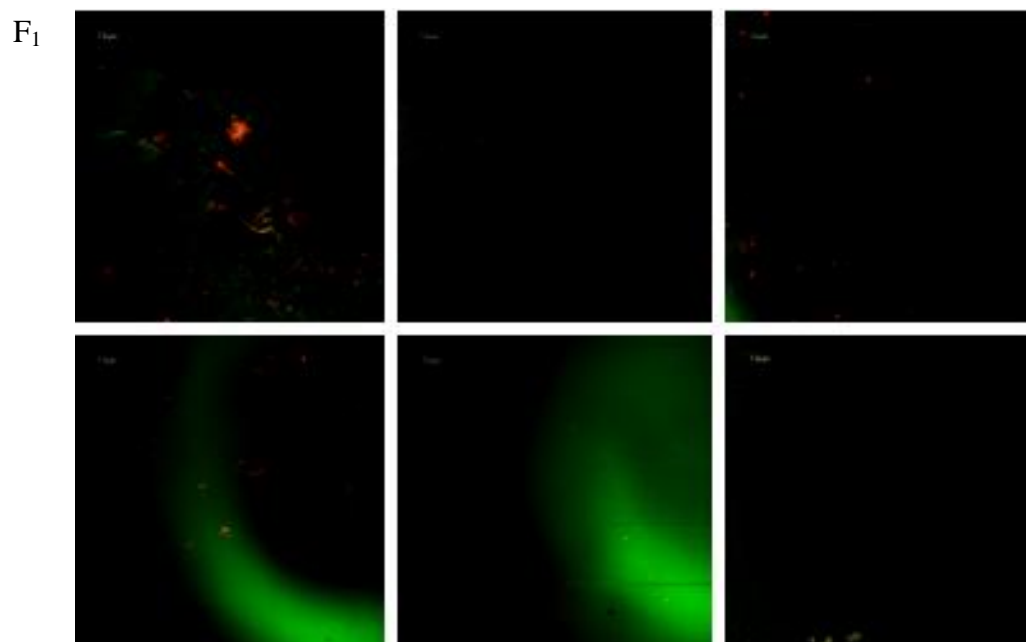
F<sub>1</sub>



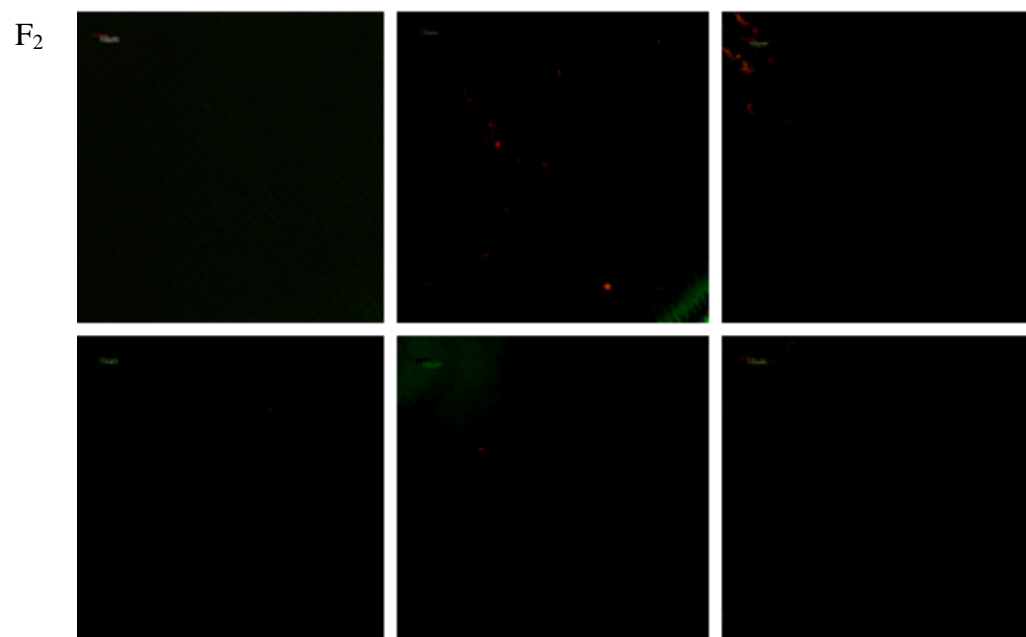
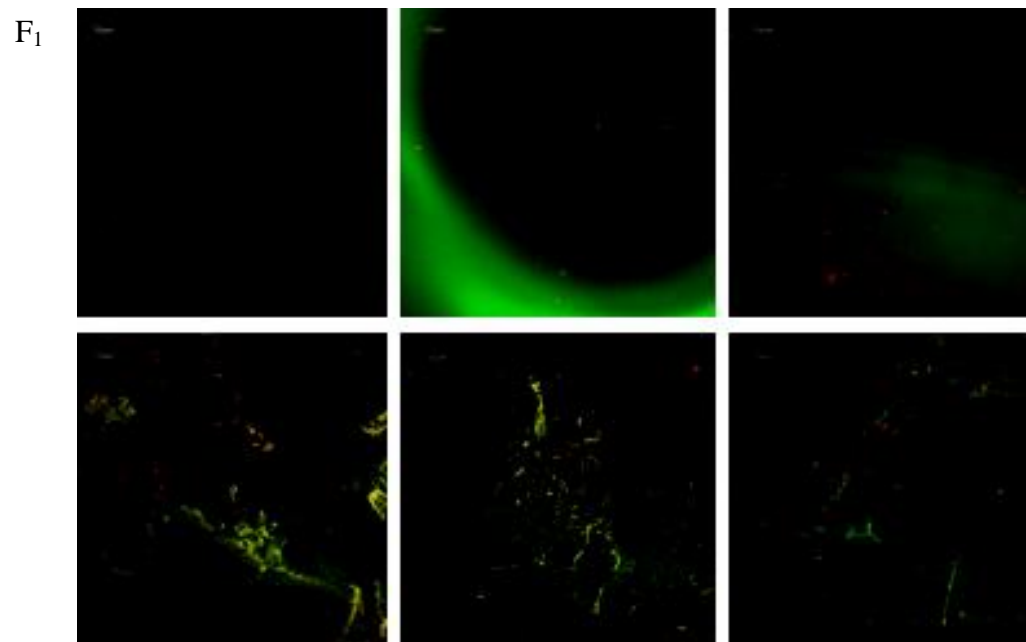
19.5 mm normal plane – 17 mm location on rear wall



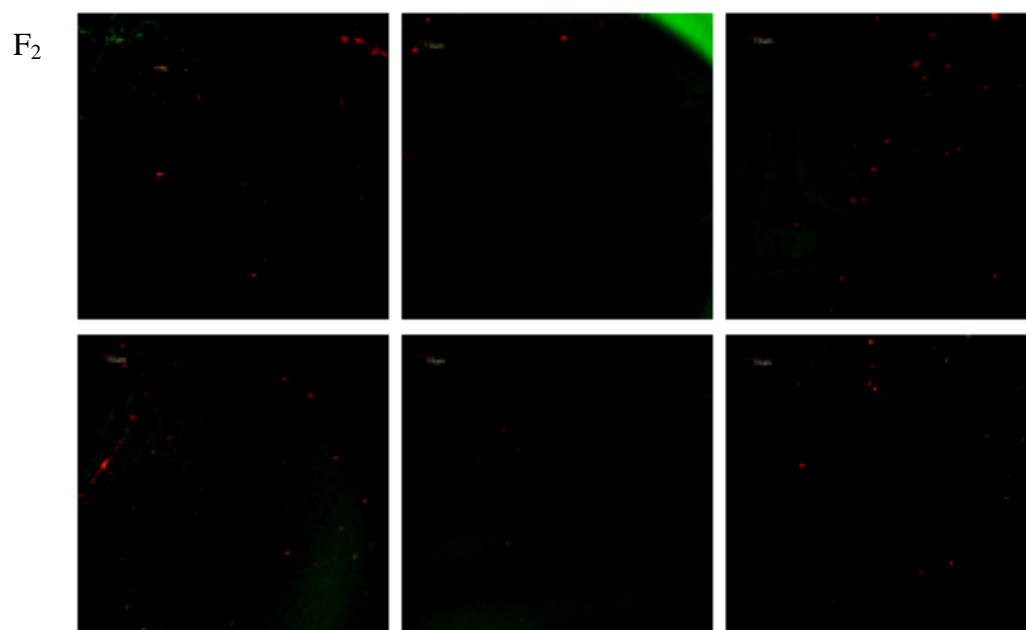
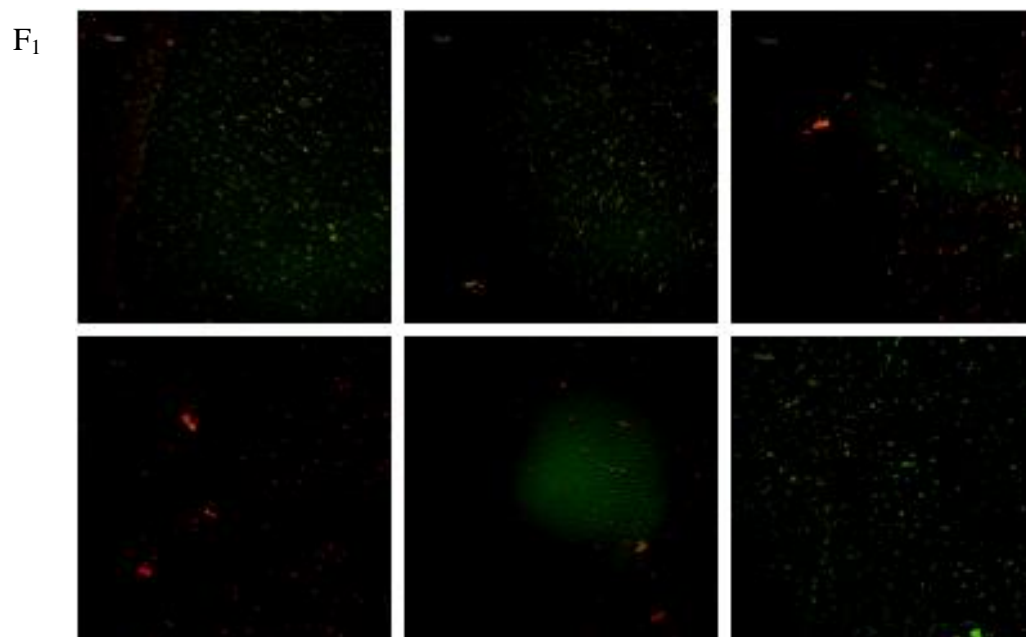
26.9 mm normal plane – front region of bottom wall



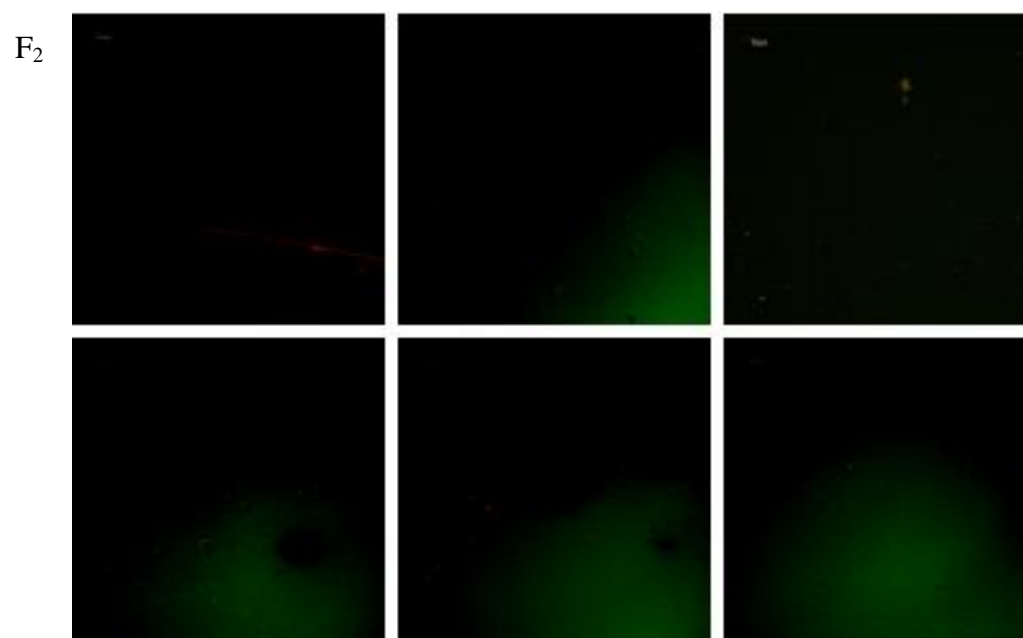
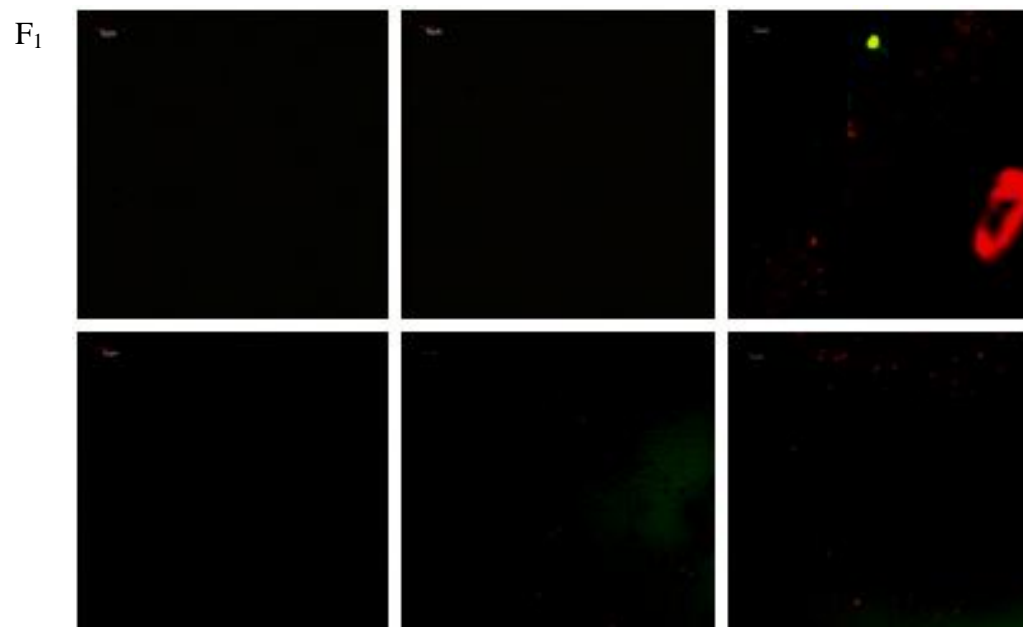
26.9 mm normal plane – center region of bottom wall



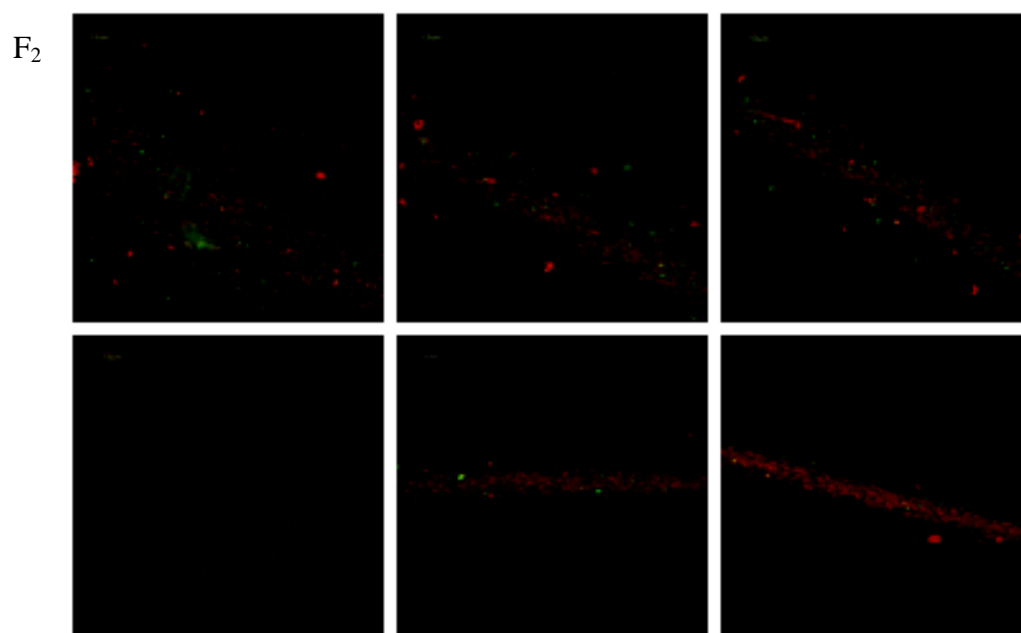
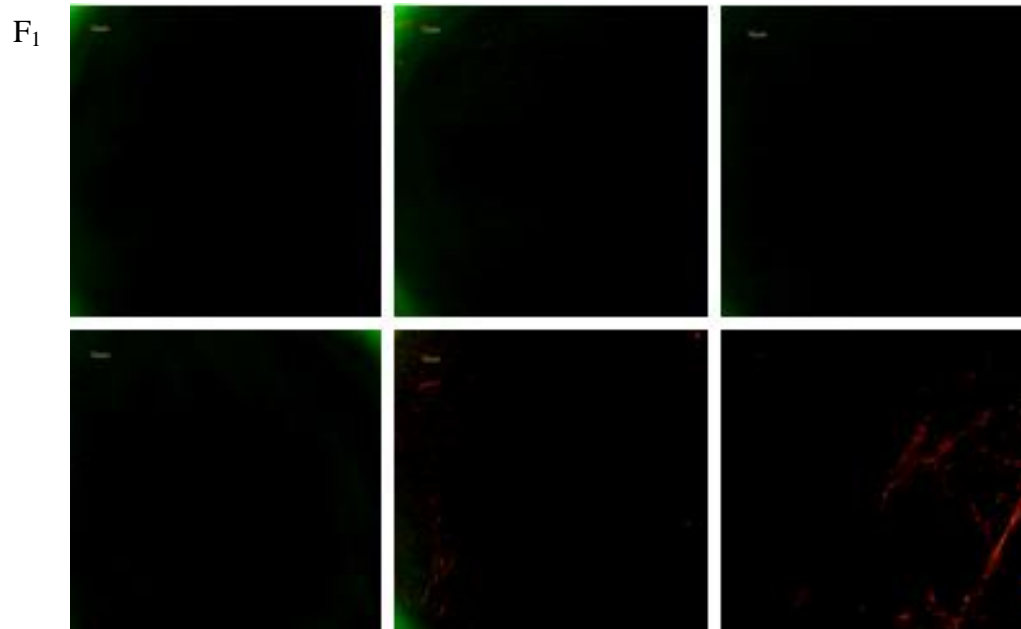
26.9 mm normal plane – rear region of bottom wall



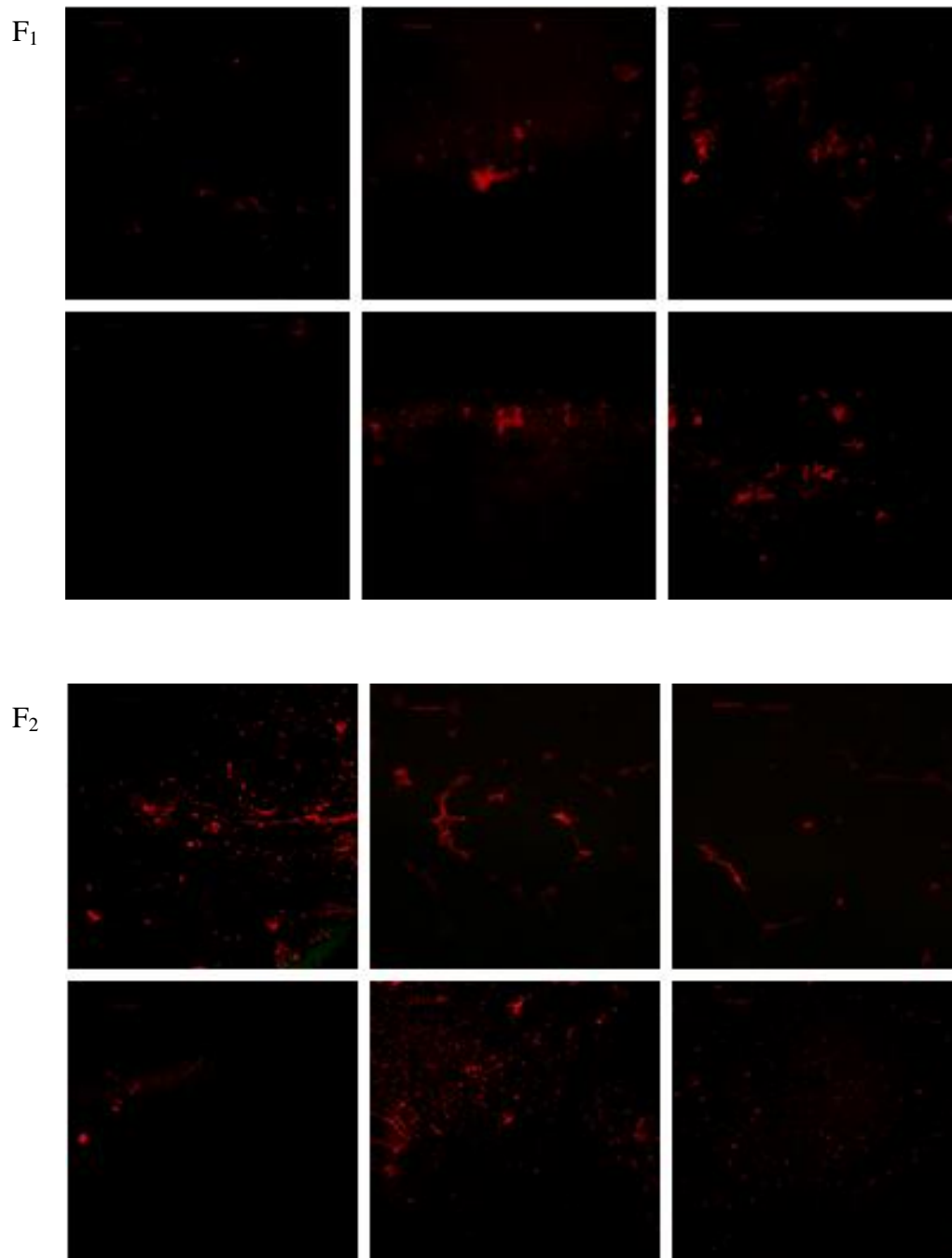
26.9 mm normal plane – 17 mm location on rear wall



34.24 mm normal plane – front region of bottom wall

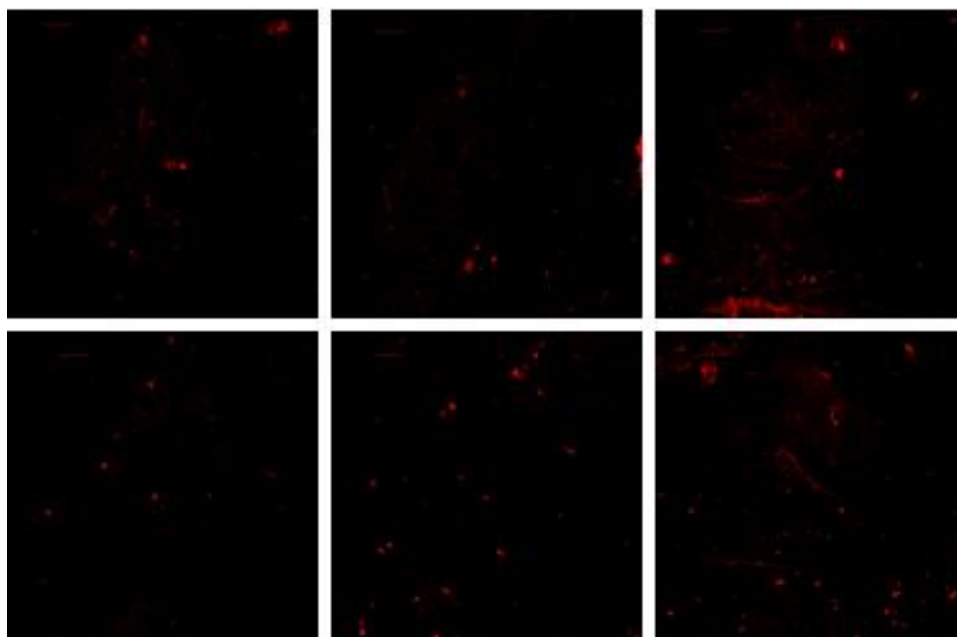


34.24 mm normal plane – center region of bottom wall

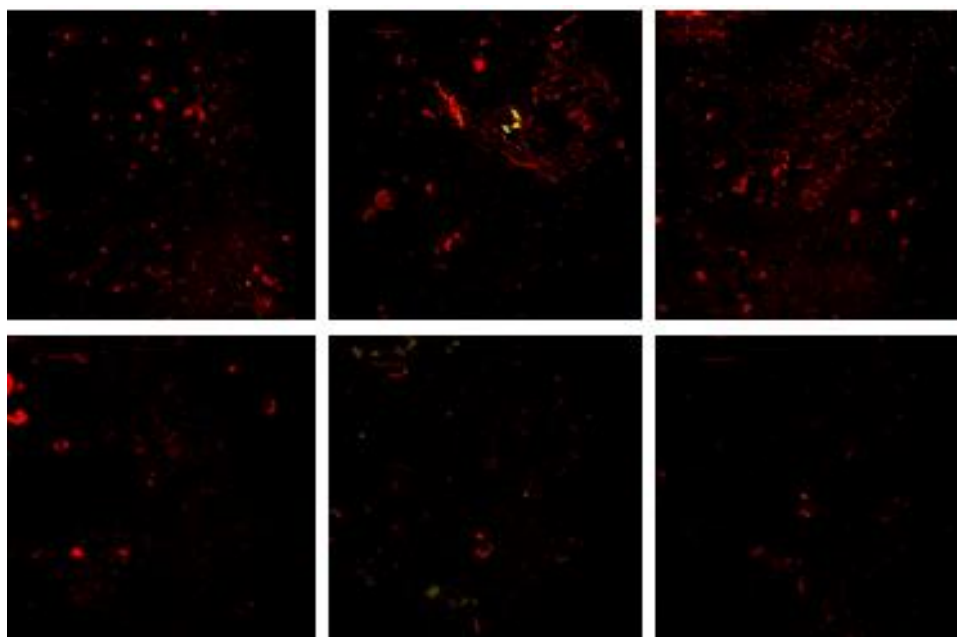


34.24 mm normal plane – rear region of bottom wall

F<sub>1</sub>

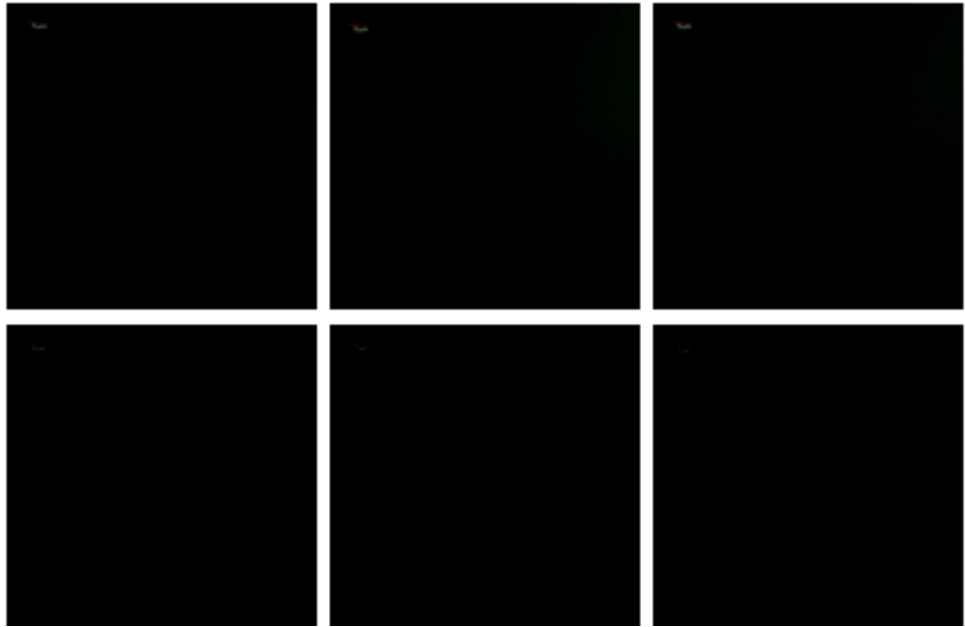


F<sub>2</sub>

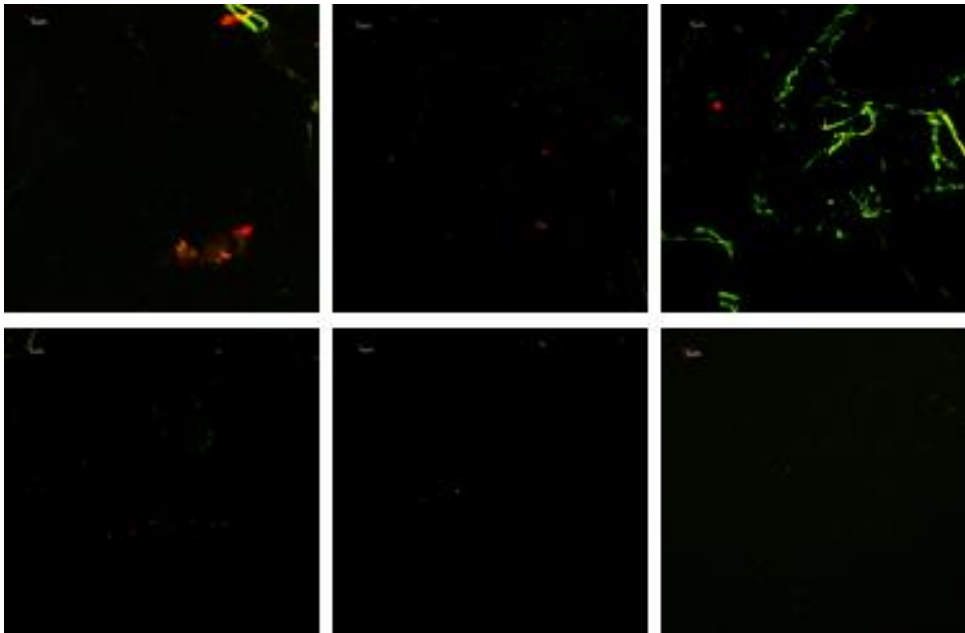


34.24 mm normal plane – 17 mm location on rear wall

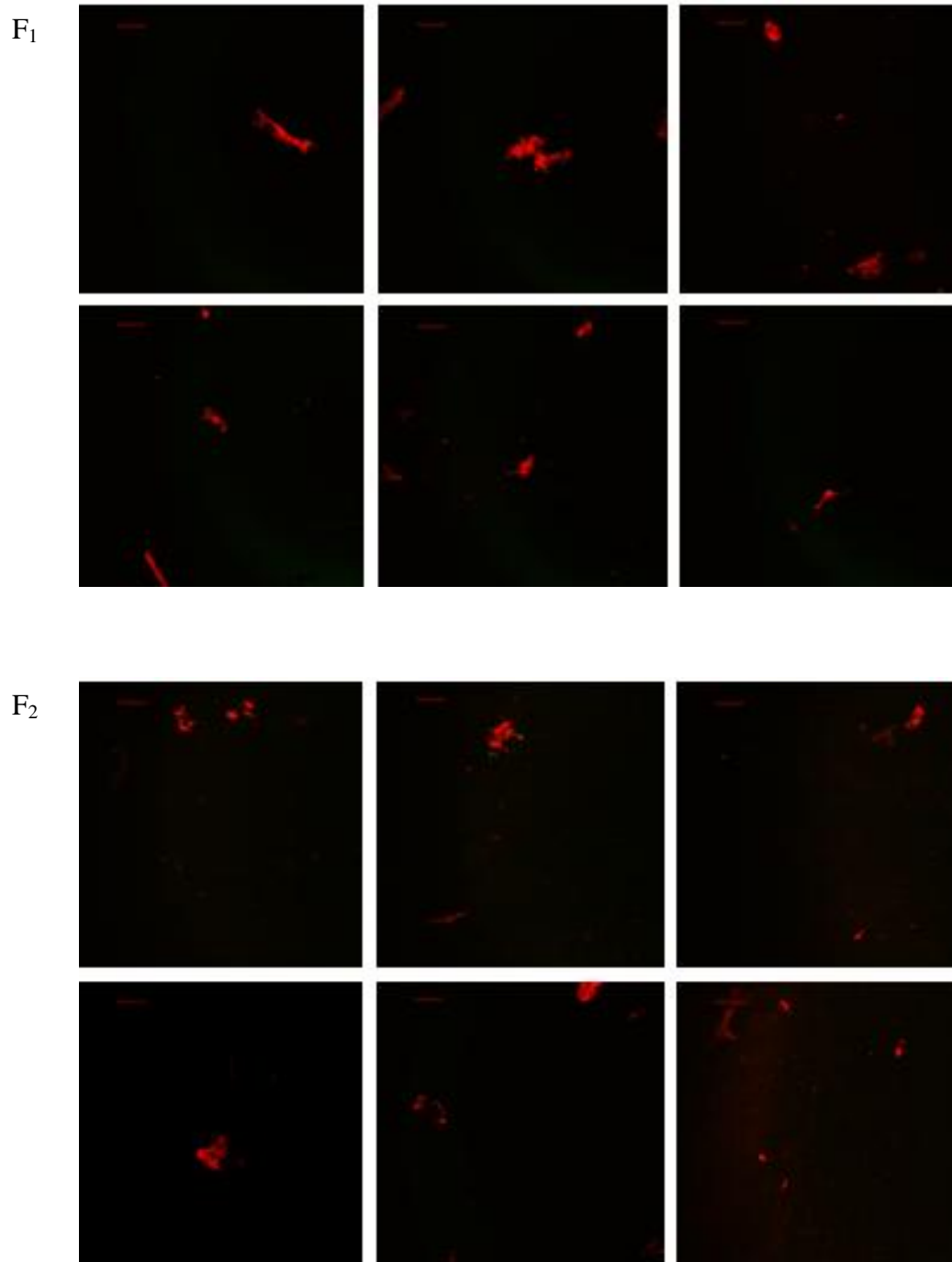
F<sub>1</sub>



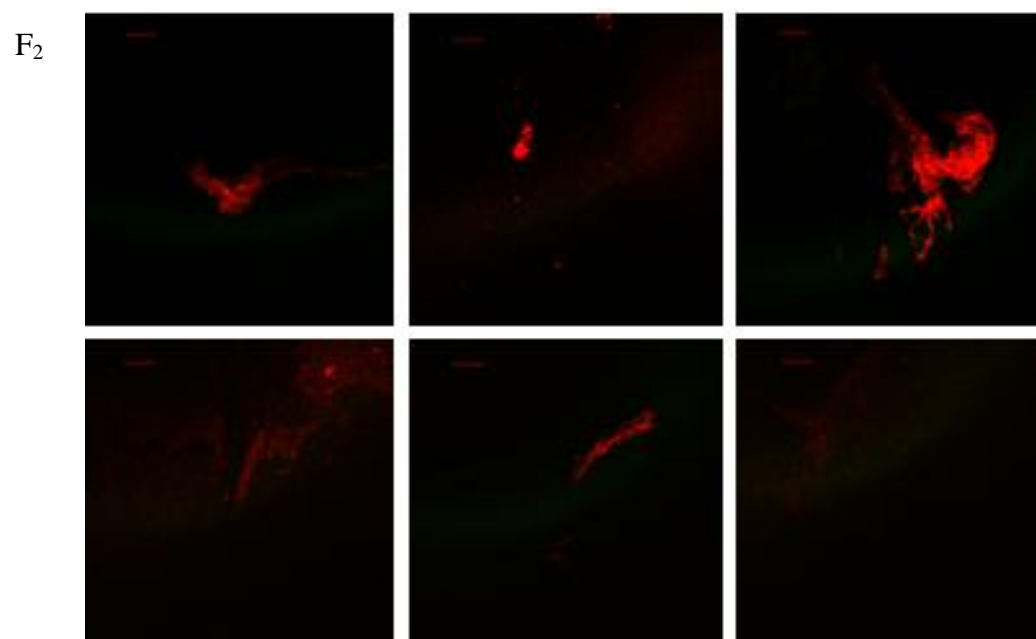
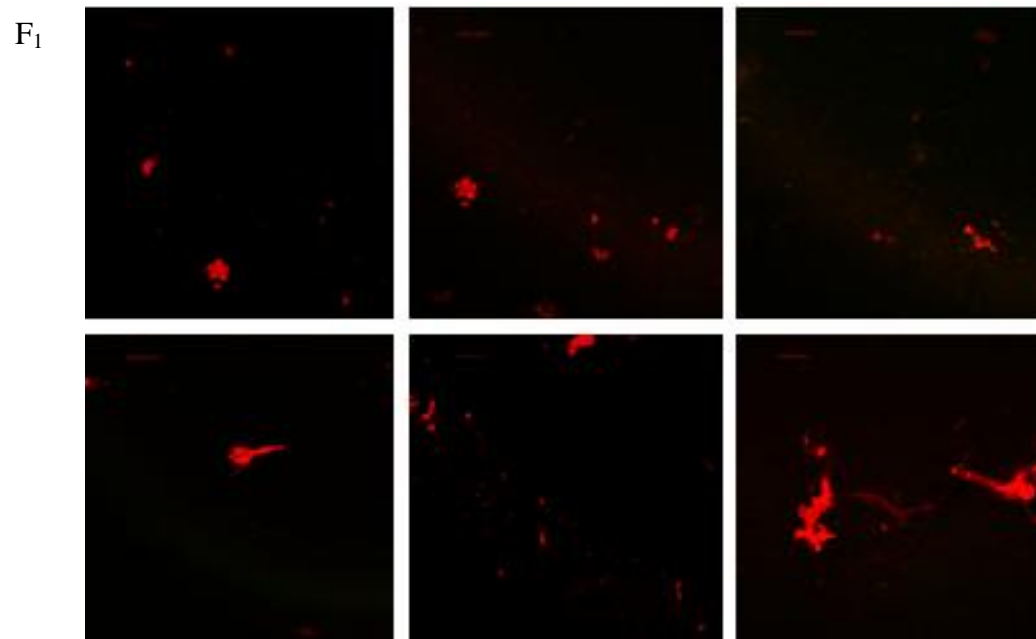
F<sub>2</sub>



42.5 mm normal plane – front region of bottom wall

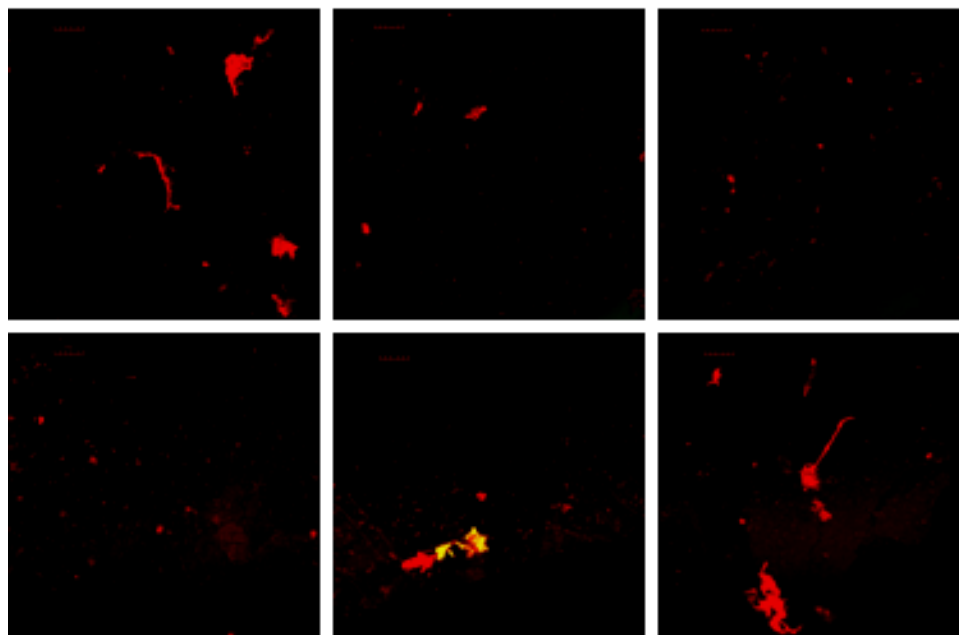


42.5 mm normal plane – center region of bottom wall

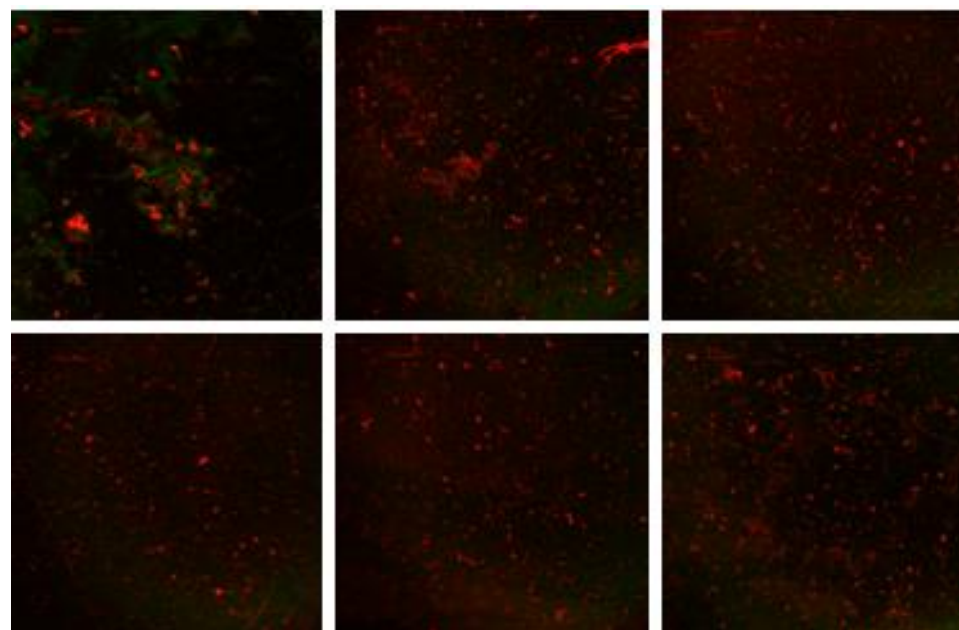


42.5 mm normal plane – rear region of bottom wall

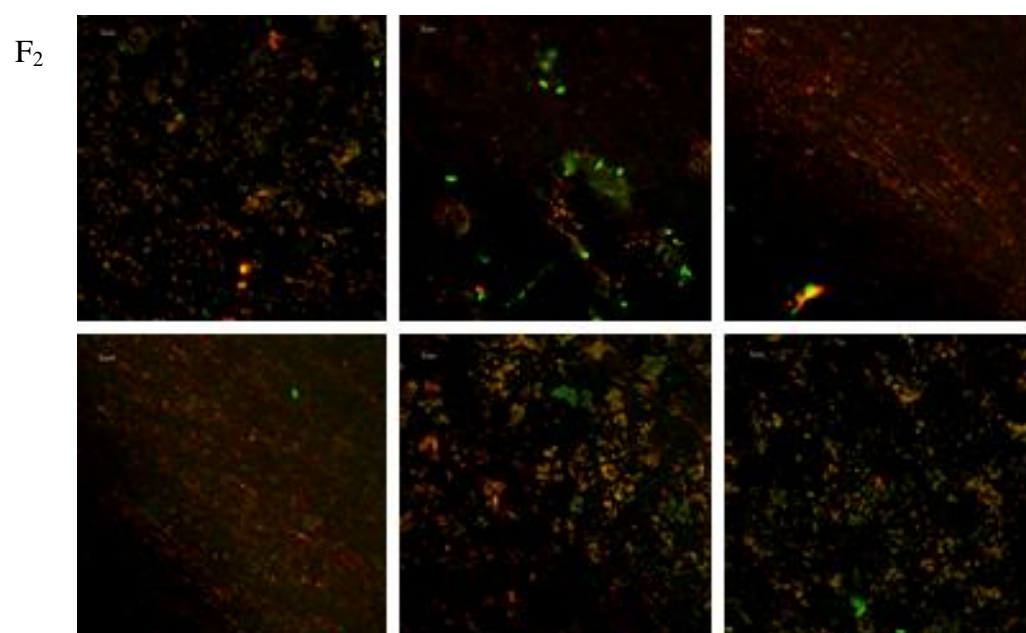
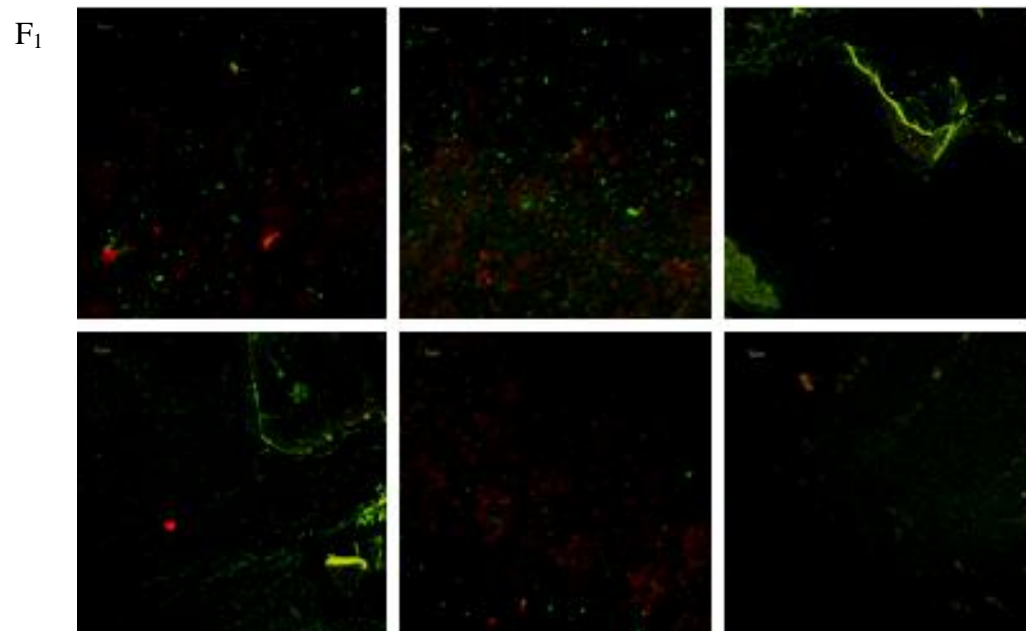
F<sub>1</sub>



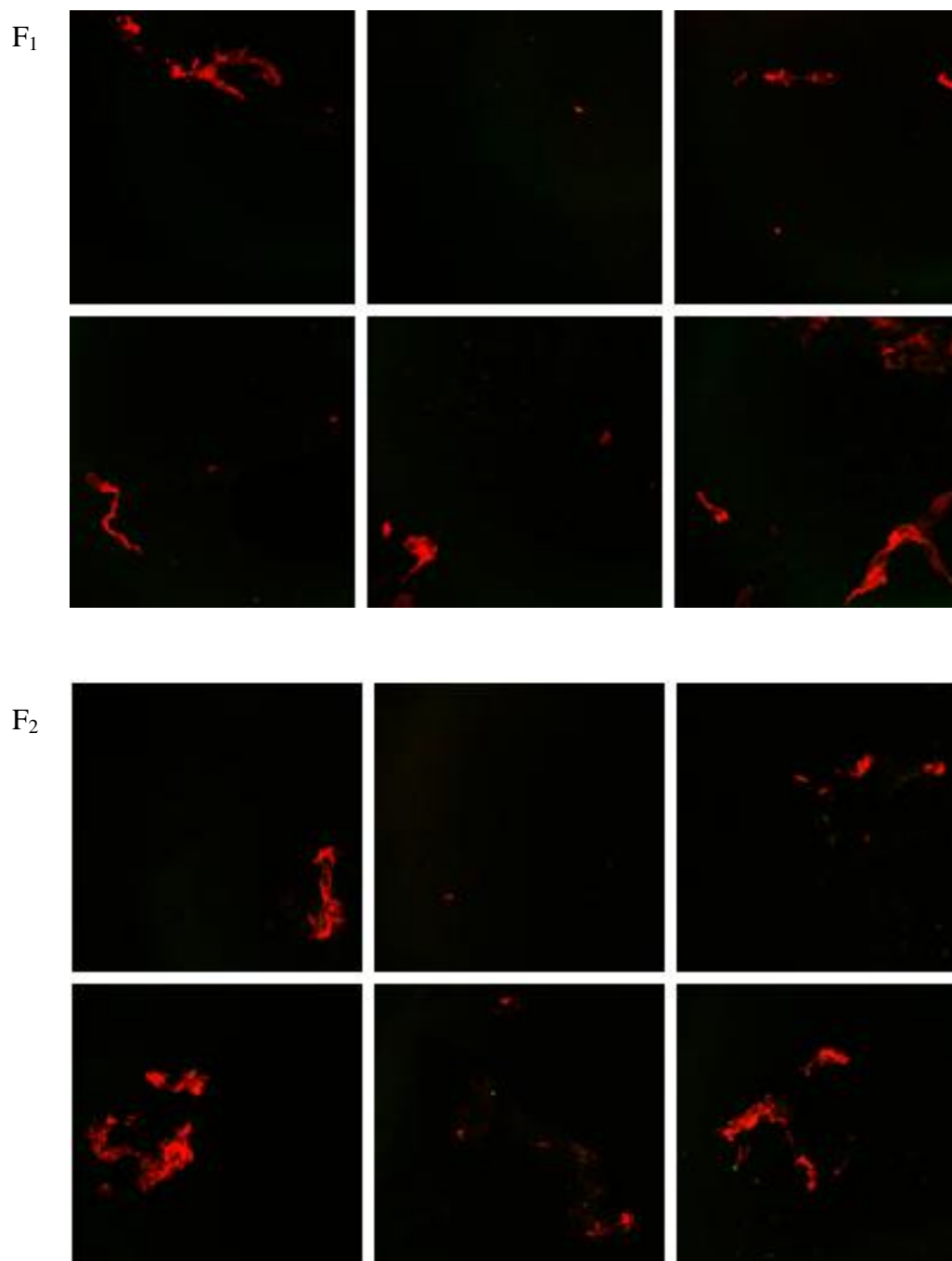
F<sub>2</sub>



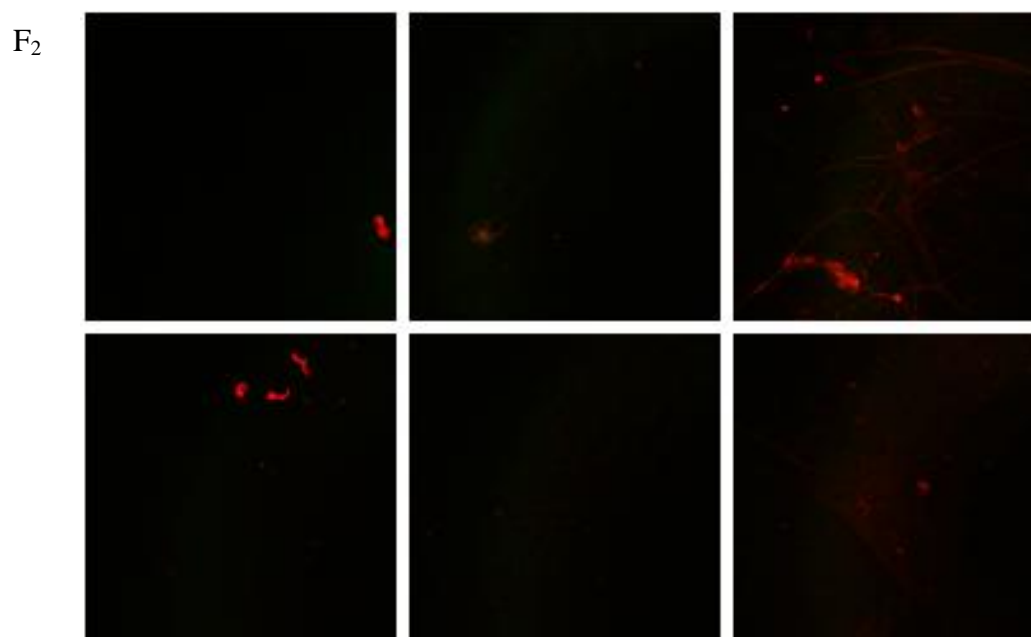
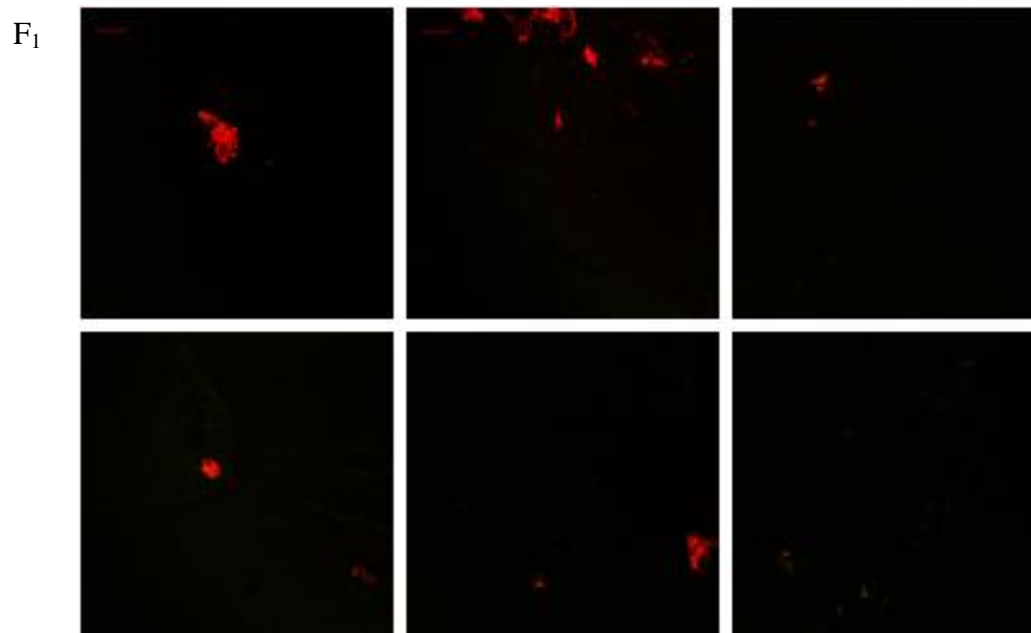
42.5 mm normal plane – 17 mm location on rear wall



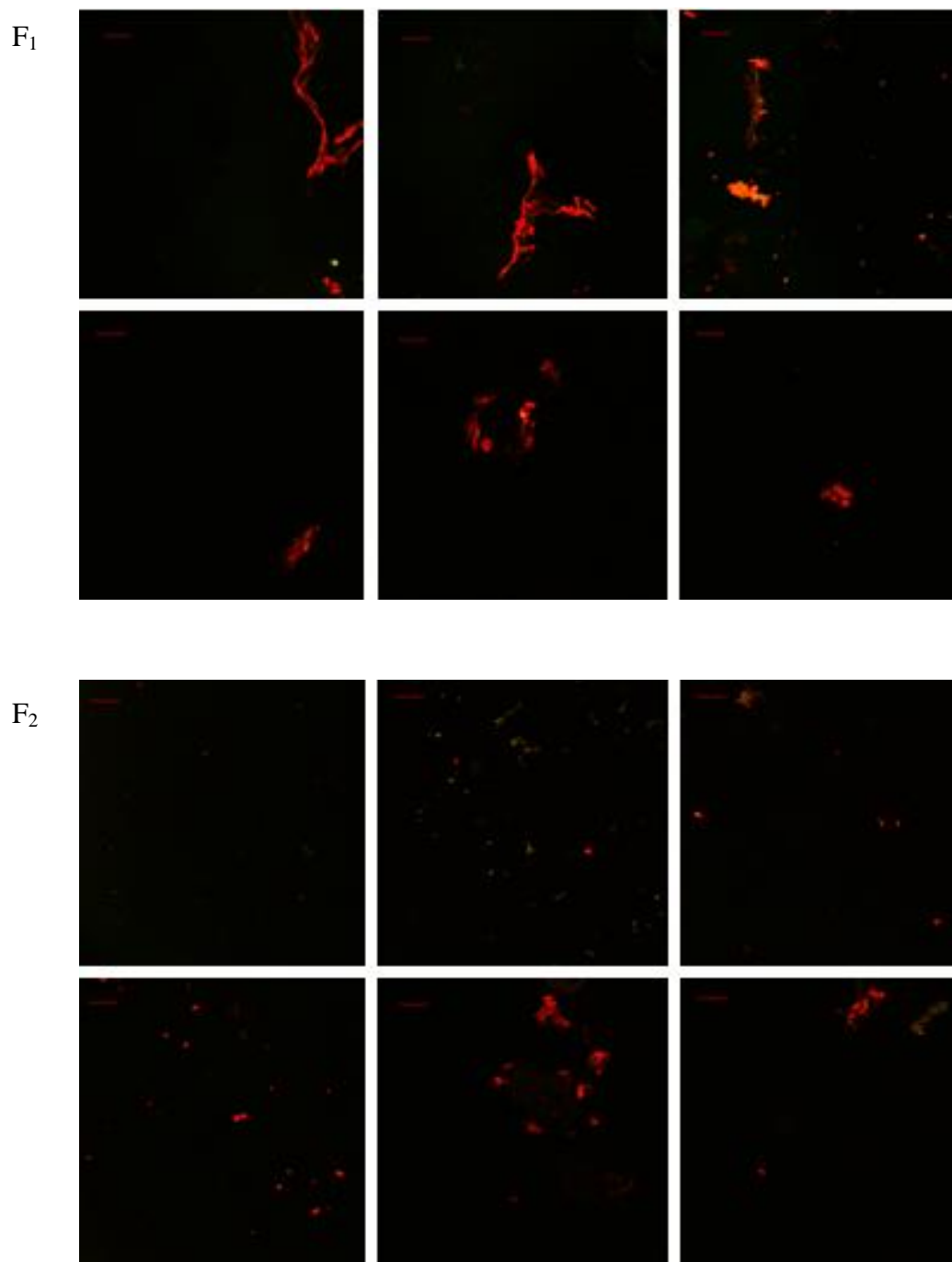
50.8 mm normal plane – front region of bottom wall



50.8 mm normal plane – center region of bottom wall

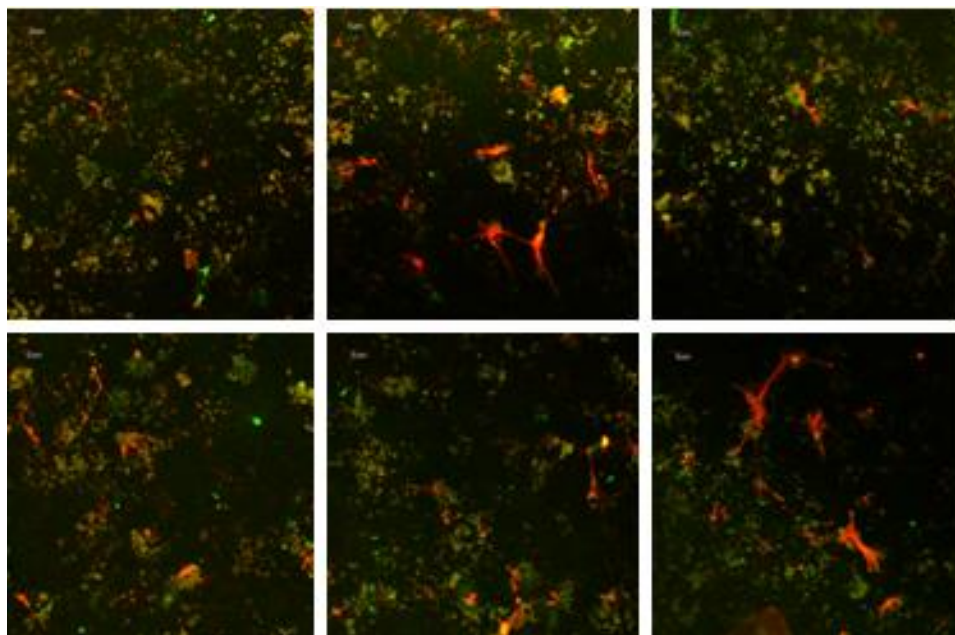


50.8 mm normal plane – rear region of bottom wall

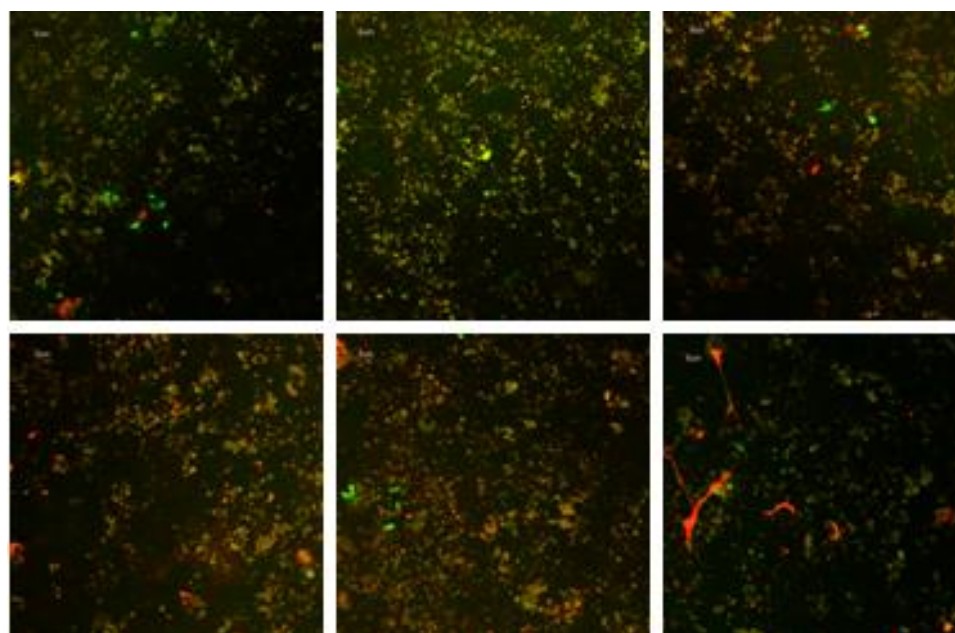


50.8 mm normal plane – 17 mm location on rear wall

F<sub>1</sub>

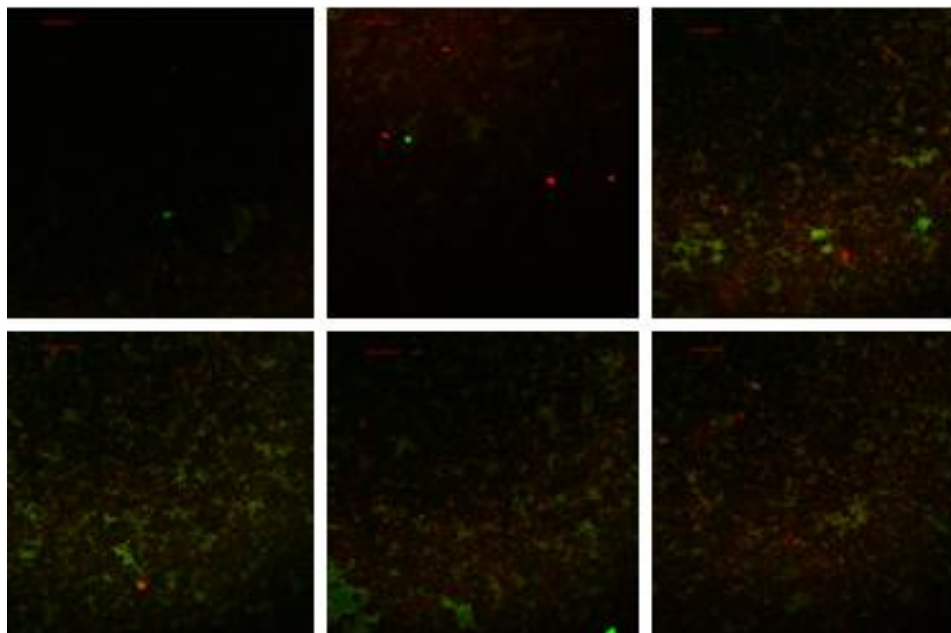


F<sub>2</sub>

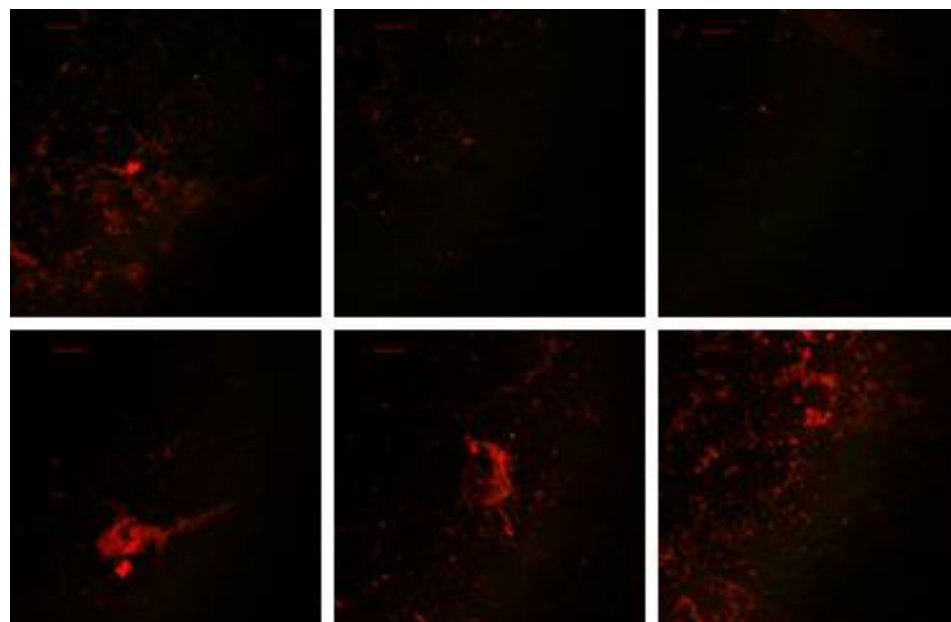


50.8 mm normal plane – 25 mm location on rear wall

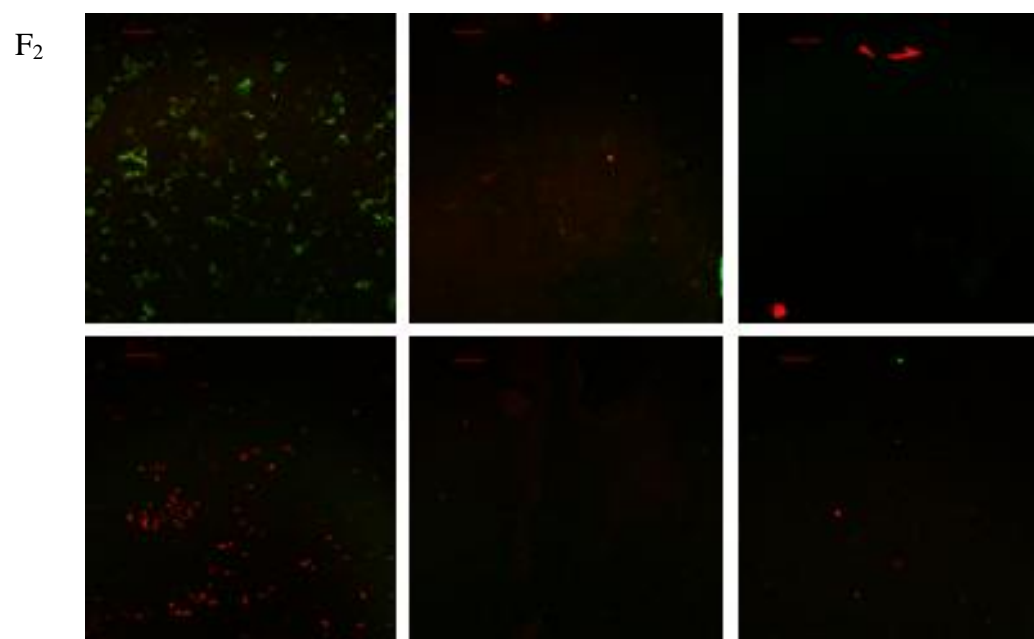
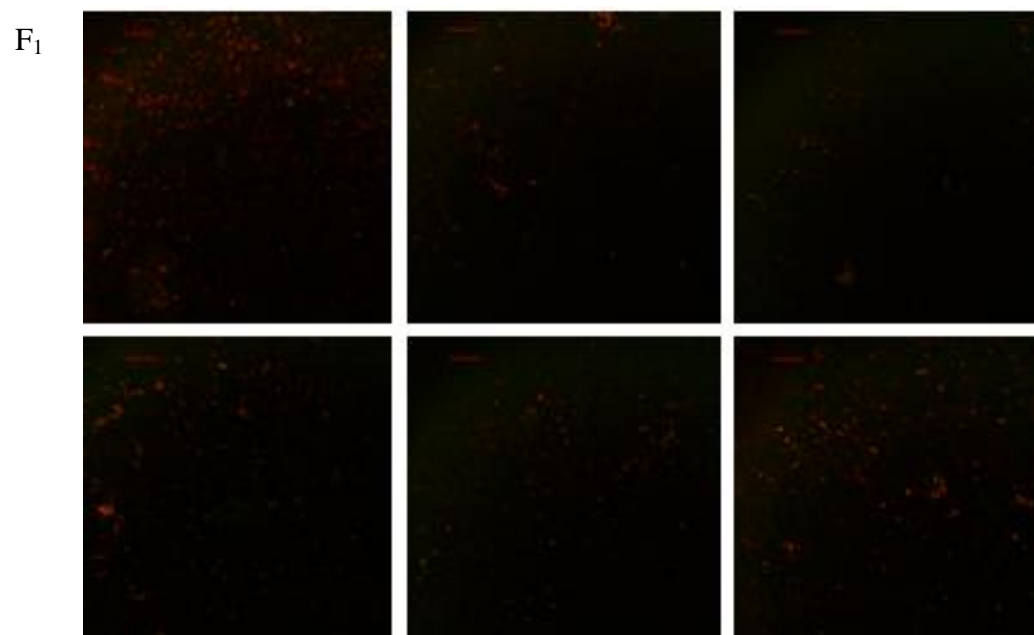
F<sub>1</sub>



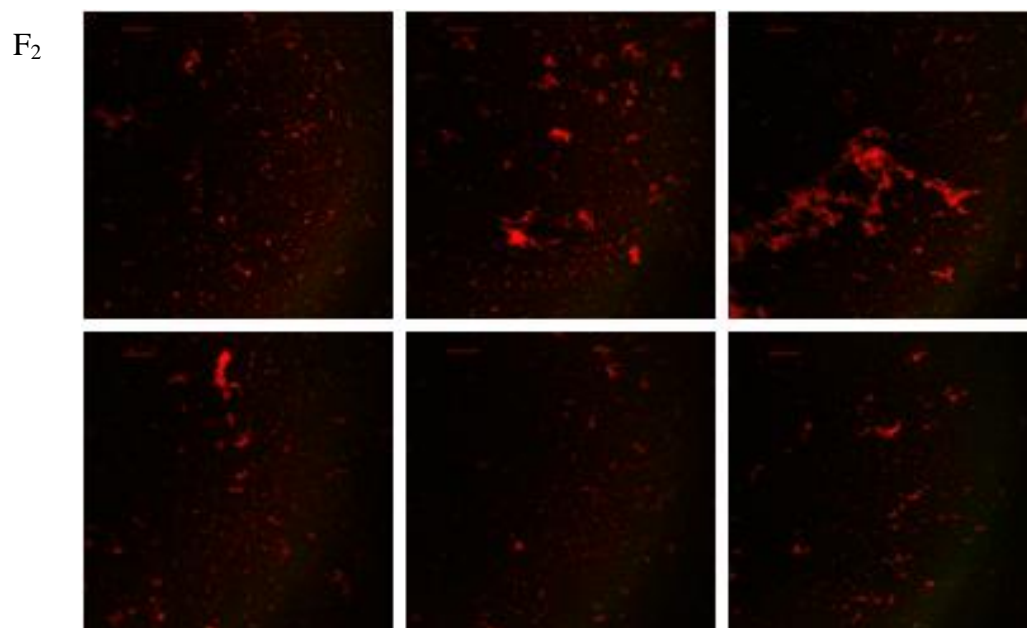
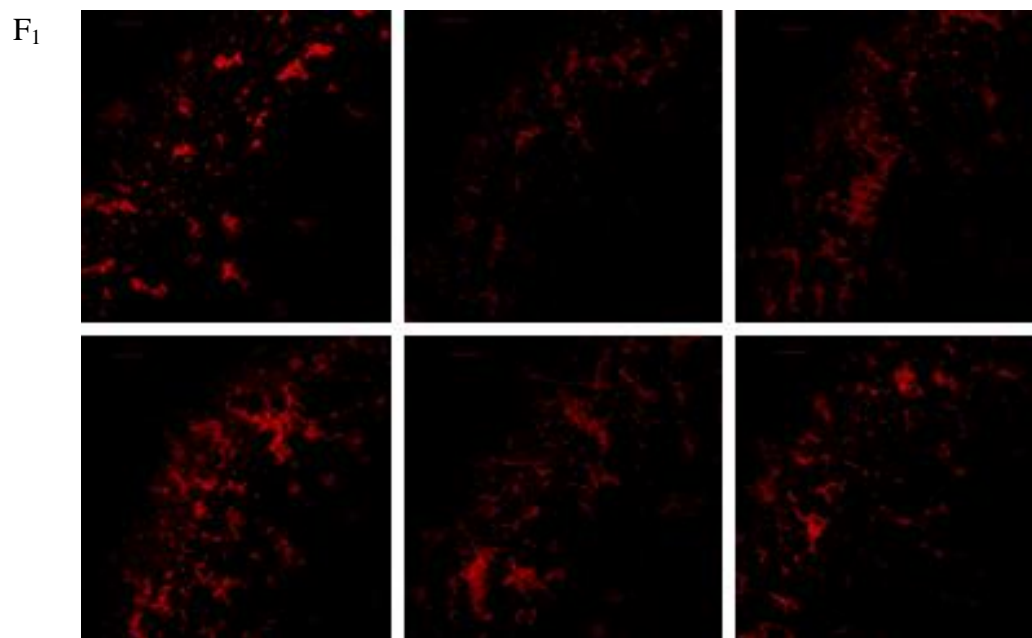
F<sub>2</sub>



50.8 mm normal plane – 35 mm location on rear wall



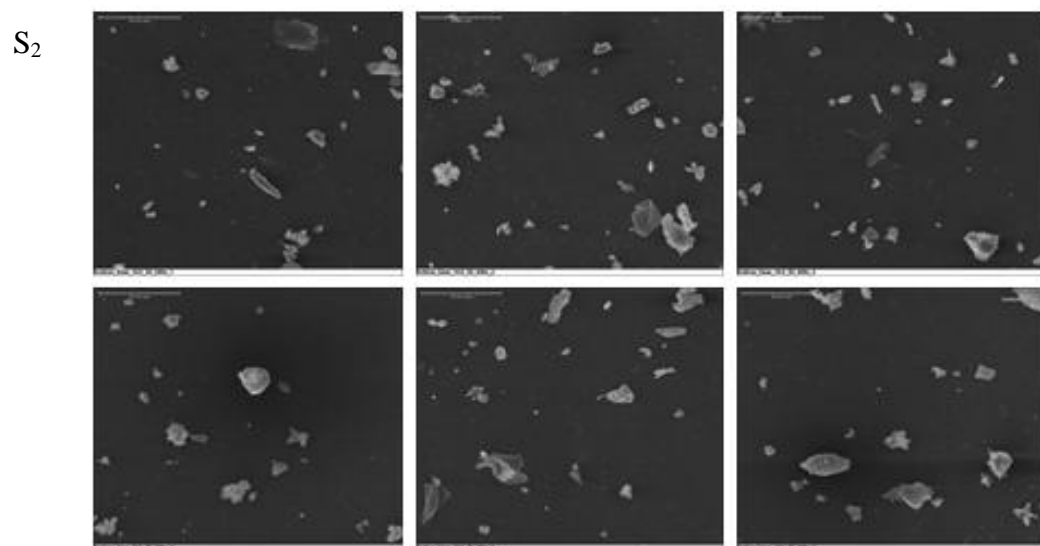
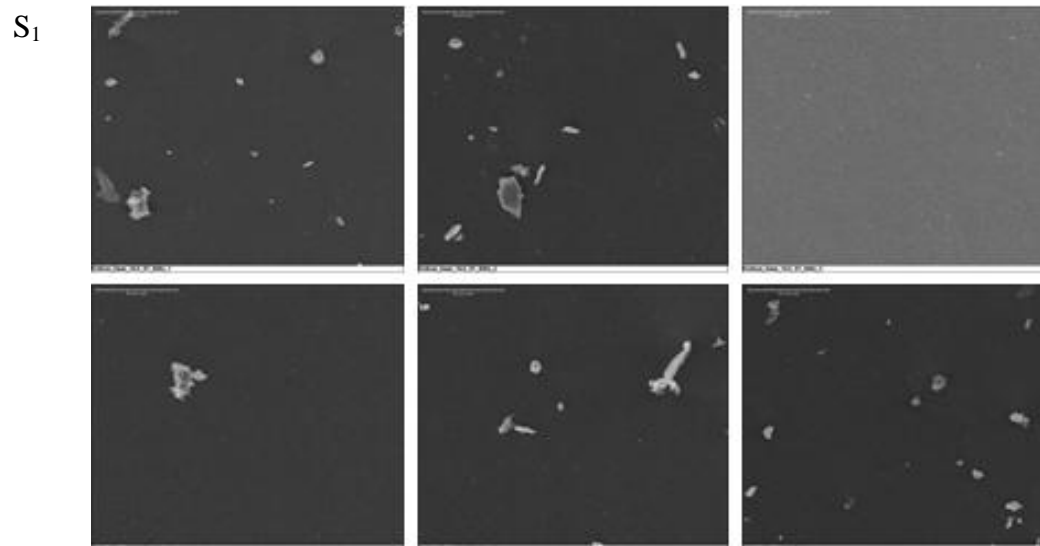
56.8 mm normal plane – rear region of bottom wall



**Appendix B****Complete set of images acquired with scanning electron microscopy**

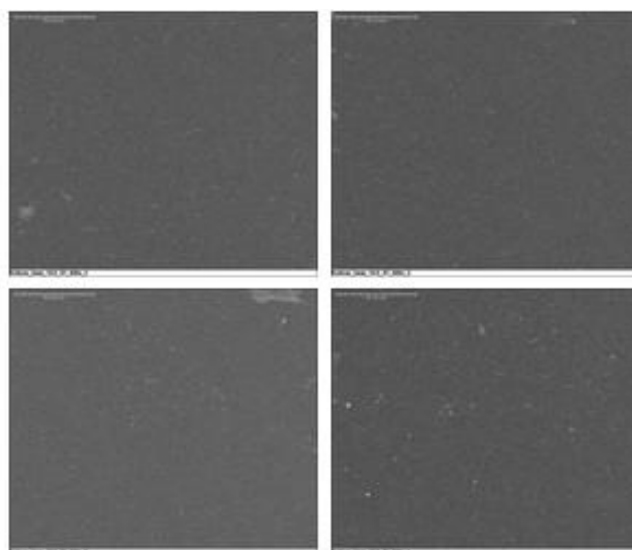
Locations of  $S_1$  and  $S_2$  are shown in Figure 2-1.

19.5 mm normal plane – front region of bottom wall

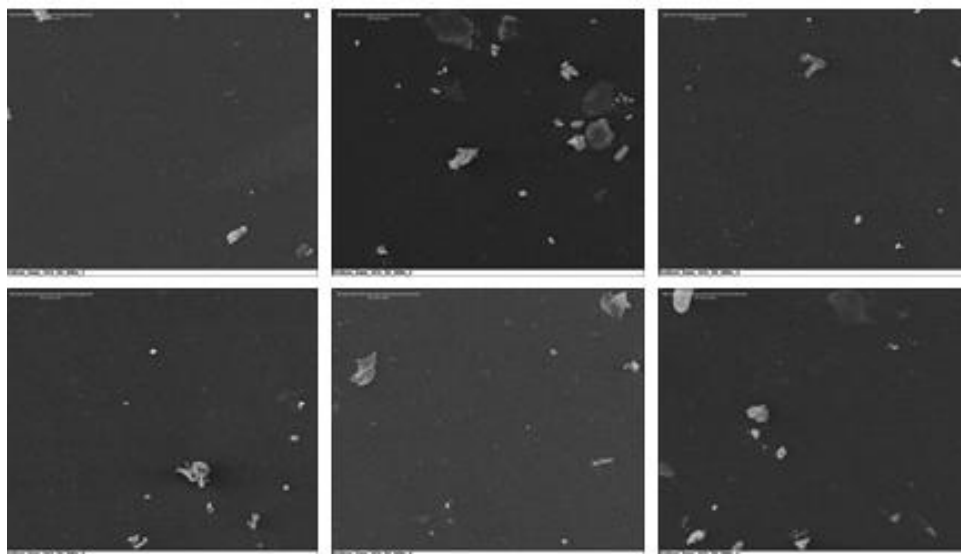


19.5 mm normal plane – center region of bottom wall

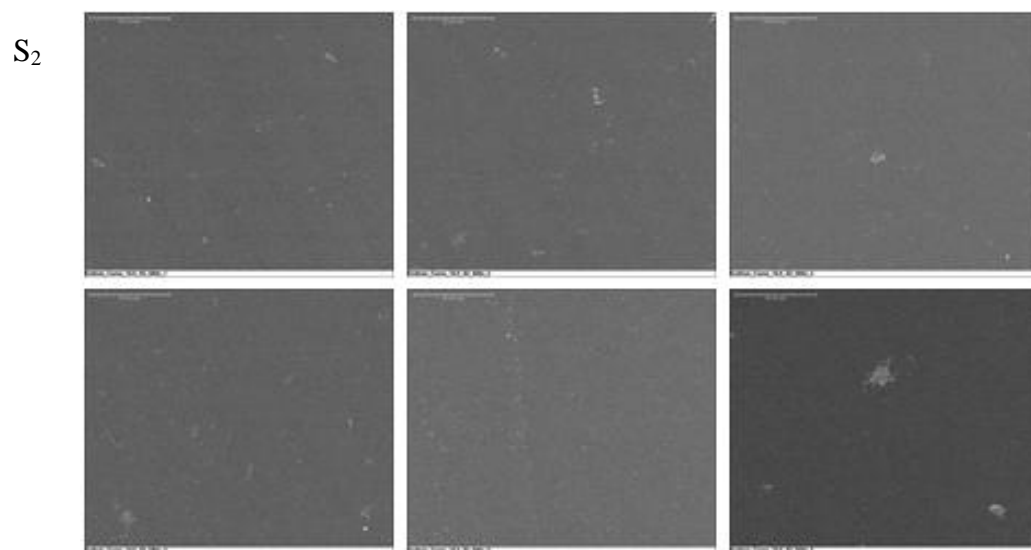
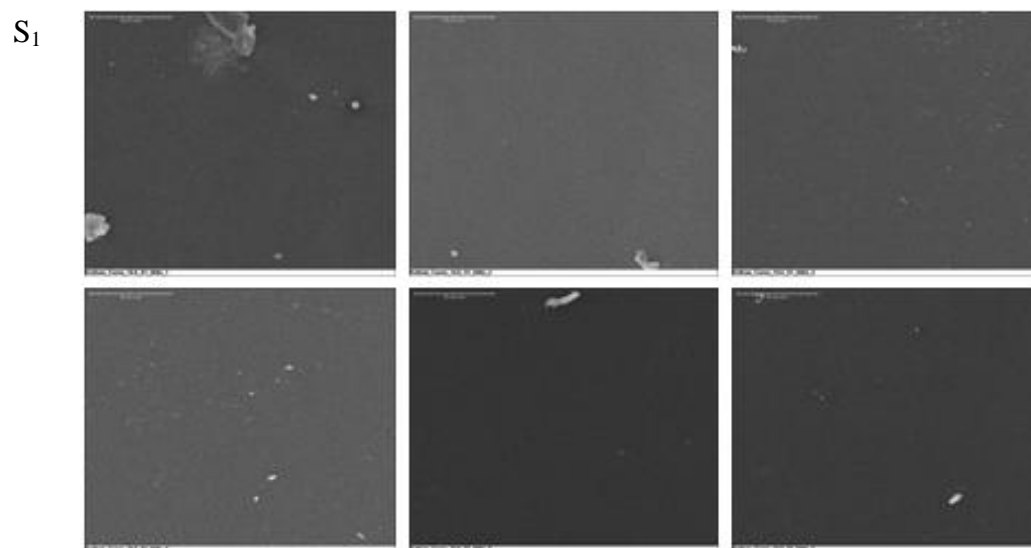
$S_1$



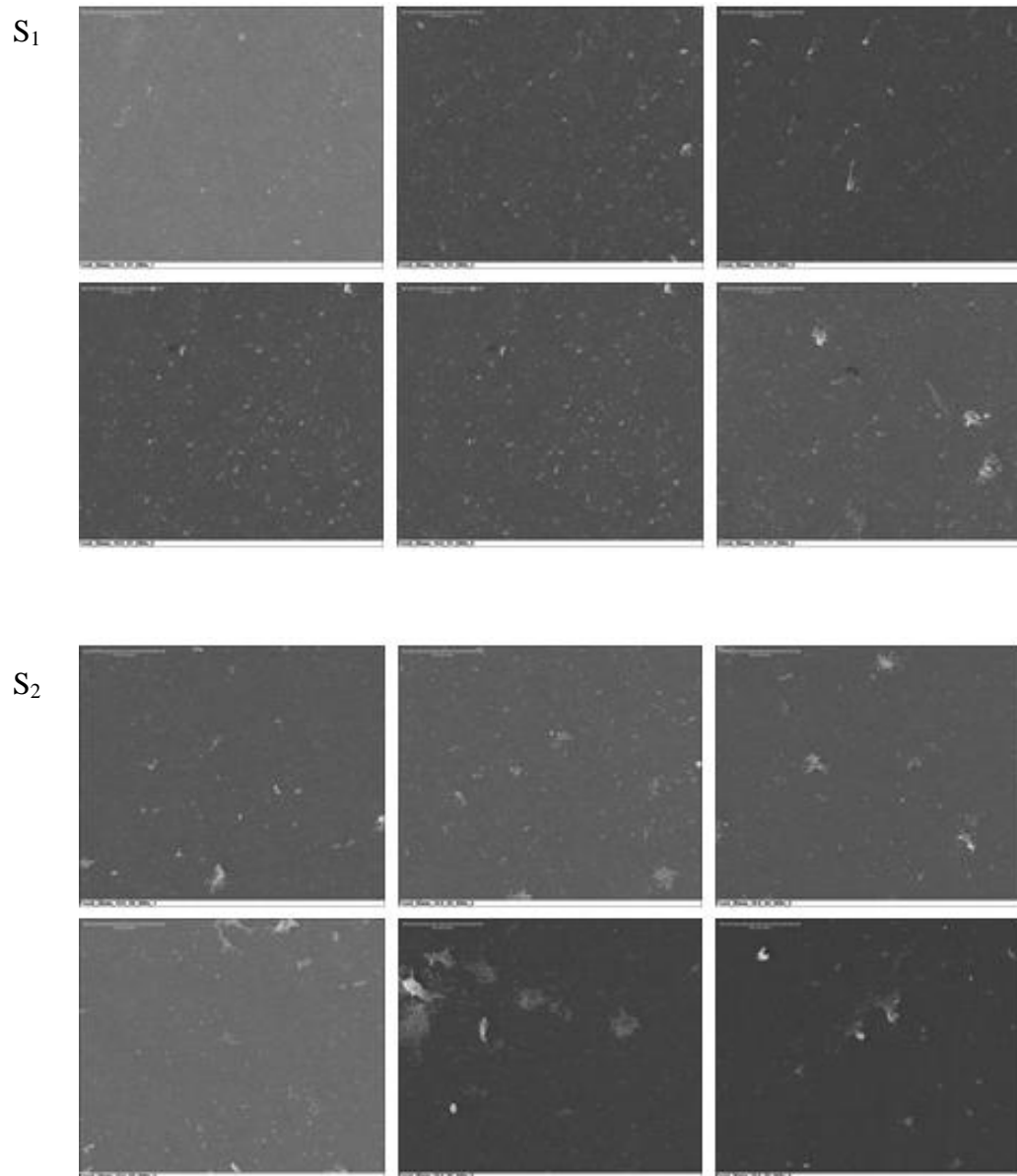
$S_2$



19.5 mm normal plane – rear region of bottom wall

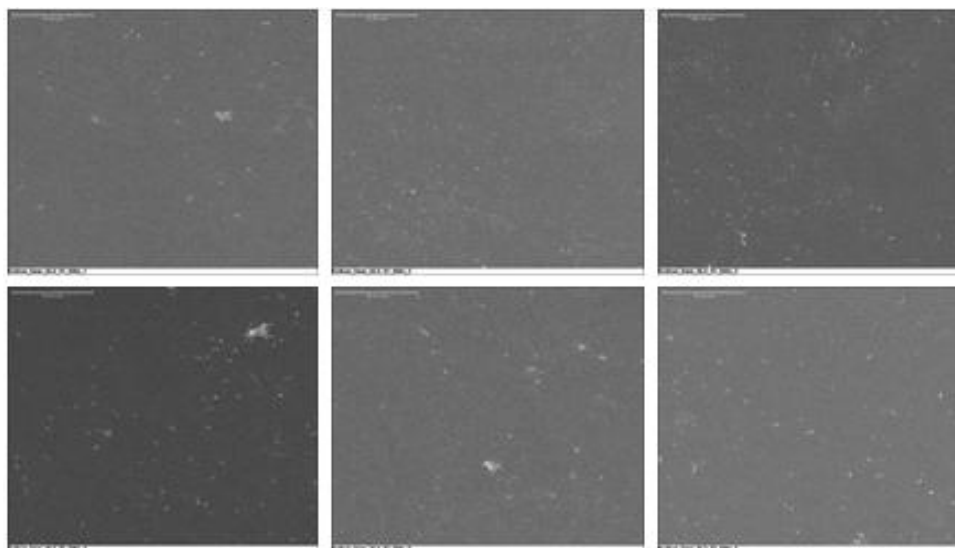


19.5 mm normal plane – 17 mm location on rear wall

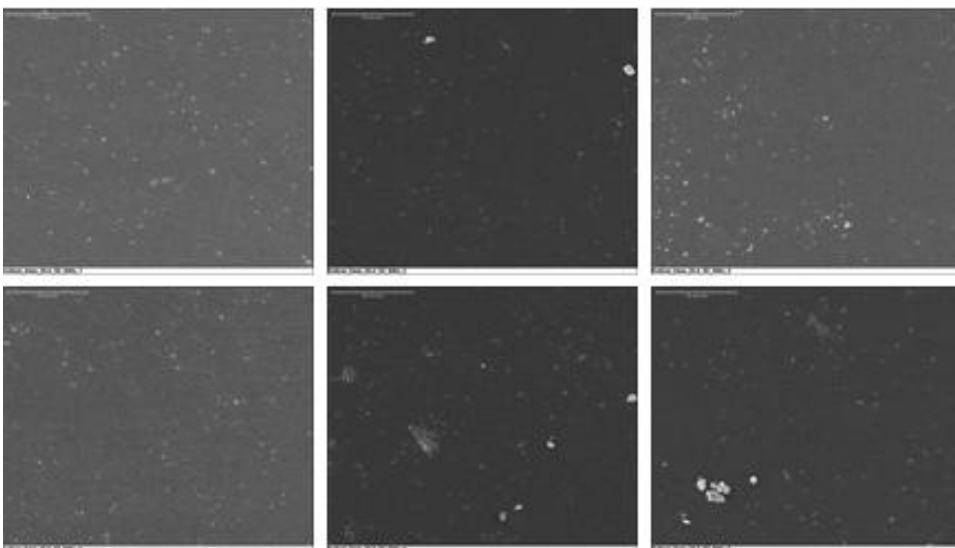


26.9 mm normal plane – front region of bottom wall

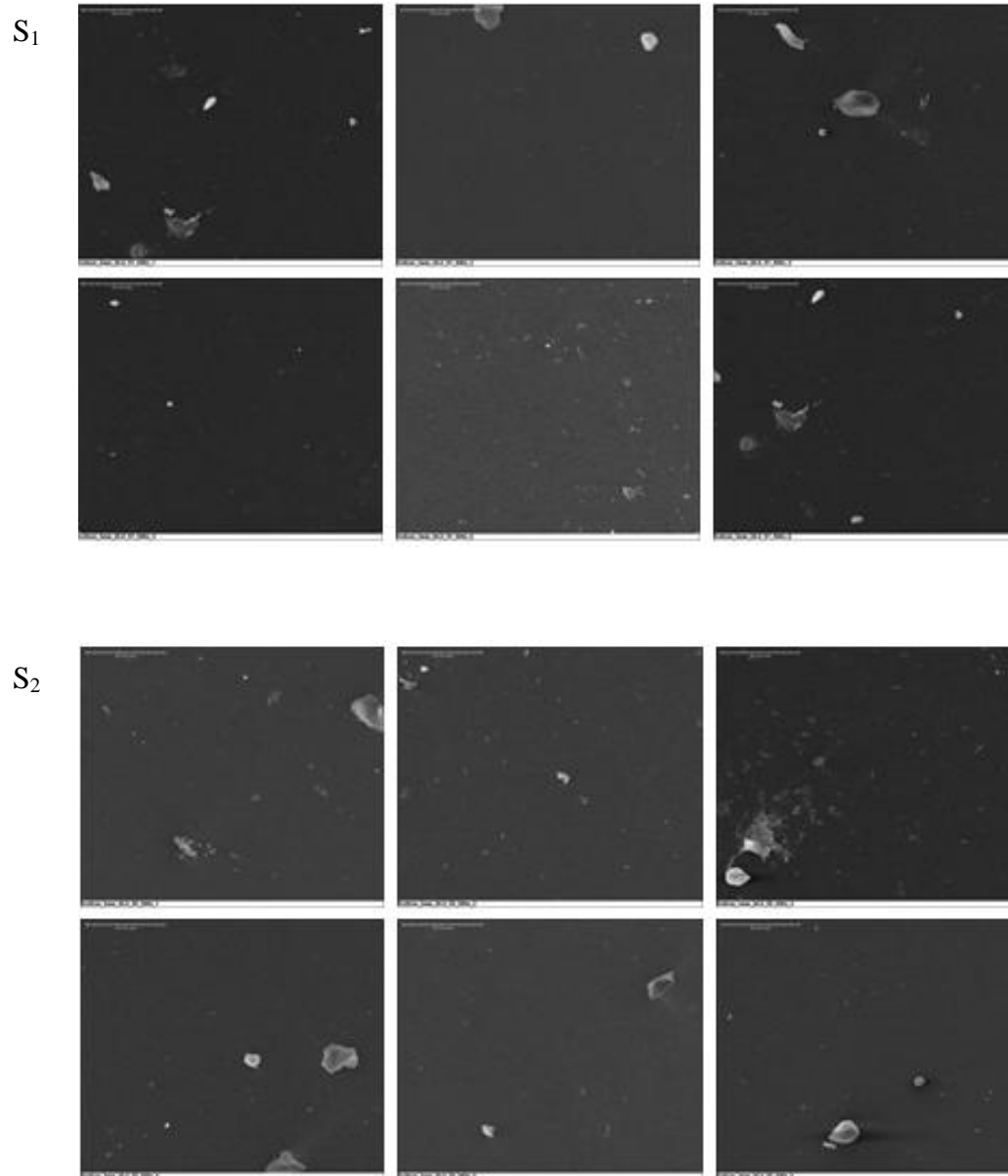
S<sub>1</sub>



S<sub>2</sub>

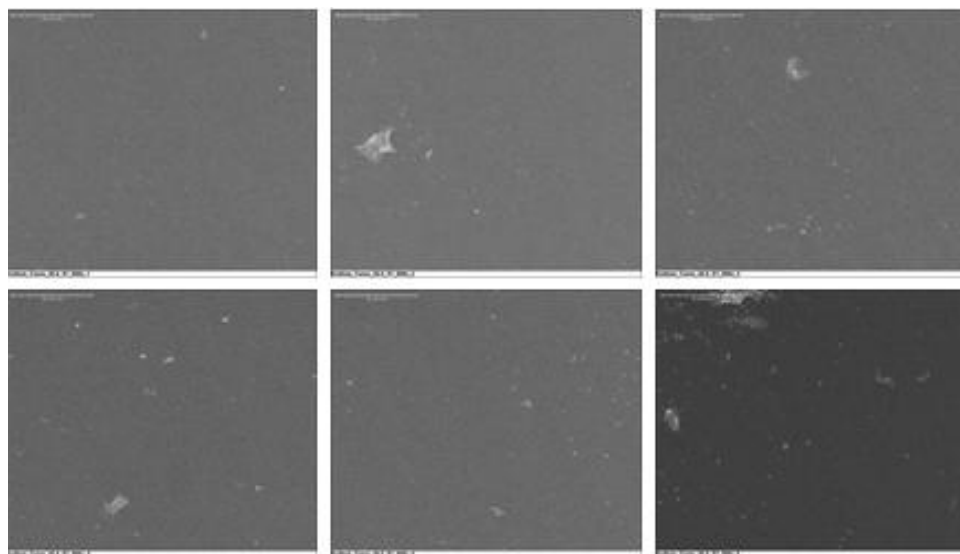


26.9 mm normal plane – center region of bottom wall

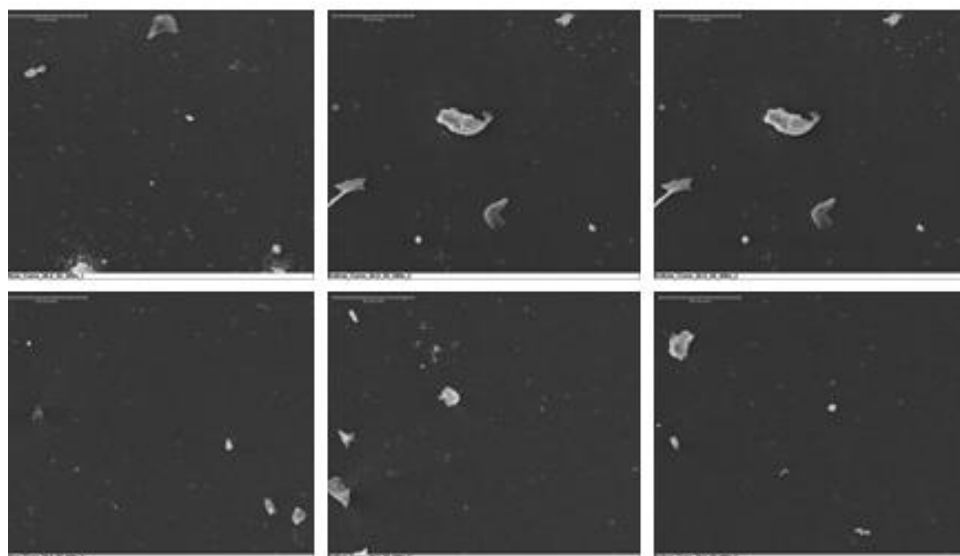


26.9 mm normal plane – rear region of bottom wall

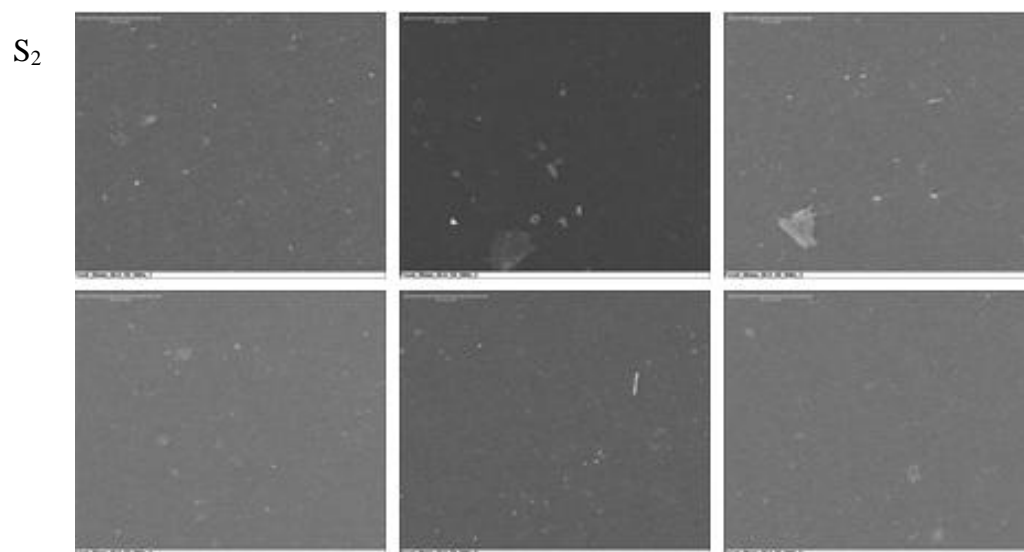
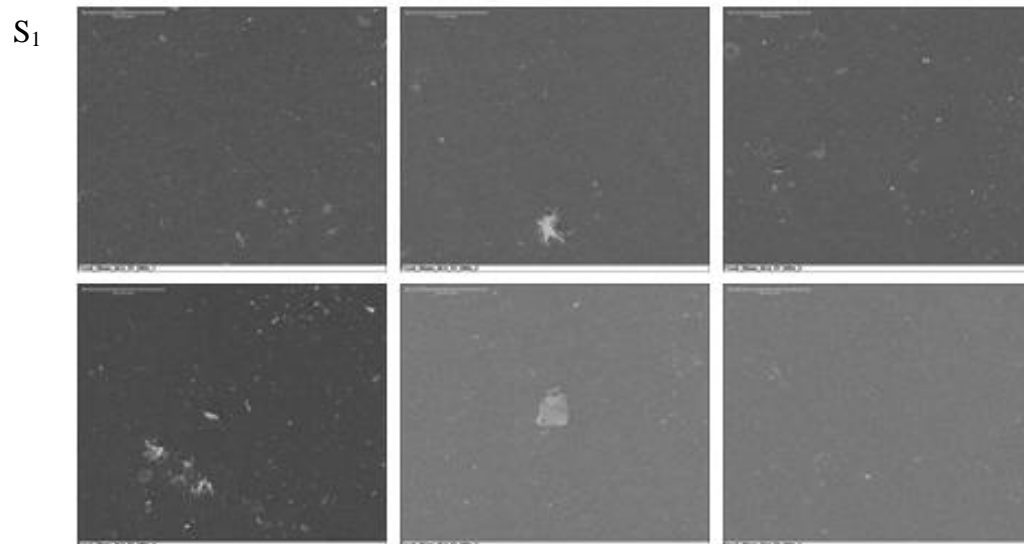
S<sub>1</sub>



S<sub>2</sub>

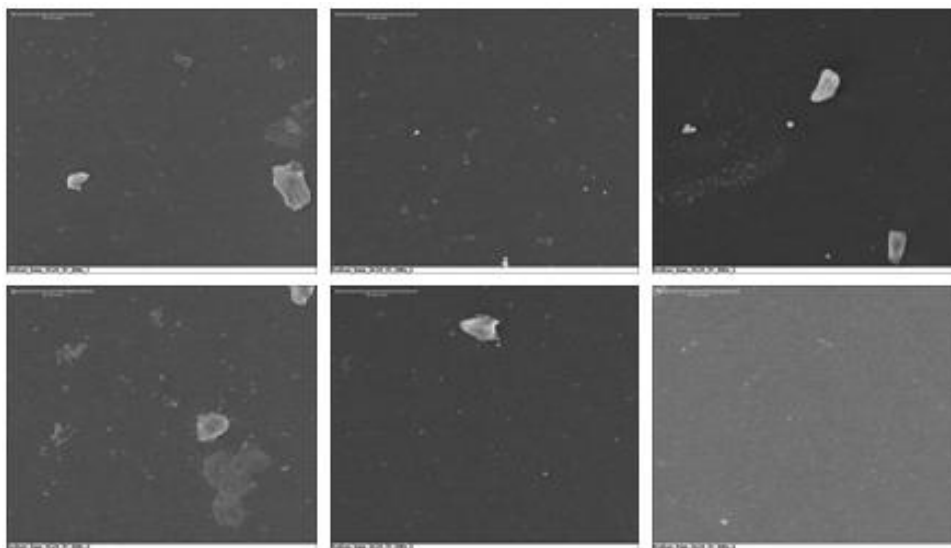


26.9 mm normal plane – 17 mm location on rear wall

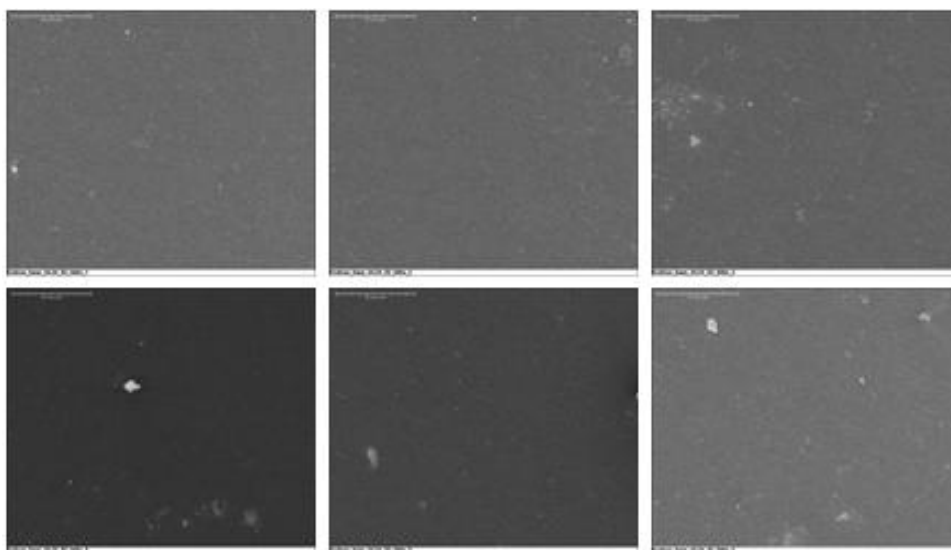


34.24 mm normal plane – front region of bottom wall

S<sub>1</sub>

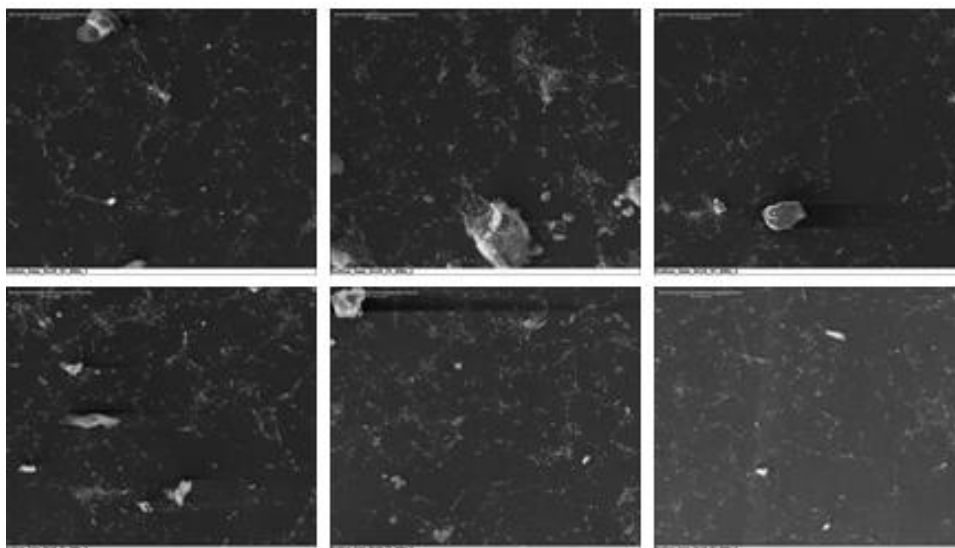


S<sub>2</sub>

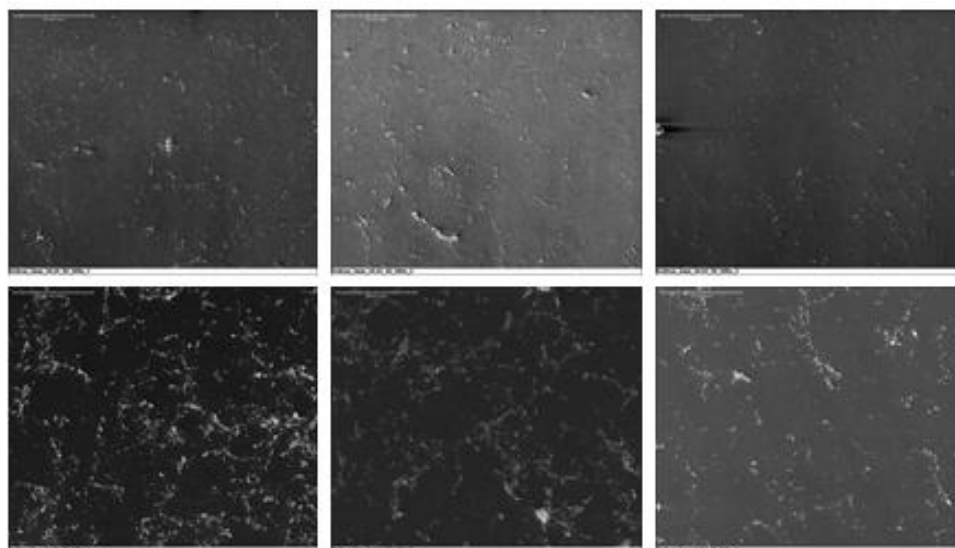


34.24 mm normal plane – center region of bottom wall

S<sub>1</sub>

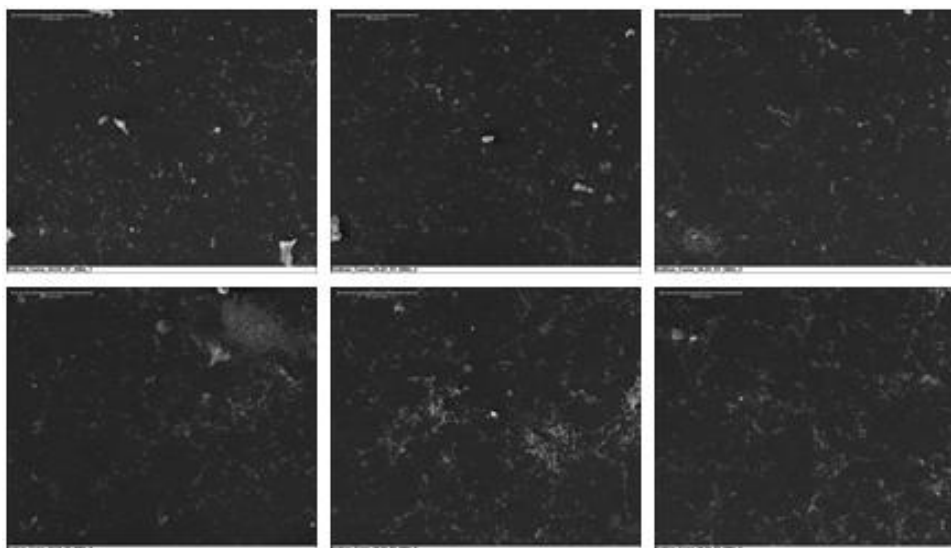


S<sub>2</sub>

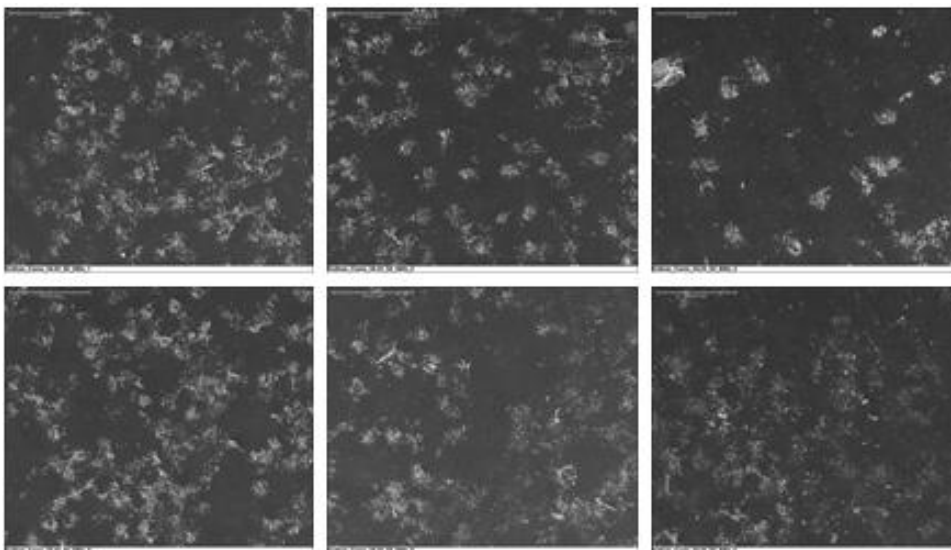


34.24 mm normal plane – rear region of bottom wall

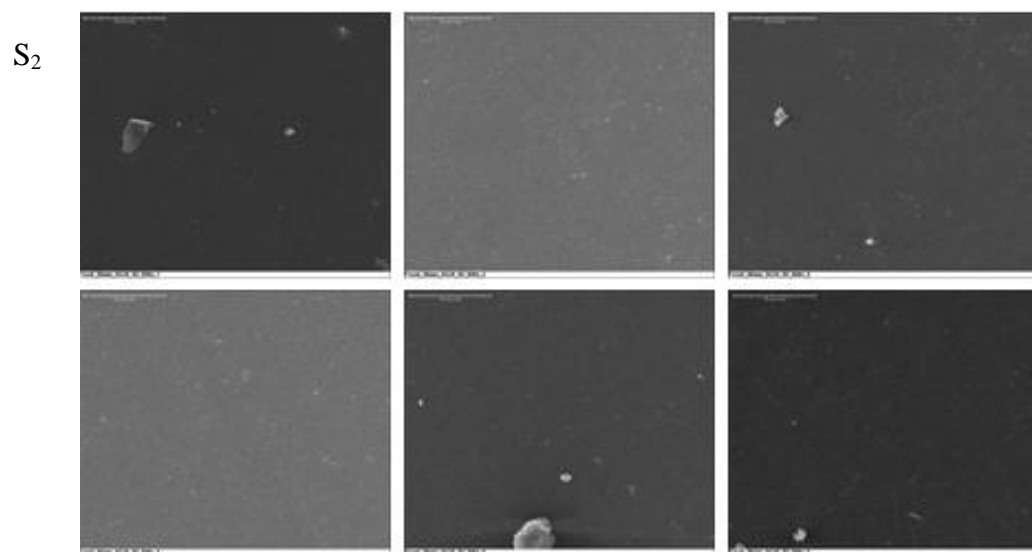
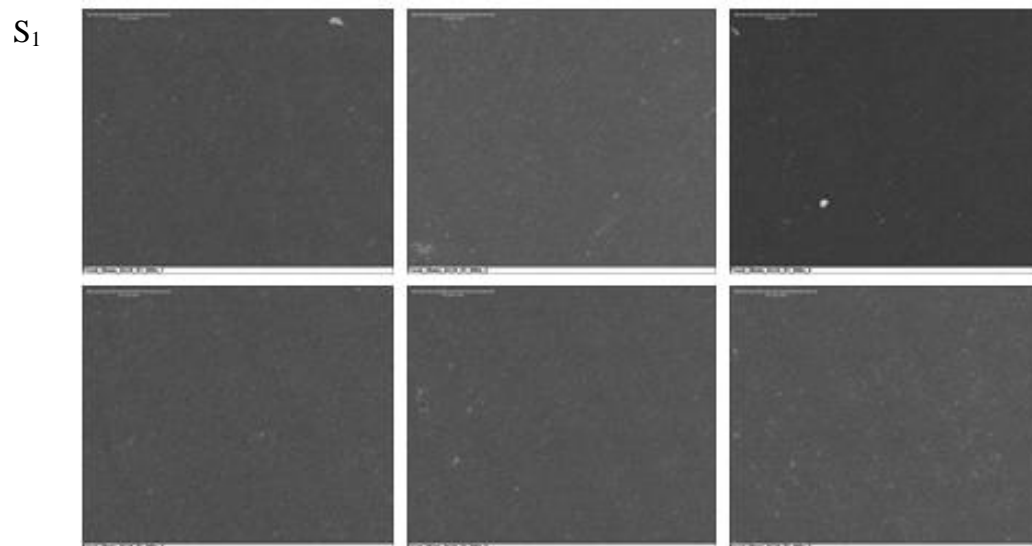
S<sub>1</sub>



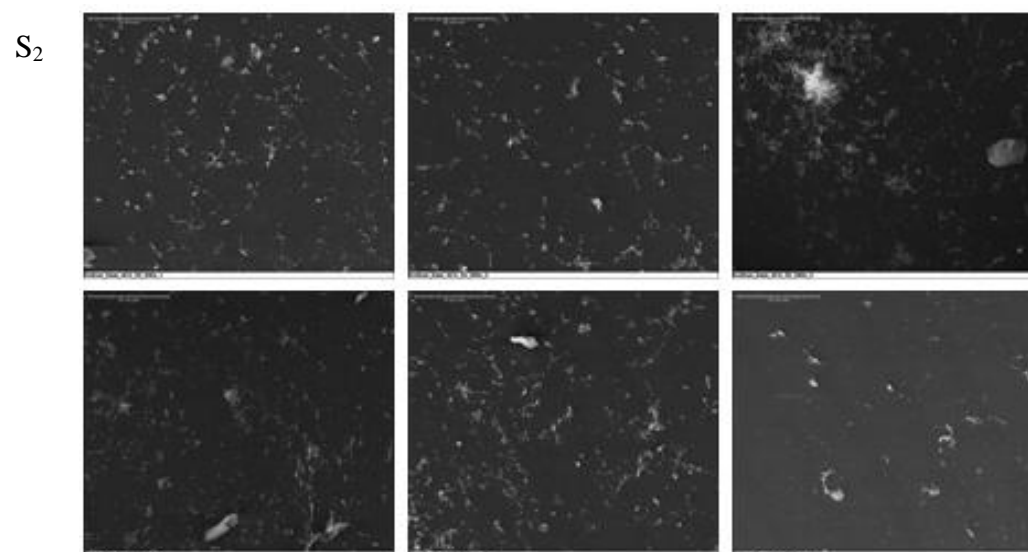
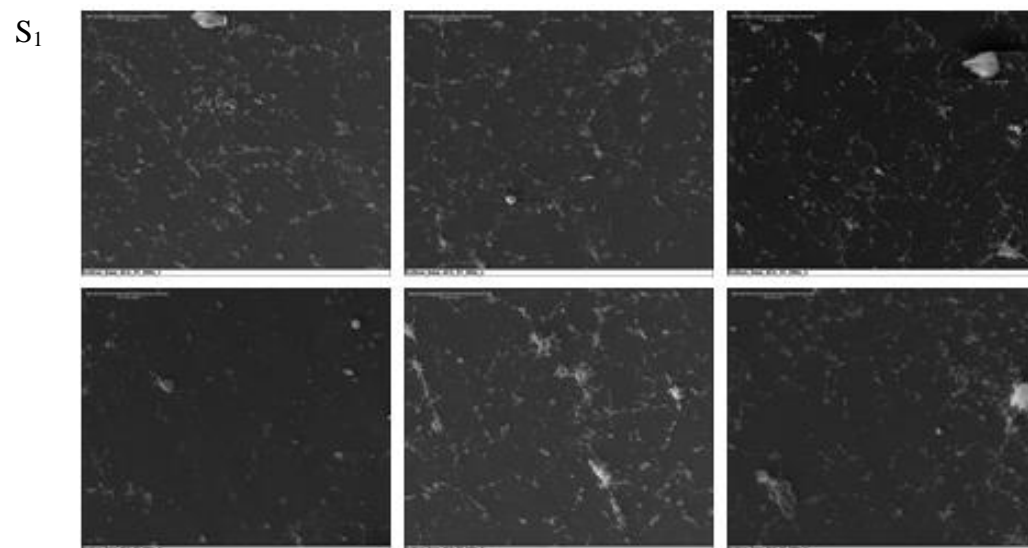
S<sub>2</sub>



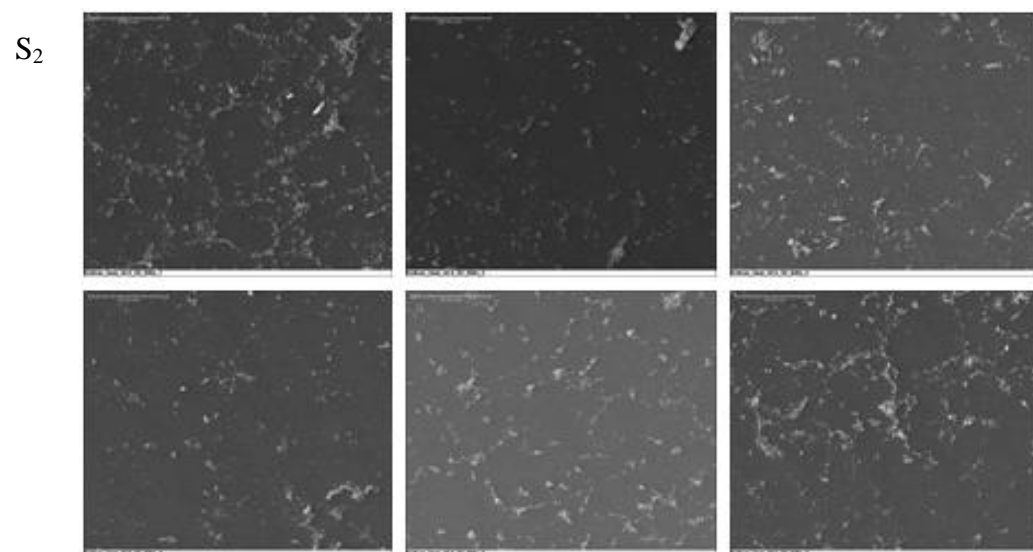
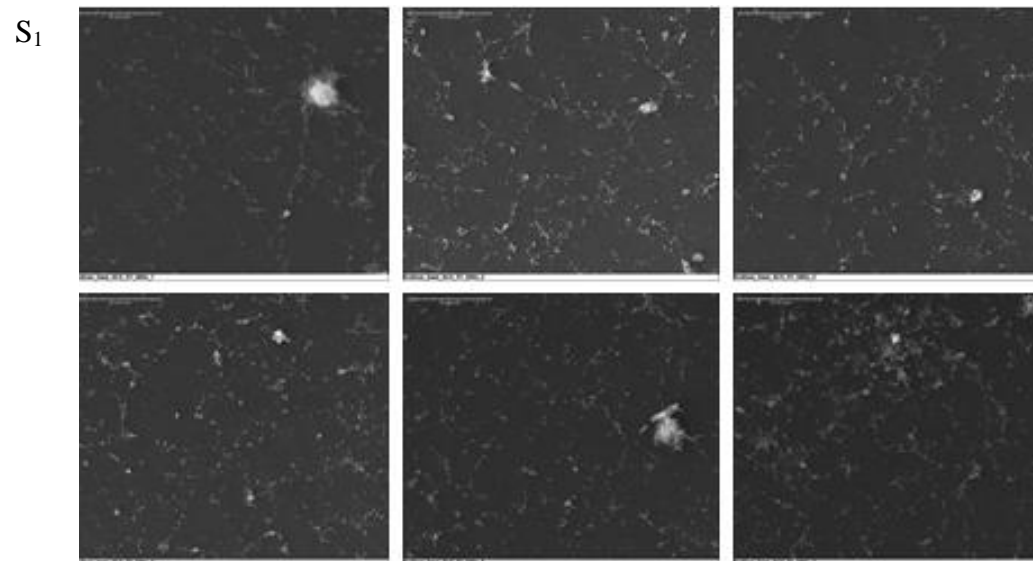
34.24 mm normal plane – 17 mm location on rear wall



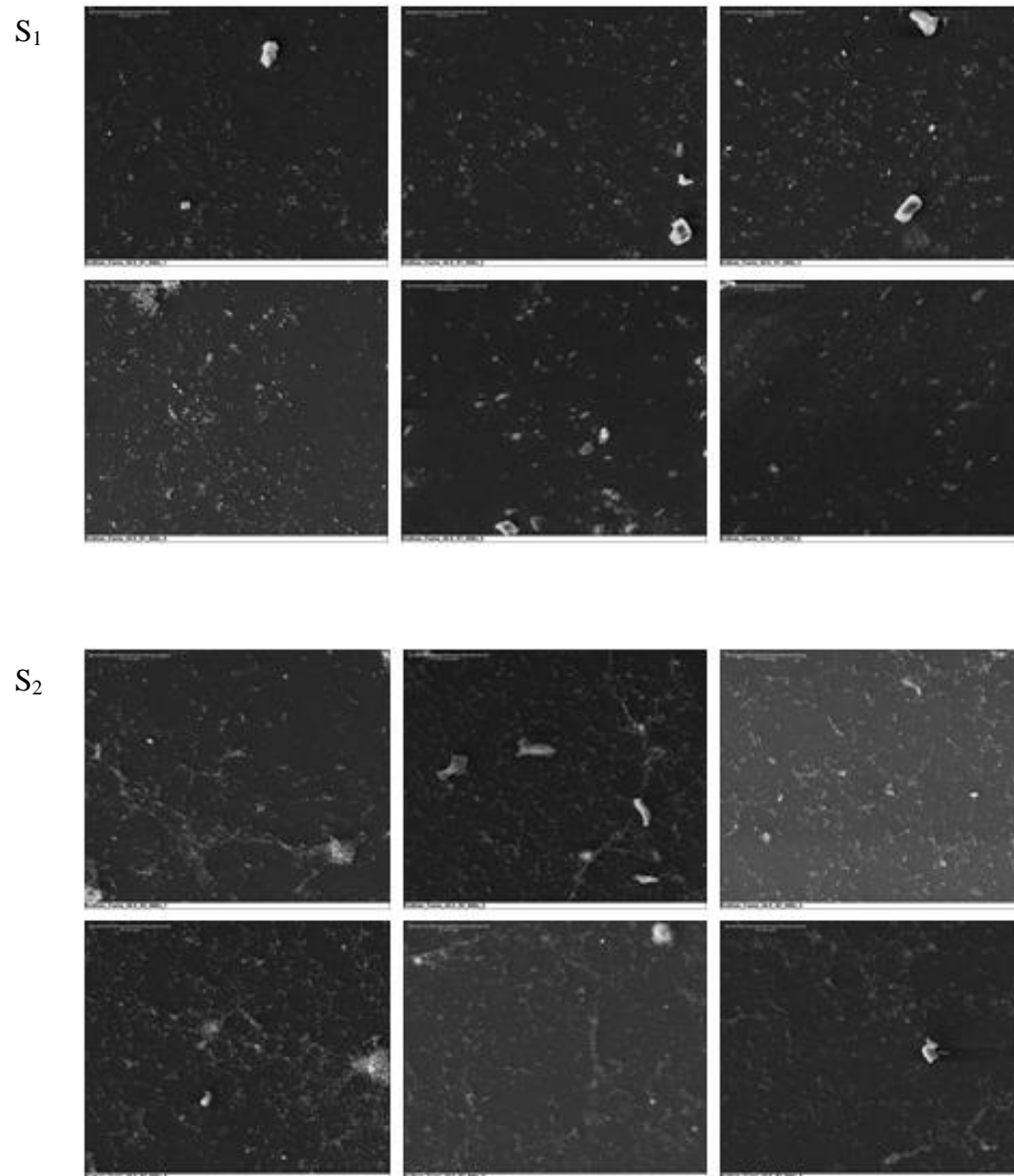
42.5 mm normal plane – front region of bottom wall



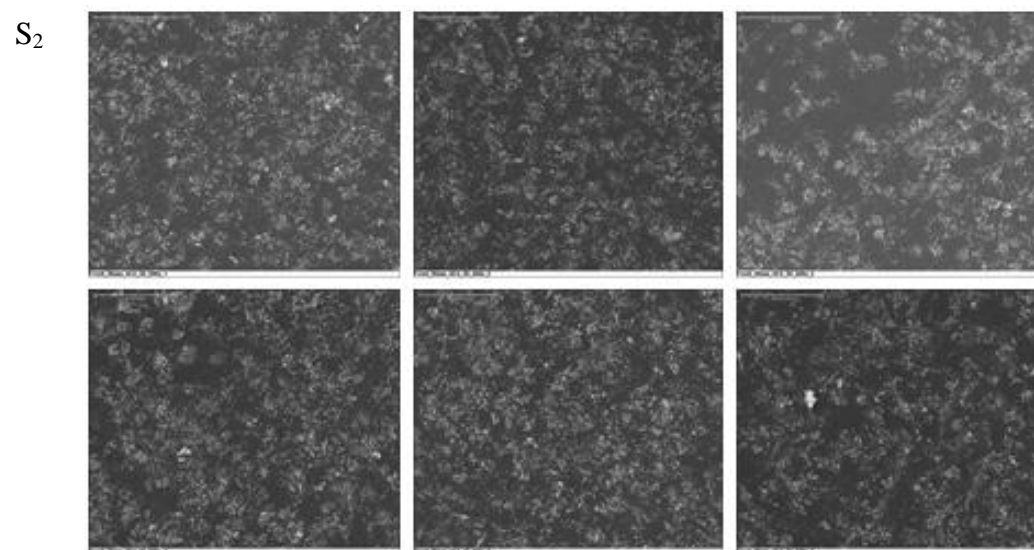
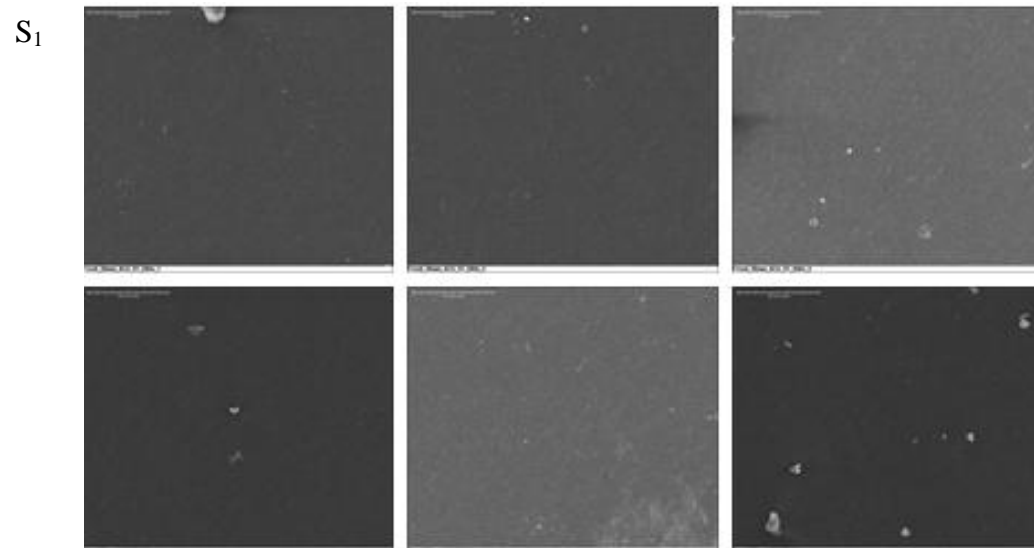
42.5 mm normal plane – center region of bottom wall



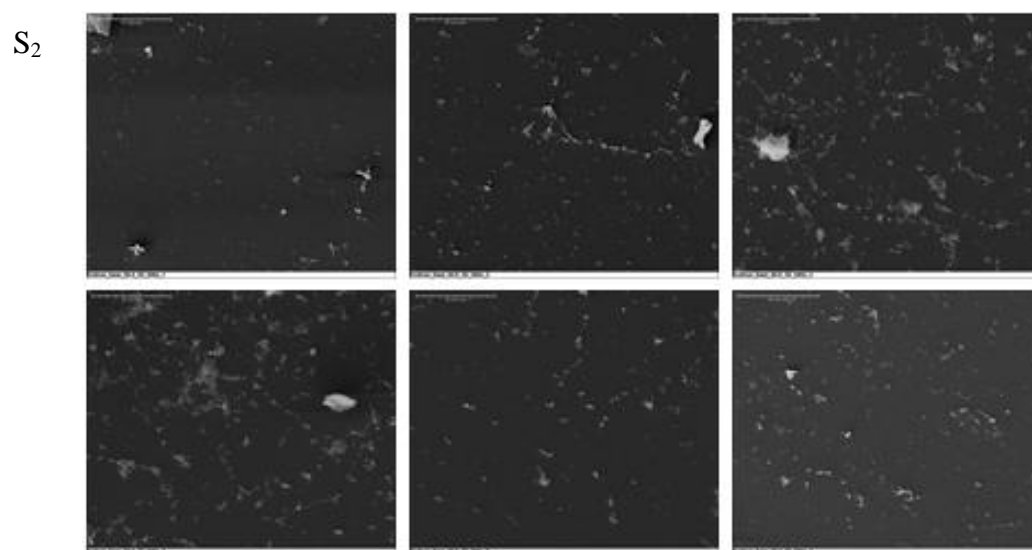
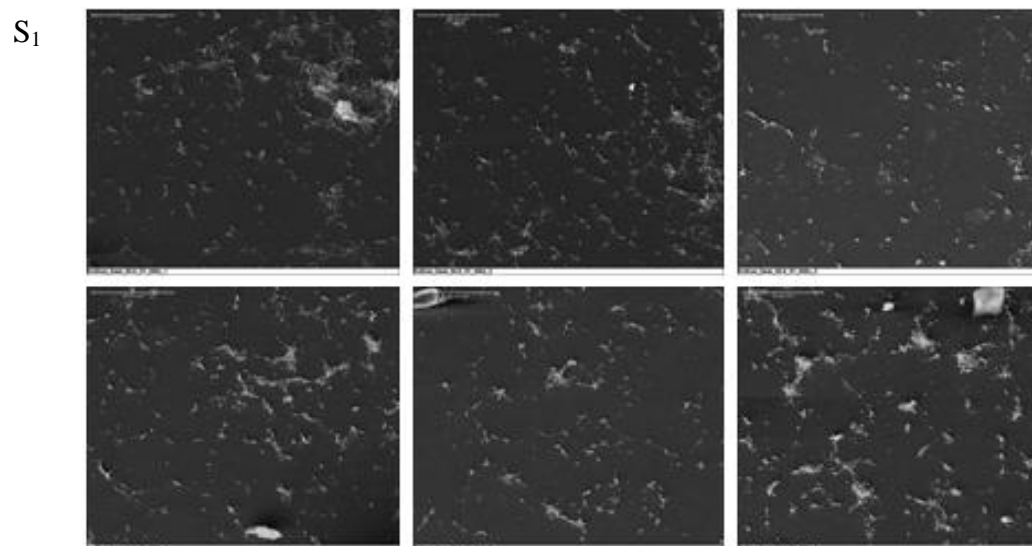
42.5 mm normal plane – rear region of bottom wall



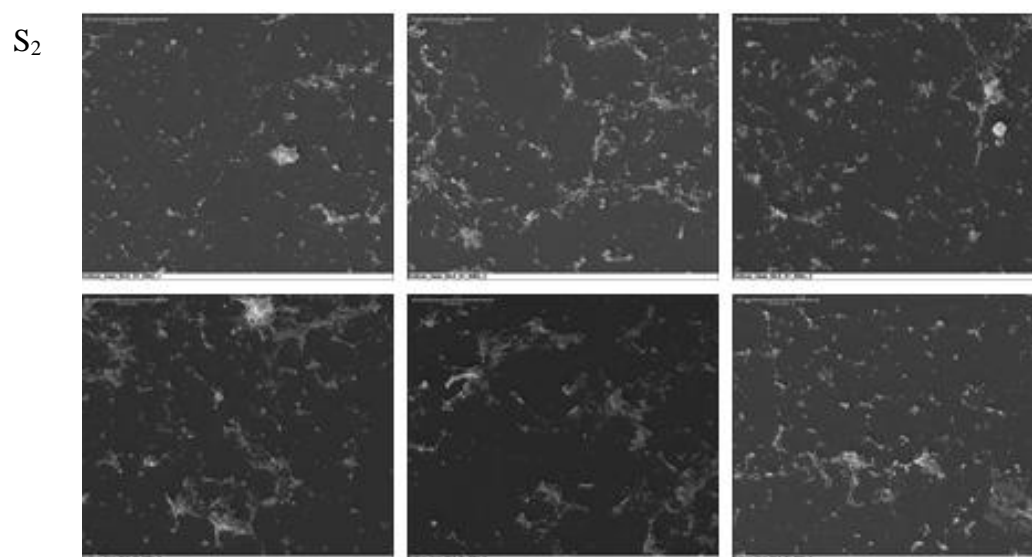
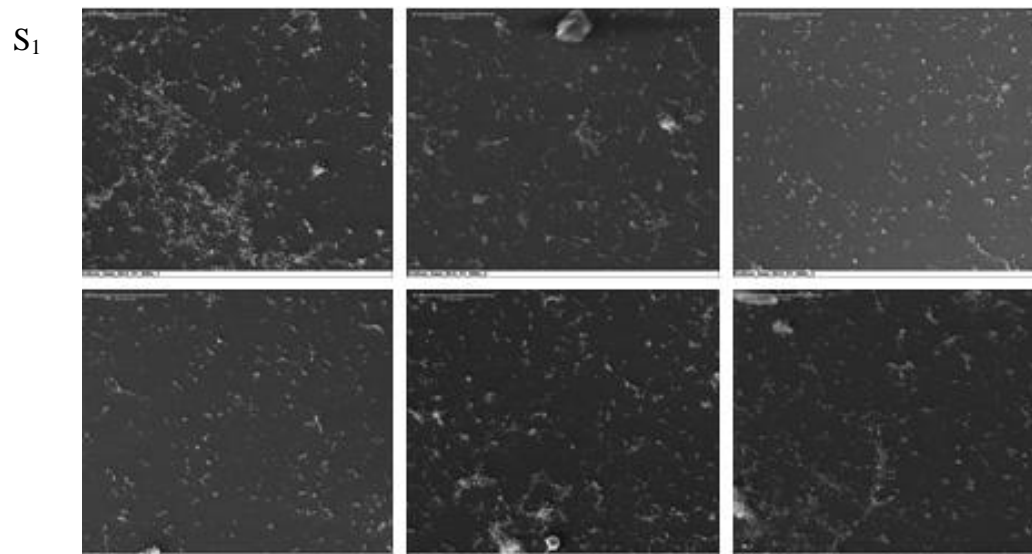
42.5 mm normal plane – 17 mm location on rear wall



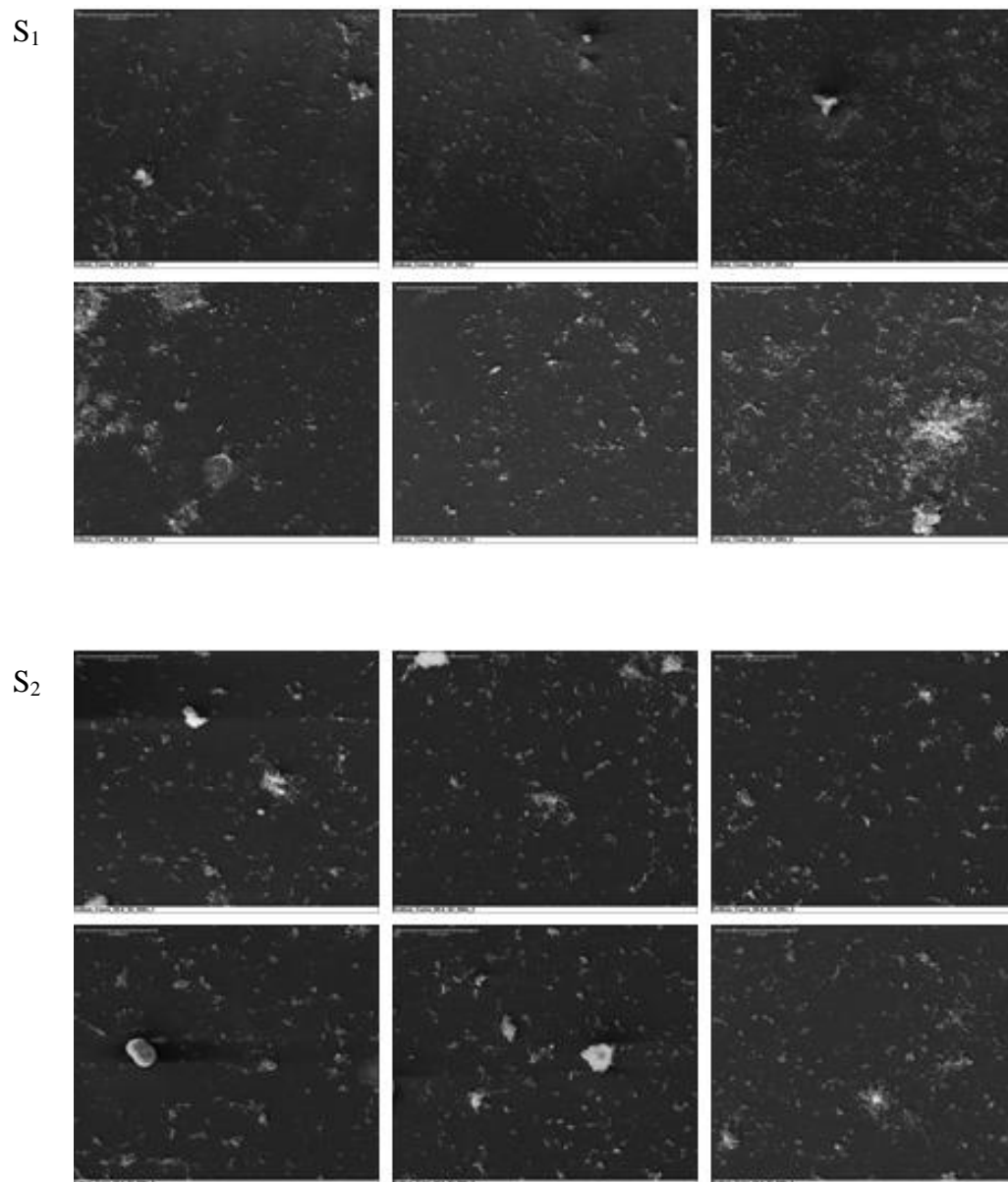
50.8 mm normal plane – front region of bottom wall



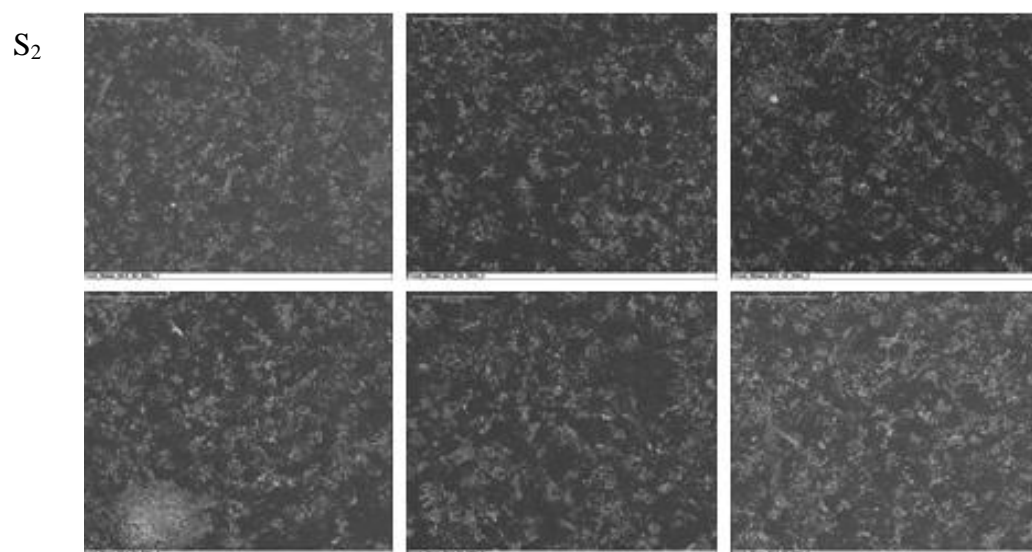
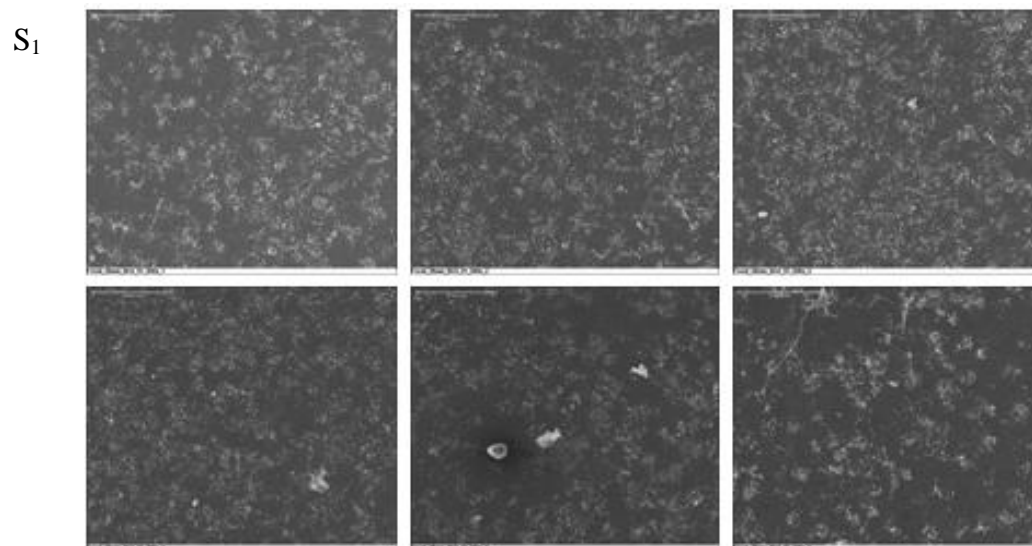
50.8 mm normal plane – center region of bottom wall



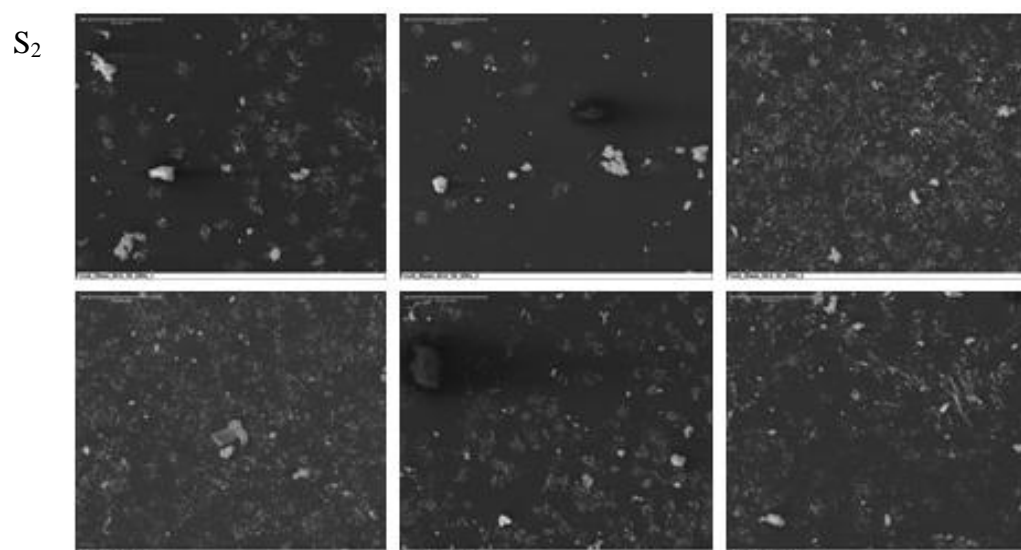
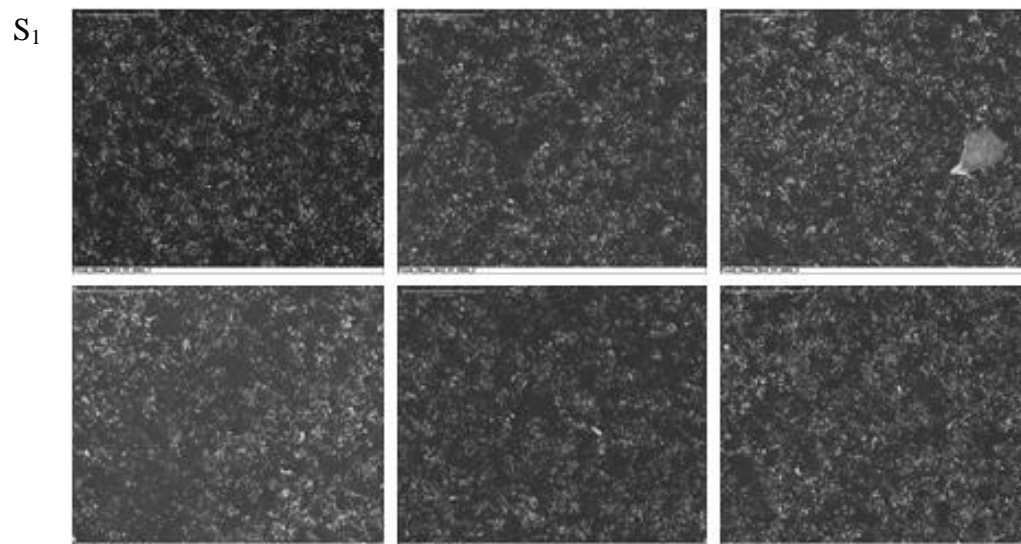
50.8 mm normal plane – rear region of bottom wall



50.8 mm normal plane – 17 mm location on rear wall

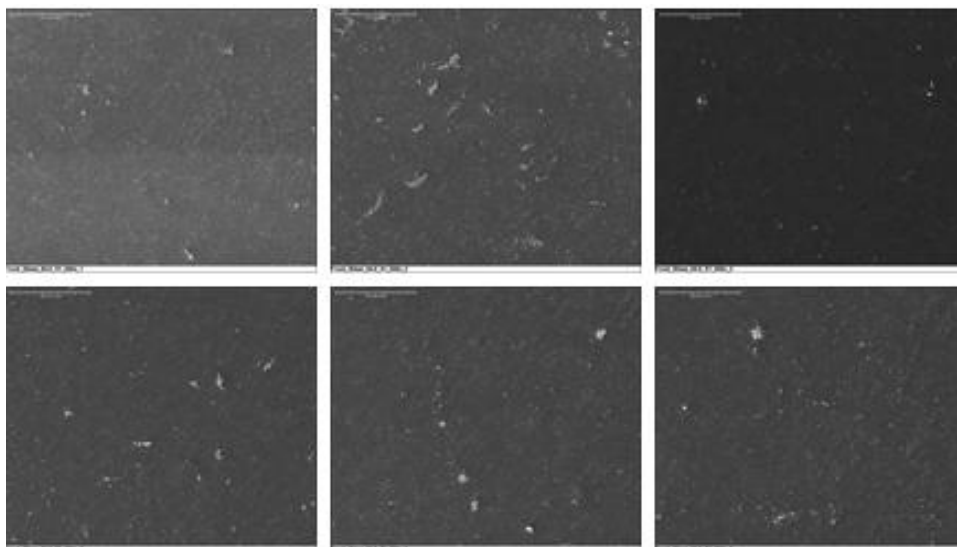


50.8 mm normal plane – 25 mm location on rear wall

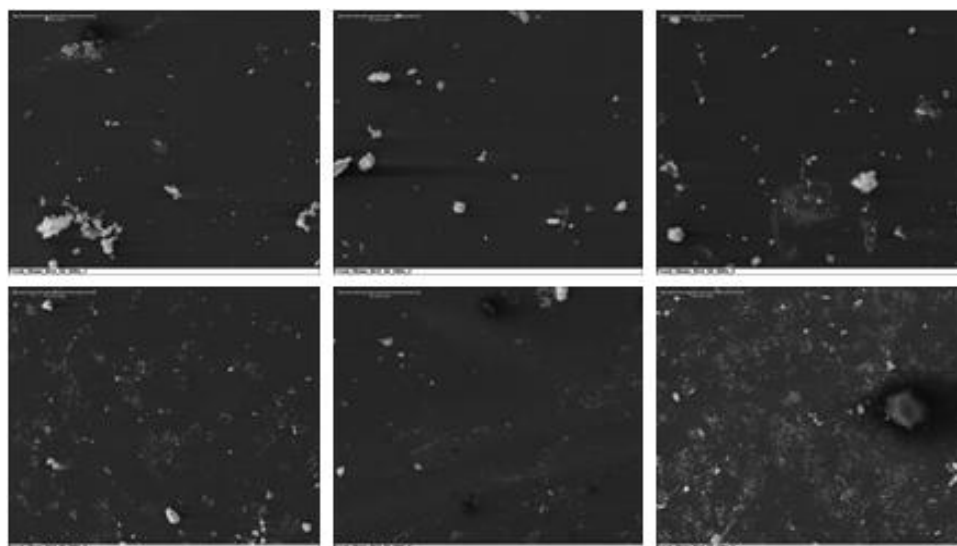


50.8 mm normal plane – 35 mm location on rear wall

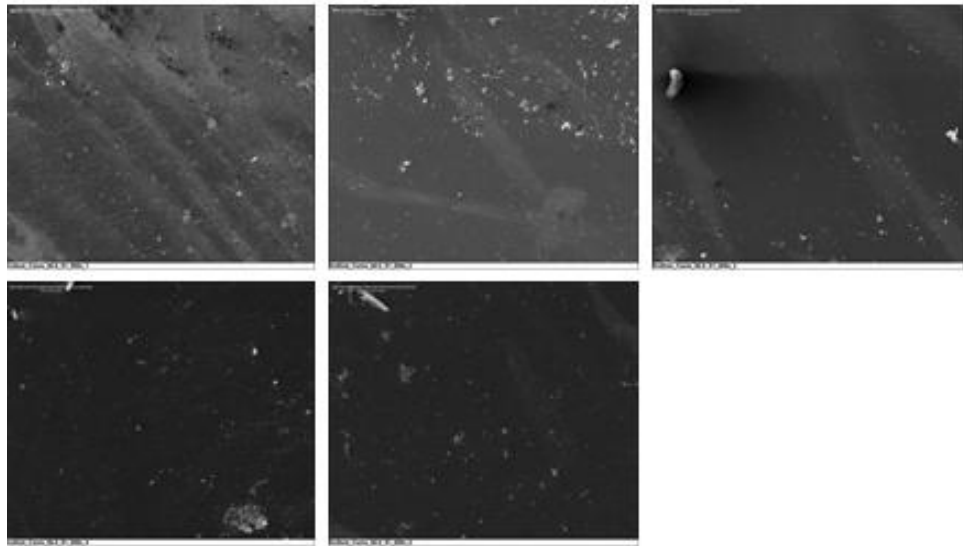
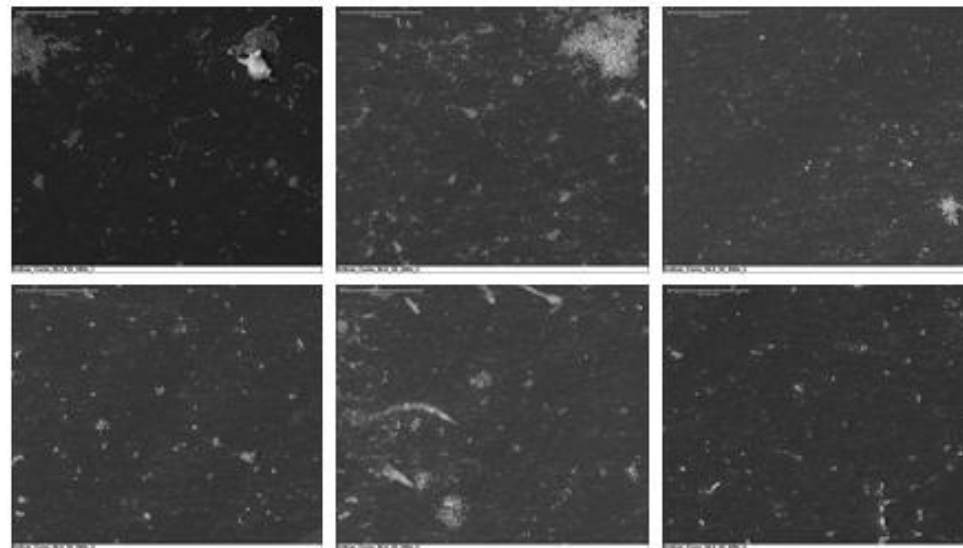
S<sub>1</sub>



S<sub>2</sub>



## 56.8 mm normal plane – rear region of bottom wall

S<sub>1</sub>S<sub>2</sub>

## ACADEMIC VITA

### **Stephen Robert Topper**

#### Education:

Bachelor of Science Degree in Bioengineering, Penn State University,  
Spring 2005  
Honors in Bioengineering  
Thesis title: A correlative study of fluid mechanics and evidence of  
thrombus formation within the penn state 50 cc v-2 left ventricular  
assist device  
Thesis Supervisor: Dr. Keefe B. Manning

#### Related Experience:

Research Assistant at the Penn State Artificial Heart Lab  
Supervisor: Dr. Keefe B. Manning  
Fall 2009 to present

#### Publications:

J. C. Nanna, M. A. Navitsky, **S.R. Topper**, S. Deutsch, K. B. Manning.  
“A Fluid Dynamics Study in a 50 CC Pulsatile Ventricular Assist Device:  
Influence of Heart Rate Variability.” The Journal of Biomechanical  
Engineering. June, 2011.

**S.R. Topper**, J.C. Nanna, R.S. Meyer, S. Deutsch, K.B. Manning. “The  
Scaling Effects in Comparing Pediatric and Adult Mechanical Heart  
Valves.” American Society for Artificial Internal Organs Conference. May  
27-29, 2010, Baltimore, MD.

J.C. Nanna, **S.R. Topper**, N. Yang, B.N. Roszelle, S. Deutsch, K.B.  
Manning. “Experimental Wall Shear Estimation as a Means of Predicting  
Thrombus Formation Within a 50cc Penn State Blood Pump.” ASME  
2010 Summer Bioengineering Conference. June 16-19, 2010, Naples, FL.

J. C. Nanna, **S.R. Topper**, B.N. Roszelle, N. Yang, S. Deutsch, K.B.  
Manning. “The Effectiveness of Particle Image Velocimetry and  
Computational Fluid Dynamics in Predicting Thrombus Formation in A  
Penn State Left Ventricular Assist Device.” 6<sup>th</sup> World Congress on  
Biomechanics. Aug. 1-6, 2010, Singapore.

Awards:

The Schreyer Honors College Academic Scholarship  
The Penn State Summer Discovery Grant  
Dean's List  
Second Place at the Penn State Undergraduate Exhibition  
National Honors Society

Presentations/Activities:

Presenter at the American Society for Artificial Organs Conference  
Baltimore, MD, 2010  
Presenter at the Penn State Undergraduate Exhibition  
University Park, PA, 2010 and 2011